NASA TECHNICAL NOTE

NASA TN D-8151

NASA TN D-8151

FUNDAMENTALS OF FLUID SEALING

John Zuk

Lewis Research Center

Cleveland, Ohio 44135

NATIONAL AERONAUTICS AND SPACE ADMINISTRATION • WASHINGTON, D. C. • MARCH 1976

1. Report No.	2. Government Accession No.	3. Recipient's Catalog No.
NASA TN D-8151		

4. Title and Subtitle	5. Report Date
FUNDAMENTALS OF FLUID SEALING	March 1976
	6. Performing Organization Code

7. Author(s)	8. Performing Organization Report No.
John Zuk	E-6910
	10. Work Unit No.
	505-04

9. Performing Organization Name and Address	11. Contract or Grant No.
Lewis Research Center National Aeronautics and Space Administration Cleveland, Ohio 44135	
	13. Type of Report and Period Covered
	Technical Note

12. Sponsoring Agency Name and Address	14. Sponsoring Agency Code
National Aeronautics and Space Administration Washington, D.C. 20546	

15. Supplementary Notes

16. Abstract

The fundamentals of fluid sealing, including seal operating regimes, are discussed. The general fluid-flow equations for fluid sealing are developed. Seal performance parameters such as leakage and power loss are presented. Included in the discussion are the effects of geometry, surface deformations, rotation, and both laminar and turbulent flows. The concept of pressure balancing is presented, as are differences between liquid and gas sealing. Also discussed are mechanisms of seal surface separation, fundamental friction and wear concepts applicable to seals, seal materials, and pressure-velocity (PV) criteria.

17. Key Words (Suggested by Author(s))	18. Distribution Statement
Seal; Face seal; Gas-film seals; Labyrinth seals; Lubrication; Incompressible flow; Compressible flow; Narrow slots; Noncontacting seals; Fluid-film seals; Hydrodynamic seals; Hydrostatic seals; Friction; Wear; Boundary lubrication; Seal materials	Unclassified - unlimited STAR Category 37 (rev.)

19. Security Classif. (of this report)	20. Security Classif. (of this page)	21. No. of Pages	22. Price*
Unclassified	Unclassified	166	$6.25

* For sale by the National Technical Information Service, Springfield, Virginia 22161

CONTENTS

FUNDAMENTALS OF FLUID SEALING

by John Zuk

Lewis Research Center

SUMMARY

The fundamentals of fluid sealing, including seal operating regimes, are discussed. The general fluid-flow equations for fluid sealing are developed. Seal performance parameters such as leakage and power loss are presented. Included in the discussion are the effects of geometry, surface deformations, rotation, and both laminar and turbulent flows. The concept of pressure balancing is presented, as are differences between liquid and gas sealing. Also discussed are mechanisms of seal surface separation, fundamental friction and wear concepts applicable to seals, seal materials, and pressure-velocity (PV) criteria.

INTRODUCTION

In fluid sealing as in every branch of engineering, one must draw on the experience and knowledge of many other disciplines and fields. The engineering of seals can involve fluid mechanics, heat transfer, lubrication theory, structural and solid mechanics, thermodynamics, chemistry, physics, metallurgy, and dynamics, as well as other fields. Seal problems may consist of a superposition of effects which can be interrelated. Usually each effect can be analyzed by itself. Then integrated effects must be evaluated.

Fluid sealing is generally the same as any other branch of engineering except for the importance of small-scale effects. Seals are characterized by surfaces in relative motion separated by a very narrow gap. In order to maintain proper operation, very small differences in the dimensions of seal parts must be maintained. Deformations in geometry due to imposed thermal gradients, frictional heating, pressure gradients, and mechanical and inertial forces must be held to a minimum. Actually, in some cases, deformations must be no more than microvalues.

The fundamentals of fluid flow are important to understanding the various sealing devices. This presentation discusses those fundamentals as they apply to seals. Basic

principles of incompressible (liquid) and compressible (gas) sealing flows are studied. The mechanism of film pressure generation between relatively moving surfaces is described. Fundamental friction and wear concepts, various seal lubrication operating regimes, and surface topography effects are also presented.

Generally, sealing flow is a direct opposite of conventional fluid flow through pipes, ducts, and nozzles, where it is desired to have as efficient a flow process as possible (low friction). In seals it can be desirable to have an inefficient flow process because this results in low leakage; however, a trade-off must be made with power loss.

This presentation is intended to provide the background necessary for a fundamental understanding of fluid sealing in general and of specific seal types in particular. Unfortunately, this discussion of the theory leaves much of the subject uncovered. Derivations are omitted unless they are essential to the understanding or illustration of a concept. A remark, perhaps, should be made concerning the accuracy of the applicable equations contained herein. When we are dealing with fluids and seal configurations for which test data are available, design accuracy of perhaps 25 percent may be realized. When we are dealing with different configurations or using fluids that deviate from ideal properties, present knowledge is rated as fair or poor and testing becomes necessary in the design.

Fundamentals of fluid sealing can also be found in a textbook by Mayer (ref. 1). A survey report (ref. 2) should be useful. Each topic covered includes, where possible, a reference wherein more information can be found. The seal nomenclature used is that adapted by the ASLE Seals Technical Committee (ref. 3).

In all references cited, the U. S. customary system of units was used. The International System of Units (SI) has been added to the text and figures for this report only.

SEAL OPERATING REGIMES

Seals operate in many lubrication regimes depending on the type of seal, the sealed fluid, the application, and so forth. A plot of friction coefficient against seal duty parameter illustrates the various seal operating (lubricating) regimes that can exist (fig. 1).

For illustrative purposes, consider a lift-off type of seal that is in rubbing contact at startup and shutdown. The way this seal may change from one lubricating regime to another within an application is shown in figure 1 for liquid lubrication. The figure shows the variation in friction coefficient a seal undergoes from startup under a load (e.g., spring force and pressure) in the boundary lubricating regime to the steady-state operating speed in the full-film lubricating regime. (The mechanism for achieving full-film operation could be an external pressurization source, or it could be self-generated by hydrodynamic lubrication. At startup the parts are in solid-to-solid contact and the

seal runner (rotating member) begins to turn under essentially dry conditions and starts to follow the path AB. If sufficient lubricant is available, the lubricant is ordinarily drawn between the sliding surfaces at once (by capillary action or a forced pumping mechanism) and the seal immediately enters the thin-film (or mixed film) regime, following the path ABC. When the speed reaches the value corresponding to point C, the seal enters the full-film regime, in which it remains until coming to operating speed at point D. It can be seen in figure 1 that, if the lubricant were not present, the seal would be forced to operate dry at a speed corresponding to point A. The resulting temperature rise could be extreme because of the high friction.

Now some of the details are examined more closely. The curves shown in figure 1 were originally for journal bearings, but the same principles apply for a seal. Friction coefficient is plotted against a seal duty parameter $\mu N/P_n$, where μ is the fluid viscosity, N is the rotational speed, and P_n is the net seal-face load. (All symbols are defined in appendix A.) To the right of the second dashed vertical line is the region of full-film fluid lubrication, that is, thick-film lubrication, where the surface asperities are completely separated by an oil film of such thickness that no metal-to-metal contact can occur (fig. 2(a)). The friction coefficient for a hydrodynamic film can be calculated from

$$\eta = \frac{\tau A}{\text{Net normal closing force}}$$

where τA is the traction force. Hydrodynamic lubrication theory applies, and the flow is laminar. At sufficiently large values of the seal duty parameter, turbulent flow can occur (transition occurs at point D and turbulent flow exists beyond point E of fig. 1). The friction here rises significantly and increases at a more rapid rate with speed than in the laminar flow regime. To the left of the dashed vertical lines are the regions of boundary and thin-film lubrication. As noted in figure 2(c), the film thickness in boundary lubrication is so small that asperities make contact through the fluid film. The thin-film regime is one that combines hydrodynamic and boundary lubrication. This is also the regime where elastohydrodynamic effects may be important. Friction coefficients in the boundary and thin-film regimes are empirically determined.

In full-film fluid lubrication, since the asperities do not contact, only bulk lubricant physical properties are important. In boundary and thin-film lubrication, the properties of the metals as well as surface physics and chemistry are of primary importance since there is metal-to-metal contact by asperities. Lubricant chemical properties can influence the type of damage that occurs.

The lubricating regimes can similarly be associated with seal-face loading and speed. The three regimes are shown from this point of view in figure 2. That is, the full-film lubricating regime is characterized by the film thickness being several times

greater than the surface roughness. The thin-film regime has the film thickness of the order of the surface roughness. In the boundary regime, asperity contact characterizes the interface.

The friction coefficient behavior is different for a gas (fig. 3). Since gases are poor boundary lubricants, the friction coefficient values are almost those obtained for a solid sliding on a solid at low seal duty parameters. Since a gas has a much lower viscosity than a liquid, friction forces can be one or two orders of magnitude less in the full-film lubricating regime. For a gas film seal to operate in this regime, incorporation of a lift geometry to the seal faces is usually required. Operating gaps are inherently smaller for gas film seals (due to the low viscosity); therefore, these seals are more sensitive to face distortions. This, coupled with the poor boundary lubricating properties of gases, means that stable self-induced hydrodynamic operation is unlikely in gas film seals. The friction coefficient variation is qualitatively similar to that for liquid lubrication in the full-film regime until compressibility effects become significant. Generally, compressibility effects become important before turbulence occurs. However, for large gaps and sufficiently high pressures or speeds, turbulent flow may occur.

GENERAL EQUATIONS OF MOTION FOR VISCOUS FLUID FLOW

A brief derivation of the fluid-flow equation governing many seal flow situations will now be given. More details can be found in any fluid mechanics textbook, such as reference 4. However, we will follow the development given in reference 5, which derived the equations for seal applications.

Consider the elemental fluid particle dx dy dz moving in a pressure field, as shown in figure 4. The element dx dy dz is small enough that we can use differential and integral calculus but large enough for a representative statistical average. That is, the density of the fluid varies smoothly. The general conditions for equilibrium will be formulated; no stipulation will be made as to the nature of the fluid other than that it is viscous and follows Newton's law of viscous flow. (Viscosity and both Newtonian and non-Newtonian fluids are discussed briefly in appendix B.) Newton's law of viscous flow states that the shear stress resulting from the shear deformation is a linear function of the rate of deformation. That is, the fluid property is a function of the thermodynamic state only. Mathematically in rectilinear Cartesian coordinates, this can be expressed as

$$\tau_{xy} = \tau_{yx} = \mu\left(\frac{\partial w}{\partial x} + \frac{\partial u}{\partial y}\right) \tag{1}$$

$$\tau_{xz} = \tau_{zx} = \mu\left(\frac{\partial v}{\partial x} + \frac{\partial u}{\partial z}\right) \tag{2}$$

$$\tau_{yz} = \tau_{zy} = \mu\left(\frac{\partial v}{\partial y} + \frac{\partial w}{\partial z}\right) \tag{3}$$

This is an empirical observation. It is the only empiricism used in deriving the equations of motion.

According to the conservation-of-momentum principle, which is Newton's second law, dynamic equilibrium of forces on the element dx dy dz requires that

$$\sum F_x = m\bar{\alpha}_x$$

which yields

$$\underbrace{X\rho\ dx\ dy\ dz}_{\text{Body force}} + \underbrace{\frac{\partial P_x}{\partial x}\ dx\ dy\ dz}_{\text{Normal stress}} + \underbrace{\frac{\partial \tau_{xy}}{\partial y}\ dx\ dy\ dz}_{\text{Shear stress}} + \underbrace{\frac{\partial \tau_{xz}}{\partial z}}_{\text{Stress gradient}} \underbrace{dx\ dy\ dz}_{\text{Differential surface area}} = \underbrace{\rho\ dx\ dy\ dz}_{\text{Mass}}\ \underbrace{\bar{\alpha}_x}_{\text{Acceleration}}$$

Figure 5 illustrates the elemental volume forces acting in the x-direction:

$$Y\rho\ dx\ dy\ dz + \frac{\partial P_y}{\partial y}\ dx\ dy\ dz + \frac{\partial \tau_{xy}}{\partial x}\ dx\ dy\ dz + \frac{\partial \tau_{yz}}{\partial z}\ dx\ dy\ dz = \rho\ dx\ dy\ dz\ \bar{\alpha}_y$$

$$Z\rho\ dx\ dy\ dz + \frac{\partial P_z}{\partial z}\ dx\ dy\ dz + \frac{\partial \tau_{xz}}{\partial x}\ dx\ dy\ dz + \frac{\partial \tau_{yz}}{\partial y}\ dx\ dy\ dz = \rho\ dx\ dy\ dz\ \bar{\alpha}_z$$

or

$$X + \frac{1}{\rho}\left(\frac{\partial P_x}{\partial x} + \frac{\partial \tau_{xy}}{\partial y} + \frac{\partial \tau_{xz}}{\partial z}\right) = \bar{\alpha}_x \tag{4}$$

$$Y + \frac{1}{\rho}\left(\frac{\partial P_y}{\partial y} + \frac{\partial \tau_{xy}}{\partial x} + \frac{\partial \tau_{yz}}{\partial z}\right) = \bar{\alpha}_y \tag{5}$$

$$Z + \frac{1}{\rho}\left(\frac{\partial P_z}{\partial z} + \frac{\partial \tau_{xz}}{\partial x} + \frac{\partial \tau_{yz}}{\partial y}\right) = \bar{\alpha}_z \tag{6}$$

Each of the pressure terms in equations (4) to (6) are normal stresses and can be shown to be a function of an average pressure P and velocity gradients. The result is

$$P_x = -P - \frac{2}{3}\mu\left(\frac{\partial u}{\partial x} + \frac{\partial w}{\partial y} + \frac{\partial v}{\partial z}\right) + 2\mu\frac{\partial u}{\partial x} \tag{7}$$

$$P_y = -P - \frac{2}{3}\mu\left(\frac{\partial u}{\partial x} + \frac{\partial w}{\partial y} + \frac{\partial v}{\partial z}\right) + 2\mu\frac{\partial w}{\partial y} \tag{8}$$

$$P_z = -P - \frac{2}{3}\mu\left(\frac{\partial u}{\partial x} + \frac{\partial w}{\partial y} + \frac{\partial v}{\partial z}\right) + 2\mu\frac{\partial v}{\partial z} \tag{9}$$

Equations (7) to (9) are the constitutive equations for a Newtonian fluid. The pressure P is the thermostatic (isotropic) pressure. If equations (1) to (3) and (7) to (9) are successively differential and substituted into equations (4) to (6), the following equations result:

$$X - \frac{1}{\rho}\frac{\partial P}{\partial x} + \frac{\mu}{3\rho}\frac{\partial}{\partial x}\left(\frac{\partial u}{\partial x} + \frac{\partial w}{\partial y} + \frac{\partial v}{\partial z}\right) + \frac{\mu}{\rho}\nabla^2 u = \frac{Du}{Dt} = \bar{\alpha}_x \tag{10}$$

$$Y - \frac{1}{\rho}\frac{\partial P}{\partial y} + \frac{\mu}{3\rho}\frac{\partial}{\partial y}\left(\frac{\partial u}{\partial x} + \frac{\partial w}{\partial y} + \frac{\partial v}{\partial z}\right) + \frac{\mu}{\rho}\nabla^2 w = \frac{Dw}{Dt} = \bar{\alpha}_y \tag{11}$$

$$Z - \frac{1}{\rho}\frac{\partial P}{\partial z} + \frac{\mu}{3\rho}\frac{\partial}{\partial z}\left(\frac{\partial u}{\partial x} + \frac{\partial w}{\partial y} + \frac{\partial v}{\partial z}\right) + \frac{\mu}{\rho}\nabla^2 v = \frac{Dv}{Dt} = \bar{\alpha}_z \tag{12}$$

where

$$\frac{D}{Dt} = \overbrace{\frac{\partial}{\partial t}}^{\text{Local}} + \overbrace{u\frac{\partial}{\partial x} + v\frac{\partial}{\partial z} + w\frac{\partial}{\partial y}}^{\text{Convective}}$$

is the material or Eulerian derivative. It is composed of the local acceleration (temporal velocity change) and the convective acceleration (spatial velocity change). The convective acceleration is due to the coordinate system, which is fixed relative to fluid motion (laboratory coordinate system). Thus, the Navier-Stokes equations are written

in the Eulerian coordinate system.

Equations (10) to (12) are the Navier-Stokes equations, which are the most general equations of motion for viscous flow. For specific problems they are simplified, which hopefully results in equations that can be solved. In this general form they are much too complex to solve even on the most advanced computers. Solutions to specific problems require satisfaction of the boundary conditions and satisfaction of the continuity equation (conservation of mass). The continuity equation can similarly be derived as the momentum conservation equation and is

$$\frac{\partial \rho}{\partial t} + \frac{\partial(\rho u)}{\partial x} + \frac{\partial(\rho w)}{\partial y} + \frac{\partial(\rho v)}{\partial z} = 0 \tag{13}$$

This is the differential form of the mass balance equation for a control volume.

The continuity equation with the three Navier-Stokes equations yields a well-posed mathematical problem, that is, four equations and four unknowns for liquids (appropriate boundary conditions must be specified).

Now the equations will be further simplified. The resulting form will be mathematically tractable and yet will retain the important physics of sealing flows:

(1) For steady flow,

$$\frac{\partial \rho}{\partial t} = \frac{\partial u}{\partial t} = \frac{\partial w}{\partial t} = \frac{\partial v}{\partial t} = 0$$

(2) Generally, the flows can be described as two dimensional; hence,

$$\frac{\partial}{\partial y} = 0$$

(3) The flow is constrained to flow in one direction only, which can arbitrarily be assigned to be parallel to the x-direction; thus, $v \equiv 0$ with its derivatives (fig. 6). The planes are considered to be infinite in the y-direction, but practically they are of finite width W. Any end-wall effects are thus neglected. The velocity must be zero at the boundaries because of the physical "no slip" of the fluid at the boundary. Since the z-dimensions are much smaller than the x-dimensions, only the velocity derivatives taken with respect to z are appreciable. Therefore,

$$\left(\frac{\partial u}{\partial x}, \frac{\partial u}{\partial y}, \frac{\partial^2 u}{\partial x^2}, \frac{\partial^2 u}{\partial y^2}\right) \cong 0$$

In the general case of converging or diverging channels, v and its derivatives may be of appreciable magnitude. However, the assumption that they are vanishingly small has practical validity in seal performance analysis since converging or diverging angles of actual seal faces are, of necessity, extremely small.

Assume that the fluid is incompressible, which is the case for liquids (not true for gases). That is,

$$\rho = \text{Constant}$$

The resulting simplification of equations (10) to (13) yields

Momentum conservation:

$$X - \frac{1}{\rho}\frac{\partial P}{\partial x} + \frac{\mu}{\rho}\frac{\partial^2 u}{\partial z^2} = 0 \tag{14}$$

$$Z - \frac{1}{\rho}\frac{\partial P}{\partial z} = 0 \tag{15}$$

$$Y = 0 \tag{16}$$

Mass conservation:

$$\frac{\partial u}{\partial x} + \frac{\partial v}{\partial z} = 0 \tag{17}$$

We can assume that the body force Z is due only to the static (gravitational) head so

$$Z = \frac{\partial}{\partial z}(gz) = g \tag{18}$$

Thus,

$$\frac{1}{\rho}\frac{\partial P}{\partial z} = \frac{1}{\rho}\frac{dP}{dz} = g$$

Hence,

$$P = \int_0^h \rho g \, dz = \rho g h + f(x) \tag{19}$$

This indicates that the z-direction pressure variation is strictly hydrostatic, which is consistent with the unidirectional, two-dimensional flow assumption.

Equations (14) to (17) are the classical forms of the incompressible, purely viscous flow equations. A number of revelant cases can be solved from this set. In the section LAMINAR FLOW, details will be given for flow between parallel plates in relative motion because this illustrates the basic concepts. Other important cases will follow without details. Details can be carried out readily as an exercise or by referring to the cited references. In the next section the usual physical quantities of interest will be described.

PHYSICAL QUANTITIES OF INTEREST

Typically, in fluid-film sealing the pressurized fluid conditions and ambient conditions are given (e.g., sealed pressure and temperature). Geometric envelope constraints are almost always known, although it is usually desirable to refine the geometry. The geometric orientation may also be dictated by system considerations (e.g., radial face seal or circumferential seal). Information on seal leakage flow rate, pressure distribution, separating (or opening) force, frictional horsepower requirements, film stiffness, center of pressure, and film temperature rise is usually desired and will be evaluated herein for most common cases. Figure 7 illustrates a pressure-balanced face seal which can be used as a reference.

Leakage Flow Rate

The desired information may be the volumetric flow rate Q for incompressible fluids, where

$$Q = \int_A u \, dz \, dx$$

or mass flow rate

$$\dot{M} = \rho Q = \rho u_{av} A$$

This is the measure of seal leakage.

Pressure Distribution

Pressure distribution is especially necessary for pressure-balanced seals. It is usually found from an analytical expression which is a function of the flow rate.

Opening Force

Since there is a pressure drop when a fluid flows, the integrated effect yields a net force. This force is called the separating force (also called opening force). This force can be found by integrating the pressure over the total surface that the pressure acts on. In seal work, it is generally desirable to know only the increment of lifting force due to the pressure differential rather than the absolute pressure force. Hence, the pressure force due to ambient (reference) conditions must be subtracted. Thus,

$$F_{net} = \int_A P \, dA - P_a A$$

Frictional Horsepower Requirements

Power requirements are also important. Seal friction can be generalized to the extent that the surfaces in contact may be either "dry" or "wet." In either case the frictional horsepower requirements are found from

$$HP = \frac{2\pi NT}{396\,000}$$

In dry friction, where F is the net seal-face force acting between the two rubbing surfaces at some effective hydraulic diameter D, the tangential force opposing rotation is the product of F and the coefficient of Coulomb friction η. For wet friction, where a viscous film separates the surfaces, the horsepower requirement is predicated on the rate of energy dissipation in viscous shear. The common assumption of Newtonian fluid applies, such that

$$\tau = \mu \frac{\partial u}{\partial z}$$

Thus, the torque is

$$\int_A \tau x \, dA$$

Film Stiffness

The film stiffness is important for maintaining positive surface separation when the seal is operating under severe conditions, such as high sealed-fluid pressure differentials and/or speeds. The axial film stiffness is defined as

$$K = - \frac{dF_{net}}{dz}$$

Center of Pressure

The center of pressure is important in determining the net twisting moment that the fluid film exerts on the seal nosepiece. The material of the rotor must accommodate the residual stress due to this moment or deflect in a satisfactory way. The net twisting moment can be found from

$$X_c = \frac{\int (P - P_a) x \, dx}{\frac{F}{W}}$$

Film Temperature Rise

The film temperature rise due to viscous shearing is also important. It is desirable to know this value to assure that the seal can tolerate this temperature rise. A very rough estimate of the film temperature rise due to viscous shearing can be made by equating the heat generated by viscous shearing with the heat transferred by convection. Thus,

$$T_{film, av} - T_{seal\ surface} = \frac{\tilde{Q}_g}{c_p \dot{M}}$$

This calculated film temperature rise will be higher than the actual film temperature

rise. The predominant mode of heat transfer is usually conduction by the seal surfaces, not convection.

Seal fluid flow can be analyzed by using either an exact or an approximate analysis. Seal flows which are purely viscous laminar flows are amenable to a differential analysis. This type of analysis yields finely detailed behavior of the fluid flow. Unfortunately, there are situations where the differential analysis yields equations which are impossible or impractical to solve for design analysis purposes. Such cases include turbulent flow, where exact physical knowledge is unknown, and choked flow, where nonlinear behavior characterizes the flow. In these cases, approximate methods, such as integrated average methods, must be used. Although the integral models satisfy only mean conditions in the flow field, they yield good results on gross quantities, such as seal leakage and pressure distribution.

SEAL PRESSURE-BALANCING FUNDAMENTALS

One of the primary objectives in fluid-film, face-seal design is to ensure that the face loading is sufficiently low so that high heat generation and high wear are prevented. However, contact or close clearance must be maintained at all operating conditions. Seal balance can be achieved, at least theoretically, by properly adjusting the secondary seal diameter (fig. 8). A common term used by seal designers is the geometric balance ratio (or modulus). This modulus is defined as the ratio of the hydrostatic closing area A_{HS} to primary seal-face (dam) area A_{SD} and is used to determine the location of the secondary seal diameter. It is desirable to predict this location analytically.

Unfortunately, a fluid-film seal may be "balanced" only at one combination of operating conditions. Balancing is strongly dependent on the variation in film thickness and the pressure profile load factor. For gases the pressure profile factor varies with the sealed-gas pressure differential. The pressure profile factor is defined as the ratio of the net or average seal-face pressure to the sealed-fluid pressure differential. Hereinafter, the pressure profile load factor will be referred to as the load factor. Both the load factor and the geometric balance ratio have other names in the literature (refs. 1 and 6 to 9) and are sometimes defined in slightly different ways. Some of these names are listed in table I. Since the load factor can equal the geometric balance ratio at only one set of operating conditions, it is impossible to completely balance an ordinary face seal for all situations. Engineering judgment must be employed to select the proper design.

The importance of the load factor and the geometric balance ratio can be illustrated by considering a face-seal force balance. The basic equation defining seal hydrostatic closing force is (fig. 8).

$$\text{Net hydrostatic closing force} = F_S \pm (F_F + F_I) + A_{HS}\,\Delta P - W\int_0^L P\,dx$$

Design philosophies differ; however, a common pressure-balancing practice for gas film seals is to select the spring force F_S to overcome only the frictional forces F_F and the inertial forces F_I. (The frictional forces are due to the secondary seals (e.g., O-rings and piston rings) and the antirotation lugs (e.g., torque pins) rubbing on the housing.)

A fundamental consideration in designing pressure-balanced seals is the selection of the secondary seal diameter. This diameter determines the hydrostatic closing force, as illustrated in figure 7. By proper positioning of the secondary seal diameter, the closing force can be equal to the seal opening force or, at least theoretically, to any degree of seal-face loading. The secondary seal diameter can be found from the geometric balance ratio, where

$$\text{Geometric balance ratio} = \frac{A_{HS}}{A_{SD}}$$

Another important parameter is the pressure profile load factor $\overline{F}$, which is defined as the pressure (pneumatic) opening force normalized to the sealed-pressure differential force acting over the entire seal-face (sealing dam) area or

$$\overline{F} = \frac{\text{Pressure opening force}}{\Delta P\, A_{SD}}$$

Across a seal face,

$$\text{Opening force} = W\int_0^L P\,dx$$

If the seal opening force is equated to the hydrostatic closing force

$$W\int_0^L P\,dx = \Delta P\, A_{HS}$$

Substituting this condition into the load factor relation results in

$$\overline{F} = \frac{A_{HS}}{A_{SD}} = \text{Geometric balance ratio}$$

When this situation exists, that is, when the load factor is equal to the geometric balance ratio, the seal is said to be perfectly balanced.

Once the load factor is known, the seal balance diameter can be simply calculated.

$$\text{Seal balance diameter} = \overline{F}(2R_2 - 2R_1) + 2R_1$$

(For a perfectly balanced seal, the seal balance diameter equals the secondary seal diameter.) For some cases the seal opening force can be evaluated analytically, and hence the load factor can be predicted analytically.

LAMINAR FLOW

Flow Between Parallel Plates in Relative Motion

The case of parallel flow (fig. 6) of an incompressible viscous fluid is probably the simplest exact solution of the Navier-Stokes equations of motion. However, it is a reasonable approximation to many sealing flows. Since the flow is incompressible and assumed to be isothermal, ρ and μ will be constant; also the body force is neglected. Since the flow is only in the x-direction, solutions are sought where $v = w = 0$. Sidewall effects or side leakage effects are neglected. From the continuity equation we find $\partial u/\partial x = 0$, so $u = u(z)$. Thus, the governing equation for this flow is

$$\frac{dP}{dx} = \mu \frac{d^2u}{dz^2} \tag{20}$$

Physically, this means that the pressure drop is proportional to the viscous friction, as expected. This equation is integrated twice with respect to z, yielding

$$u = \frac{1}{\mu}\left(\frac{\partial P}{\partial x}\frac{z^2}{2} + C_1 z + C_2\right) \tag{21}$$

Now apply the boundary conditions (which are the "no slip" boundary conditions since the fluid wets the solid wall)

$$u = U_1 \qquad \text{at} \quad z = 0$$

$$u = U_2 \qquad \text{at} \quad z = h$$

Successive substitution into equation (21) yields two simultaneous equations for the constants of integration C_1 and C_2. The result is

$$C_1 = \frac{\mu}{h}(U_2 - U_1) - \frac{h}{2}\frac{dP}{dx}$$

$$C_2 = \mu U_1$$

These constants are substituted into equation (21), giving

$$u = \frac{1}{2\mu}\frac{dP}{dx}(z^2 - hz) + \frac{(U_2 - U_1)}{h}z + U_1 \tag{22}$$

It is useful to examine the situation when $U_1 = 0$. Thus, letting $U_2 = U$,

$$u = \underbrace{\frac{1}{2\mu}\frac{dP}{dx}(z^2 - hz)}_{\text{Pressure flow component}} + \underbrace{\frac{Uz}{h}}_{\text{Shear flow component}} \tag{23}$$

This is known as the general Couette flow velocity distribution equation. For the case $U = 0$, that is, when both surfaces are at rest, equation (23) gives a parabolic velocity profile such as that shown in figure 9. This is known as plane Poiseuille flow. The general behavior of the velocity profile is shown in figure 10. For $\partial P/\partial x = 0$ and $U \neq 0$, the velocity profile is linear and is known as simple Couette flow. In general, the velocity profile is made up of both the pressure flow component and the shear flow component. Also depending on the value of dP/dx, the profile may be convex or concave, or it may even reverse itself. The point at which the flow will occur in a direction opposite to U can be calculated by letting $du/dx = 0$ at the stationary surface. The result is that, for $dP/dx > 2U\mu/h^2$, the flow will reverse itself over certain values of z. (This type of velocity profile characterizes flow in a viscoseal.) For incompressible flow the velocity profile does not vary with axial flow distance. Also since the governing equations are linear, the pressure flow and shear flow components can be analyzed separately and then superimposed.

Leakage flow rate. - The continuity equation in differential form can be replaced by the condition that the volume of flow in every flow cross section must be constant.

$$Q = Wh \int_0^h \frac{u}{h}\, dz = \text{Constant} \tag{24}$$

Physically, this means the flow cross-sectional area is multiplied by the average velocity. Hence, for this parallel-flow case

$$Q = W \int_0^h u\, dz = W \int_0^h \left[\frac{1}{2\mu}\frac{\partial P}{\partial x}(z^2 - hz) + (U_2 - U_1)\frac{z}{h} + U_1\right] dz \tag{25}$$

After integration and substitution of limits the volumetric flow rate becomes

$$Q = -\frac{Wh^3}{12\mu}\frac{dP}{dx} + \frac{Wh}{2}(U_2 + U_1) \tag{26}$$

Note the strong cubic dependence of the leakage flow rate on the gap h. If the gap were doubled, the leakage would increase eight times for laminar flow. Although there is lesser dependence on gap for turbulent flow and in labyrinth seals, tight control of the flow cross-sectional area is essential. The clearance between the seal and shaft that forms the flow path should be as small as possible. However, the minimum clearance possible is limited by shaft deflections, variations in the film thicknesses, fabrication and assembly tolerances, unequal expansions, and so forth. Because of variations present in any seal, the gap in equation (26) can be the "mean effective separation" between the sealing surfaces.

Pressure distribution. - The pressure distribution is still unknown but now can be found. Rearranging terms and integrating with respect to x yields

$$P - P_1 = -\frac{12\mu Q}{Wh^3}\int_0^x dx + \frac{6\mu}{Wh^2}(U_2 + U_1)\int_0^x dx$$

$$= -\frac{12\mu Qx}{Wh^3} + \frac{6\mu}{Wh^2}(U_2 + U_1) \tag{27}$$

Therefore, at any point x in the sealing passage

$$P = P_1 + \frac{6\mu x}{h^2 W}\left(-\frac{2Q}{h} + U_2 + U_1\right) \tag{28}$$

at the end of the passage ($x = L$, $P = P_2$). Hence, the volume flow rate can now be found in terms of the usual known physical quantities in fluid-film sealing. Thus,

$$Q = \frac{Wh^3}{12\mu L}(P_1 - P_2) + \frac{h}{2}(U_2 + U_1)W \tag{29}$$

Comparing equation (29) with (26) shows that the constant pressure distribution is merely

$$\frac{dP}{dx} = \frac{P_2 - P_1}{L} \tag{30}$$

for plane Poiseuille flow. Now the static pressure at any point in the flow is found by substituting equation (29) into (28). The result is

$$P = P_1 - \frac{x}{L}(P_1 - P_2) \tag{31}$$

There is no pressure distribution associated with shear flow. Also the pressure is independent of the gap and the fluid properties.

Opening force. - The seal opening force is found by integrating the pressure over the surface area on which it acts:

$$F = \int_A P\, dA = W \int_0^L \left[P_1 - \frac{x}{L}(P_1 - P_2)\right] dx \tag{32}$$

$$F = P_1 LW - \frac{LW}{2}(P_1 - P_2) \tag{33}$$

This expression defines the force represented by area abcd on the P-x diagram shown in figure 11. In seal work it is generally of interest to know the increment of lifting force due to the pressure differential rather than the absolute pressure force. This force is represented by area dec on the P-x diagram and is equal to

$$F_{net} = F - P_2 LW \tag{34}$$

or

$$F_{net} = \frac{LW}{2}(P_1 - P_2) \tag{35}$$

This expression indicates that the effective pressure tending to separate the flow boundaries is one-half of the full pressure differential (linear pressure drop).

Frictional horsepower requirements. - To determine the power dissipation or frictional horsepower requirement, recall that the assumption of a Newtonian fluid again implies

$$\tau = \mu \frac{\partial u}{\partial z} \tag{36}$$

We will consider two cases. The first case is for a ring sliding on a rod or in the bore of a cylinder. The velocity gradient term in equation (36) is found by taking the partial derivative of equation (23) with respect to z:

$$\left.\frac{\partial u}{\partial z}\right|_{z=h} = \frac{h}{2\mu}\frac{dP}{dx} + \frac{U_2}{h} \tag{37}$$

For convenience of manipulation, U_1 is taken as zero. The viscous drag force resisting the sliding motion between the two boundary surfaces is equal to the product of the shear intensity and the area over which this acts. Frictional horsepower is in turn the product of this drag force and the relative sliding velocity (for a ring or bore configuration, $W = \pi D$). Hence,

$$HP = \frac{\pi D U_2}{6600}\int_0^L \tau \, dx \tag{38}$$

Combining equations (30), (36), and (37) and substituting in equation (38) yield, after integration,

$$HP = \frac{\pi D U_2}{6600}\int_0^L \left(\frac{h}{2}\frac{\Delta P}{L} + U_2\right)dx \tag{39}$$

$$HP = \frac{\pi \mu D L U_2^2}{6600h} - \frac{\pi D h U_2}{13\,200}(P_1 - P_2) \tag{40}$$

Another important case is a clearance-type ring seal where the boundaries are ro-

tating with a relative angular velocity Ω in the y-direction ($U_1 = U_2 = 0$). Only the velocity gradient in the y-direction applies. Here we may assume a linear velocity gradient in that the fluid at each boundary has zero velocity relative to that boundary (no slip). This is a simple Couette (shear) flow profile.

$$w = \frac{D}{2} \Omega \frac{y}{h} \tag{41}$$

$$\tau = \mu \frac{\partial w}{\partial y} = \frac{\mu D}{2h} \Omega \tag{42}$$

For this case the frictional horsepower becomes, after evaluation,

$$HP = \frac{\pi \mu D^3 L \Omega^2}{26\ 400\ h} \tag{43}$$

Center of pressure. - The center of pressure in the flow passage direction can be found from

$$X_c = \int_0^L \frac{P - P_2}{\frac{F}{W}} x\, dx \tag{44}$$

$$X_c = \frac{2}{L(P_1 - P_2)} \int_0^L \left[P_1 - \frac{x}{L} (P_1 - P_2) - P_2 \right] x\, dx \tag{45}$$

$$X_c = \frac{L}{3} \tag{46}$$

By examining the triangular pressure gradient in figure 11, this result is expected. This is the value of the centroid for a triangle.

Axial film stiffness. - The axial film stiffness is found from

$$K = - \frac{dF}{dz} \tag{47}$$

$$K \equiv 0 \qquad \text{for a parallel surface} \tag{48}$$

Since the seal opening force does not depend on film thickness for parallel films, there is no axial film stiffness. Some auxiliary device, such as self-acting lift pads or a radial step, must be used to obtain axial film stiffness.

The procedures for converging and diverging surfaces and for radial and cylindrical flow are identical to the procedure for the parallel-surfaces case presented. However, the mathematics is more complex because of the geometry variation.

Flow Between Flat Converging or Diverging Plates

The governing momentum equation

$$\frac{\partial P}{\partial x} = \mu \frac{\partial^2 u}{\partial z^2} \tag{49}$$

and velocity distribution

$$u = \frac{1}{2\mu} \frac{\partial P}{\partial x} (z^2 - hz) + \frac{Uz}{h} \tag{50}$$

are the same as for parallel surfaces. The film thickness variation for converging or diverging surfaces can be expressed as (fig. 12)

$$h = h_1 + \alpha x$$

Leakage flow rate. - The leakage flow rate can be found from

$$Q = -\frac{h_1^3 W}{12\mu} \frac{\partial P}{\partial x}(1 + \alpha x)^3 + \frac{W h_1}{2} U_2 (1 + \alpha x) \tag{51}$$

Rearranging terms and integrating with respect to x yields

$$P = P_1 - \frac{6\mu L}{h_1(h_2 - h_1)} \left[\frac{Q}{h_1 h^2} \left(h^2 - h_1^2 \right) - \frac{(h - h_1)(U_2 + U_1)}{h} \right] \tag{52}$$

Thus, the volumetric leakage flow rate per unit length is

$$\frac{Q}{W} = \frac{(P_1 - P_2)}{6\mu L} \frac{h_1^3 \beta^2}{(\beta + 1)} + \frac{h_1 \beta}{(\beta + 1)} (U_2 + U_1) \tag{53}$$

where

$$\beta = \frac{h_2}{h_1}$$

When $\beta = 1$, we have parallel plates

$$Q = \frac{h_1^3 W}{12\mu L} (P_1 - P_2) + \frac{h_1 (U_2 + U_1) W}{2} \tag{54}$$

Note that

$\beta < 1$ for converging plates

$\beta > 1$ for diverging plates

Generally, tapers in seals are small, but in some applications it is desirable to machine a converging taper in order to achieve a positive film stiffness. Also it can readily be shown that

$$\frac{h_1^3 \beta^2}{\beta + 1} = \frac{h_1^2 h_2^2}{2h_m} \tag{55}$$

By defining a characteristic film thickness

$$h_{char} = \left(\frac{h_1^2 h_2^2}{h_m} \right)^{1/3} \tag{56}$$

Thus, the leakage flow rate can be expressed as

$$Q = \frac{h_{char}^3 W (P_1 - P_2)}{12\mu L} + \frac{W h_1 \beta (U_2 + U_1)}{(\beta + 1)} \tag{57}$$

When there are no tilts present, $h_1 = h_2$ (hence, $\alpha = 0$). Then $h_{char} = h$ and the classical parallel-surface mass leakage equation is evolved. However, if an effective or linear apparent tilt is desired, the effect on mass leakage can be easily calculated from the parallel-surface leakage equation. A simple computation enables leakage with deformation to be readily calculated or read from a parallel-surface leakage plot.

Pressure distribution. - For the case where the relative surface velocity in the flow direction is zero, the pressure distribution across the sealing dam is

$$P = P_1 - (P_1 - P_2)\frac{x}{L}\mathscr{T} \tag{58}$$

where the linear tilt factor $\mathscr{T}$ is defined as

$$\mathscr{T} = \frac{h_2^2(2h_1 + \alpha x)}{2h_m(h_1 + \alpha x)^2} \tag{59}$$

For parallel surfaces, $\alpha = 0$; hence, $h_m = h_1 = h_2$ and the tilt factor $\mathscr{T}$ is 1, which yields the parallel-surface pressure distribution. Representative pressure profiles for parallel, converging and diverging surfaces are shown in figure 13.

Opening force. - Upon integration of the pressure distribution, the net opening force can be found and is

$$F_{net} = \underbrace{\frac{LW}{1 + \beta}(P_1 - P_2)}_{\substack{\text{Hydrostatic} \\ \text{force}}} + \underbrace{\frac{6\mu L^2 W}{(\beta - 1)^2 h_1^2}(U_2 + U_1)\left[\frac{2(\beta - 1)}{\beta + 1} - \ln\beta\right]}_{\text{Hydrodynamic force}} \tag{60}$$

When there is no relative motion of the surfaces in the leakage flow direction, the net surface opening force is

$$F_{net} = \frac{WL\,\Delta P}{1 + \beta}$$

The load factor is

$$\overline{F} = \frac{F_{net}}{A_{SD}\,\Delta P} = \frac{1}{1 + \beta}$$

For parallel surfaces, $\beta = 1$ and

$$\overline{F} = 0.50$$

For converging faces, $\beta < 1$; and, for example, if $\beta = 1/2$,

$$\overline{F} = 0.67$$

For diverging faces, $\beta > 1$; and, for example, if $\beta = 2$,

$$\overline{F} = 0.33$$

The practical range of load factors appears to vary from 0.6 to 0.9 for liquid face seals currently in use.

For $\beta = 1$, the parallel-surface case, equation (60) reduces to

$$F_{net} = \frac{LW}{2}(P_1 - P_2) \tag{35}$$

The second term is the load-carrying capacity of a slider bearing which is infinite in y-direction.

When $P_1 = P_2$, the force induced in the classical hydrodynamic slider bearing U_1 is equal to zero. This pressure distribution is shown in figure 14. The dimensionless hydrodynamic force is defined as

$$\overline{F} = \frac{F_{net}}{P_a WL} = \frac{6\mu UL}{P_a h_1^2} = \Lambda$$

where Λ is the bearing number. The bearing number is similar to the load factor except that the ambient pressure is the reference pressure. Hydrodynamic pressure generation is discussed in the section MECHANISM OF FILM PRESSURE GENERATION BETWEEN RELATIVELY MOVING SURFACES.

Frictional horsepower requirement. - First, we consider friction on a moving surface, for example, a ring sliding on a rod or in the bore of a cylinder. From

$$\tau = \frac{h}{2}\frac{\partial P}{\partial x} + \mu\frac{U_2}{h}$$

we get

$$HP = \frac{\pi \mu DLU_2^2}{3300(\beta - 1)h_1}\left(2 \ln \beta - 3\frac{\beta - 1}{\beta + 1}\right) - \frac{\pi \alpha Dh_1 U_2 (P_1 - P_2)}{6600(\beta + 1)} \tag{61}$$

Second, for clearance-type seal rings, boundaries are rotating with relative angular velocity Ω, and $U_1 = U_2 = 0$. Only the velocity gradient in the y-direction applies; that is,

$$w = \frac{D}{2}\Omega_1 \frac{y}{h}$$

The result is

$$HP = \frac{\pi \mu D^3 L \Omega^2}{26\,400h_1} \frac{\ln \beta}{\beta - 1} \tag{62}$$

Radial Flow Between Annular Disks

The governing equation for the radial flow between annular disks, representative of mechanical face seals (fig. 15), is

$$-\rho r \Omega^2 = -\frac{\partial P}{\partial r} + \mu \frac{\partial^2 u}{\partial z^2} \tag{63}$$

The radial geometry yields a centripetal inertial force (centrifugal force) because of the curvature on the left side of equation (63). This equation yields the following velocity profile:

$$u = -\frac{\rho \Omega^2 r}{12 \mu h^2}(z^4 - h^3 z) + \frac{1}{2\mu}\frac{\partial P}{\partial r}(z^2 - hz) \tag{64}$$

Leakage flow rate. - Use the continuity equation for volumetric flow in any radial direction r

$$Q = W \int_0^h u \, dz = \frac{\rho \Omega^2 W r h^3}{40 \mu} - \frac{W h^3}{12 \mu}\frac{\partial P}{\partial r} \tag{65}$$

Let

$$W = 2\pi r$$

Integrating with respect to r between R_1 and r yields

$$P = P_1 + \frac{3\rho\Omega^2}{20}\left(r^2 - R_1^2\right) - \frac{6\mu Q}{\pi h^3}\ln\frac{r}{R_1} \tag{66}$$

At $r = R_2$, $P = P_2$; hence, the flow rate can be found from

$$Q = \frac{\pi h^3}{6\mu \ln\dfrac{R_2}{R_1}}\left[\frac{3\rho\Omega^2}{20}\left(R_2^2 - R_1^2\right) + (P_1 - P_2)\right] \tag{67}$$

$$Q = 0$$

when

$$R_2^2 - R_1^2 = \frac{20}{3\rho\Omega^2}(P_2 - P_1) \tag{68}$$

When $\Delta P \geq 0$, leakage increases due to centripetal force; when $\Delta P < 0$, leakage decreases due to centripetal force.

Frictional horsepower requirements. - The frictional horsepower can be found by using

$$\tau = \mu\frac{\partial w}{\partial z} = \frac{\mu r\Omega}{h}$$

Thus,

$$HP = \frac{2\pi\mu\Omega^2}{6600h}\int_{R_1}^{R_2} r^3\, dr \tag{69}$$

or

$$HP = \frac{\pi \mu \Omega^2}{13\ 200h}\left(R_2^4 - R_1^4\right) \tag{70}$$

Opening force. - The opening force can be found by integrating the pressure distribution equation

$$P = P_0 + \frac{3\rho\Omega^2\left(r^2 - R_1^2\right)}{20} - C \ln \frac{r}{R_1} \tag{71}$$

where

$$C = \frac{1}{\ln \dfrac{R_2}{R_1}}\left[\frac{3\rho\Omega^2}{20}\left(R_2^2 - R_1^2\right) + (P_1 - P_2)\right] \tag{72}$$

$$F_{net} = \pi\left\{(P_1 - P_2)\left[\frac{R_2^2 - R_1^2}{2 \ln \dfrac{R_2}{R_1}} - R_1^2\right] + \frac{3\rho\Omega^2\left(R_2^2 - R_1^2\right)}{40 \ln \dfrac{R_2}{R_1}}\left[\left(R_2^2 - R_1^2\right) - \left(R_2^2 + R_1^2\right)\ln \frac{R_2}{R_1}\right]\right\} \tag{73}$$

For $P_1 > P_2$, F_{net} is larger than for inward flow (when $P_1 < P_2$). For the hydrostatic case and $R_2/R_1 < 1.1$, it can be shown that the static pressure is linear and

$$F_{net} \cong \frac{\pi}{3}(P_1 - P_2)\left(R_2^2 + R_1R_2 - 2R_1^2\right) \tag{74}$$

Pressure distribution. - The pressure distribution due to the centrifugal force can be examined in more detail by solving for pressure distribution when the inner and outer diameters do not have an imposed pressure differential ($P_1 = P_2$). For this case, equation (71) becomes

$$P = P_1 + \frac{3}{20}\rho\Omega^2\left[\left(r^2 - R_1^2\right) - \left(R_2^2 - R_1^2\right)\frac{\ln \dfrac{r}{R_1}}{\ln \dfrac{R_2}{R_1}}\right] \tag{75}$$

For most face seals, R_2/R_1 is close to 1. Hence,

$$\ln \frac{R_2}{R_1} \cong - \frac{R_2 - R_1}{R_1}$$

$$\ln \frac{r}{R_1} \cong -\left(\frac{r - R_1}{R_1}\right)$$

(This is known as the face-seal approximation.)

$$P = P_1 - \frac{3}{20} \rho \Omega^2 (r - R_1)(R_2 - r) \tag{76}$$

Equation (76) indicates that the centrifugal force term is <u>always negative</u> and independent of the nature of pressurization. For both internal and external pressurization the centrifugal effect diminishes the pressures on the seal face, reducing the separation forces and resulting in a decreased seal clearance.

Axial Flow Between Annular Cylinders

<u>Concentric cylinders</u>. - The governing equation for the axial flow between concentric annular cylinders, representative of bushing and circumferential seals (fig. 16(a)), is

$$\frac{dP}{dz} = \mu\left(\frac{d^2u}{dr^2} + \frac{1}{r}\frac{du}{dr}\right) \tag{77}$$

Note the additional friction term due to curvature. The velocity distribution can be found from

$$u = \frac{P_1}{4\mu L}\left(R_1^2 - r^2 + \frac{R_2^2 - R_1^2}{\ln \frac{R_2}{R_1}} \ln \frac{r}{R_1}\right) \tag{78}$$

Upon integrating u between R_1 and R_2, the flow becomes

$$Q = \frac{\pi P_1}{8\mu L}\left(R_2^2 - R_1^2\right)\left(R_2^2 - R_1^2 - \frac{R_2^2 - R_1^2}{\ln \frac{R_2}{R_1}}\right) \tag{79}$$

For the special case of a circular cylinder ($R_1 = 0$), the velocity distribution is found from

$$u = \frac{1}{4\mu}\frac{dP}{dz}\left(R_2^2 - r^2\right) \tag{80}$$

The maximum velocity is

$$u_{max} = \frac{1}{4\mu}\frac{dP}{dz}R_2^2 \tag{81}$$

Since the velocity profile is parabolic,

$$u_{av} = \frac{u_{max}}{2} = \frac{1}{8\mu}\frac{dP}{dz}R_2^2 \tag{82}$$

Hence,

$$Q = u_{av}\pi R_2^2 = \frac{\pi R_2^4 P_1}{8\mu L} \tag{83}$$

Eccentric cylinders. - Eccentric cylinders simulate the case of two nonparallel developed surfaces. Let $h = h_m(1 + \epsilon \cos \theta)$. Thus,

$$u = -\frac{P_1}{2\mu L}y[y - h_m(1 + \epsilon \cos \theta)] = f(y, \theta) \tag{84}$$

Now

$$Q = -\int_0^{2\pi}\int_0^h \frac{P_1}{2\mu L}y[y - h_m(1 + \epsilon \cos \theta)]dy\, R\, d\theta \tag{85}$$

$$Q = \frac{\pi P_1 R h_m^3}{6 \mu L} \left(1 + \frac{3}{2} \epsilon^2\right) \tag{86}$$

The eccentricity can be due to loading, fabrication, and/or assembly tolerances. The actual eccentricity of the shaft and bushing is very seldom known; therefore, only the two limits, maximum and minimum flow, are usually computed. For $\epsilon = 0$, equation (86) reduces to equation (79). Comparing these two equations shows that the flow rate will be $2\frac{1}{2}$ times that for a concentric cylinder when the cylinders are fully eccentric ($\epsilon = 1$). An exact analytical treatment is complex. Details and a partial solution can be found in reference 10.

The higher leakage for the eccentric cylinders can be thought of as being due to a larger effective gap and, hence, a larger shear surface area.

TURBULENT FLOW

For turbulent flow, exact physical knowledge is unknown. Hence, an exact differential analysis model such as the one that describes laminar flow is impossible to solve or impractical for design analysis purposes. Thus, approximate solutions must be found. A widely used method in fluid mechanics and hydraulics is the approximate integrated average method. Although the integral models only satisfy mean conditions in the flow field, they have shown good results on gross quantities such as seal leakage and pressure distribution. However, it will be seen that an empiricism is required to find a solution.

The viscous friction is balanced by the pressure drop. This is the classical fluid-flow case. This model is widely used to describe pipe and duct flows.

Consider the control volume shown in figure 17 for situations when the fluid inertia is negligible. The momentum conservation is a balance between the pressure and the viscous friction force, which is

$$A\, dP = -\tau_w\, dA_w \tag{87}$$

Introducing the parameters hydraulic diameter D

$$D = \frac{4A}{\frac{dA_w}{dx}}$$

and mean Fanning friction factor $\bar{f}$

$$\bar{f} = \frac{\tau_w}{\frac{\rho u^2}{2}}$$

into equation (87) results in

$$D\frac{dP}{dx} = -2\rho u^2 \bar{f} \tag{88}$$

Substituting the mass flow definition

$$\dot{M} = \rho u A \tag{89}$$

yields the following useful form:

$$dP = \frac{-2\dot{M}^2 \bar{f}\, dx}{\rho D A^2} \tag{90}$$

The pressure at a position x along the leakage length can be found by integrating from the inlet to any position x

$$\int_{P_1}^{P} dP = -\int_0^x \frac{2\dot{M}^2 \bar{f}}{\rho D A^2}\, dx \tag{91}$$

or

$$P = P_1 - \frac{2\dot{M}^2 \bar{f} x}{\rho D A^2} \tag{92}$$

At the seal exit, $x = L$ and $P = P_2$; hence, the mass flow rate can be found from

$$\dot{M} = \sqrt{\frac{\rho D A^2 (P_1 - P_2)}{2\bar{f}L}} \tag{93}$$

Substituting equation (93) into equation (92) results in

$$P = P_1 - (P_1 - P_2)\frac{x}{L} \tag{94}$$

Hence, for either laminar or turbulent flow, the pressure distribution is independent of the fluid properties and the film thickness. For radial flow between coaxial parallel disks and parallel plates, the hydraulic diameter D is given by

$$D = 2h \tag{95}$$

Generally, the mean friction factor is related to Reynolds number by a expression of the following form:

$$\bar{f} = \frac{k}{(Re)^n} \tag{96}$$

It is useful to express the Reynolds number as

$$Re = \frac{2\dot{M}}{W\mu} \tag{97}$$

For laminar flow the friction factor is derived from the classical, viscous flow solution (eq. (23)) and the derivation is also shown in reference 11. The resulting mean friction factor - Reynolds number relation is

$$\bar{f} = \frac{24}{Re} = \frac{12\mu W}{\dot{M}} \tag{98}$$

Thus,

$$\dot{M} = \frac{\rho h^3 W(P_1 - P_2)}{12\mu L} \tag{99}$$

This is the identical result obtained in equation (57) by setting $U_1 = U_2 = 0$ and $M = \rho Q$.

Turbulent Flow Between Parallel Plates

The Blasius relation of friction factor and Reynolds number appears to satisfactorily describe a large class of fully developed flows even though it is experimentally deter-

mined. Thus, in equation (96), k = 0.079 and n = 0.25. Substitution in equation (93) yields

$$\dot{M} = \frac{2^{1/7}\rho^{4/7}h^{12/7}W(P_1 - P_2)^{4/7}}{(0.079)^{4/7}L^{4/7}\mu^{1/7}} \tag{100}$$

which gives the functional relation of the variables in quasi-fully-developed turbulent flow. The leakage dependence on film thickness is no longer cubic, but it is less than quadratic. However, the leakage is still most sensitive to gap. The functional variation of leakage is compared for laminar and turbulent flow in table II.

Turbulent Flow with Small Linear Deformation (and Constant Width)

Again, as in laminar flow, the surface deformation is represented by

$$h = h_1 + \alpha x \tag{101}$$

The mass leakage flow rate is identical to the parallel surface equation (eq. (100)), except that the characteristic film thickness is used:

$$\dot{M} = \frac{2^{1/7}\rho^{4/7}h_{char}^{12/7}W(P_1 - P_2)^{4/7}}{(0.079)^{4/7}L^{4/7}\mu^{1/7}} \tag{102}$$

The pressure distribution is also identical to that found for laminar flow (eq. (94)).

The dependence on flow-width is the same as for laminar flow; but there is lesser dependence (4/7) on density, flow length, and pressure differential. Also notice the weak dependence on molecular viscosity - a characteristic of turbulent flow. However, turbulent flow is characterized by large-scale momentum exchange (eddies). This macroscopic fluid behavior can be represented as apparent shear stresses. Hence, a turbulent viscosity can be orders of magnitude higher than the molecular viscosity. Thus, turbulent flow leakage is characterized by a high effective viscosity, which means lower leakage than predicted by laminar-flow models but also higher shear heating.

Turbulent Radial Flow

Equation (90) can be integrated for radial annular flow without relative seal-face

rotation by using the same restrictions as previously stated. The following result is obtained for mass flow (here $W = 2\pi r$ and $x = r$):

$$\dot{M} = \frac{2\pi\rho^{4/7}h^{12/7}(P_1 - P_2)^{4/7}}{(0.079)^{4/7}\mu^{1/7}\left(\frac{1}{R_1^{3/4}} - \frac{1}{R_2^{3/4}}\right)^{4/7}} \tag{103}$$

The pressure distribution can be found from

$$P = P_1 - \frac{(P_1 - P_2)\left(\frac{1}{R_1^{3/4}} - \frac{1}{r^{3/4}}\right)}{\frac{1}{R_1^{3/4}} - \frac{1}{R_2^{3/4}}} \tag{104}$$

The leakage flow rate with rotationally induced turbulence (p. 61) is

$$\dot{M} = \frac{3\pi\rho}{4(0.0195)}\left(\frac{h^9}{\rho^3\mu\Omega^3}\right)^{1/4}\frac{1}{\left(R_2^{3/4} - R_1^{3/4}\right)}\left[P_1 - P_2 + (0.128)\rho\left(R_2^2\Omega^2 - R_1^2\Omega^2\right)\right] \tag{105}$$

Sneck (ref. 12) used an eddy viscosity approach to derive equation (105). Details can be found in that paper.

Turbulent Flow Between Concentric and Eccentric Cylinders

When flow is turbulent, leakage is not affected as much by eccentricity as when flow is laminar. Generally, turbulent flows are less sensitive to gap, as shown in table II. This is probably due to the large momentum exchange that characterizes turbulent flow. Leakage for the fully eccentric shaft is 30 percent higher than for the perfectly concentric shaft. The analytical expression for turbulent flow through an eccentric annular gap is somewhat complicated and approximate and is given in graphical form in figure 18 (ref. 10). Figure 19 compares the effect of eccentricity on laminar and turbulent flow.

APPLICATION OF THEORY TO FACE-SEAL CONCEPTS

An application of the preceding derivations will now be cited. References 13 and 14 numerically solved six face-seal-contour cases on a digital computer, relating film thickness, leakage flow rate, opening force, and exit pressure. These contours represented converging, diverging, and symmetric faces and were compared with parallel faces. The studies of references 13 and 14 were conducted with sea water at 300 K (80° F) as the fluid medium. The seal inside diameter was 22.162 cm (8.725 in.) and the outside diameter was 24.067 cm (9.475 in.). The face contours are shown in figure 20 (from ref. 14).

The relation of minimum film thickness to inlet water pressure is shown in figure 21 for a leakage flow rate of 0.002 m^3/min (0.5 gal/min) and a change in film thickness Δh of 0.00127 cm (0.0005 in.). All nonparallel cases resulted in a decrease in minimum film thickness from the parallel case. (The centrifugal force had a negligible effect on the film thickness.)

Figure 22 shows log-log plots of the minimum film thickness h_{min} against the ratio of leakage flow rate to inlet water pressure, resulting in a single curve for each face contour.

The radial pressure profiles illustrated in figure 23 show the effect of the various contours. A rapid dropoff in pressure occurred near the outer radius with the diverging surfaces; a slow decrease occurred with the converging surfaces.

The resulting plot of seal-face load against inlet water pressure is shown in figure 24 for a constant leakage flow rate and the same inlet and outlet film thickness differences. Only the symmetrical parabolic contour is similar to the parallel case; the others differ by an increasing amount as the pressure increases. The effects of Δh and Q on the seal-face load are shown in figures 25 and 26, respectively, for a constant P_2. Only the symmetrical parabolic face load remains constant as both Δh and Q are varied. All approach the load of the parallel case as Δh approaches zero with constant Q. However, the diverging case approaches zero and the converging case approaches the full load of 1.43×10^5 N (32 150 lbf) as Q approaches zero with constant Δh.

Finally, figure 27 illustrates pressure profiles for a converging gap in the flow direction, for parallel surfaces, and for a diverging gap, including the effect of a pronounced area change.

COMPRESSIBLE FLOW OF GASES

The equations previously derived have been for liquids, which can be considered to be incompressible under most sealing conditions. The constant-density assumption

means that the equations will be simpler to solve and that pressure appears only in a dynamic role not thermodynamically. Hence, the previous solutions were obtained without use of the energy equation. This is not the case for compressible flow. Since density is now a dependent variable, the momentum equation is interrelated to the energy equation. Also another equation is necessary, the equation of state. The physics of the flow are also different and more complex. Principles of gas-film-seal fluid mechanics are discussed in great detail in reference 11. Herein only the salient features will be pointed out.

Generally, for thin films the standard lubrication assumption of isothermal surfaces can be made even for gases. This is so because gas lubricant films are very thin and in contact with relatively large masses of metal. However, at higher flow rates, an adiabatic or polytropic equation of state may be more relevant. This isothermal or polytropic equation of state enables a relation to be found which eliminates consideration of temperature in solving the set of equations. Hence, the energy equation need not be considered. The polytropic equation of state is

$$\frac{P}{\rho^{\gamma}} = \text{Constant}$$

The gas film theory, as well as gas dynamics, is based on the premise that at any point in time and space the flow is in thermodynamic equilibrium and the perfect-gas law applies

$$P = \rho \mathscr{R} T$$

In summary, it is the local change in density in the film that characterizes compressible flow. Because of the isothermal assumption, the density change results primarily from changes in pressure as predicted by the perfect-gas law. Hence, we expect to see differences from incompressible flow in physical quantities of interest. Also the viscosities of gases increase slowly with temperature, as opposed to the rather rapid decreases that liquids exhibit. This is discussed in more detail in appendix B.

Compressible Flow Equations

The set of equations that will be used for compressible fluids (gases) between narrowly spaced annular disks in polar coordinates (fig. 28) is

Continuity:

$$\frac{1}{r}\frac{\partial}{\partial r}(\rho r u) + \frac{\partial}{\partial z}(\rho v) = 0 \tag{106}$$

Radial momentum conservation:

$$\rho u \frac{\partial u}{\partial r} + v \frac{\partial u}{\partial z} - \rho \frac{w^2}{r} = -\frac{\partial P}{\partial r} + \mu \frac{\partial^2 u}{\partial z^2} \tag{107}$$

Circumferential momentum conservation:

$$\frac{\partial^2 w}{\partial z^2} = 0 \tag{108}$$

Axial momentum conservation:

$$\frac{\partial P}{\partial z} \cong 0 \tag{109}$$

Equation of state:

$$P = \rho \mathscr{R} T \tag{110}$$

Energy:

$$\rho c_p u \frac{\partial T}{\partial r} + \rho c_p v \frac{\partial T}{\partial z} = k \frac{\partial^2 T}{\partial z^2} \tag{111}$$

The formulation of the appropriate equations governing gas-film-seal behavior is detailed in reference 11.

Classical Viscous Compressible Flow Model

Parallel radial flow. - The classical hydrostatic radial leakage-flow formula illustrates the effects of compressibility. It is valid for compressible viscous flows and is the widely used gas leakage formula in the seal industry. If rotation effects are neglected and the flow is assumed to be isothermal, the governing equations reduce to the

equations for mass and radial momentum conservation. The radial momentum equation is

$$\frac{dP}{dr} = \mu \frac{\partial^2 u}{\partial z^2} \tag{112}$$

This yields

$$u = \frac{1}{2\mu} \frac{dP}{dr} z^2 + C_1 z + C_2 \tag{113}$$

Upon applying the boundary conditions the result is

$$u = \frac{1}{2\mu} \frac{dP}{dr} (z^2 - hz) \tag{114}$$

The mean velocity at any radial cross section is

$$u_m = \frac{1}{h} \int_0^h u \, dz \tag{115}$$

$$u_m = - \frac{dP}{dr} \frac{h^2}{12\mu} \tag{116}$$

Now, the mass leakage flow rate is

$$\dot{M} = \rho W h u_m$$

$$= \left(- \frac{\rho W h^3}{12\mu} \right) \left(\frac{dP}{dr} \right) \tag{117}$$

If the perfect-gas relation is substituted and equation (117) is rearranged, the radial pressure gradient can be expressed in the following forms:

$$\frac{dP}{dr} = - \frac{12\mu \mathscr{R} T \dot{M}}{P W h^3} \tag{118}$$

$$P\,dP = -\frac{12\mu\mathscr{R}T\dot{M}}{Wh^3}\,dr \tag{119}$$

Since

$$W = 2\pi r$$

$$dP^2 = -\frac{12\mu\mathscr{R}T\dot{M}}{\pi h^3}\frac{dr}{r}$$

or

$$P^2 = -\frac{12\mu\mathscr{R}T\dot{M}}{\pi h^3}\ln r + C \tag{120}$$

Applying the boundary condition at $r = R_1$,

$$P^2 = P_1^2$$

yields

$$P^2 = P_1^2 + \frac{12\mu\mathscr{R}T\dot{M}}{\pi h^3}\ln\frac{R_1}{r} \tag{121}$$

Applying the boundary condition at $r = R_2$,

$$P^2 = P_2^2$$

yields the classical mass leakage flow equation

$$\dot{M} = \frac{\pi h^3\left(P_2^2 - P_1^2\right)}{12\mu\mathscr{R}T\ln\dfrac{R_1}{R_2}} \tag{122}$$

Using equation (122) in equation (121) yields the following pressure distribution equation:

$$P = P_1\left[1 - \left(1 - \frac{P_2^2}{P_1^2}\right)\frac{\ln \frac{R_1}{r}}{\ln \frac{R_1}{R_2}}\right]^{1/2} \tag{123}$$

The classical solution for the pressure distribution is independent of both the fluid properties and the gap. Also, the velocity profile does vary with radius, and hence for compressible fluids the flow is not fully developed but is quasi-fully developed.

Face-seal approximation ($\Delta R/R_1 << 1$). - In many gas film seal faces, ΔR is much less than R_1. For this case,

$$\ln \frac{R_1}{R_2} \cong -\frac{\Delta R}{R_1}$$

By setting $W = 2\pi r$, equation (122) becomes

$$\dot{M} = \frac{Wh^3\left(P_1^2 - P_2^2\right)}{24\mu \mathscr{R} T(R_2 - R_1)} \tag{124}$$

Equation (124) can be written as

$$\dot{M} = \frac{Wh^3(P_1 + P_2)\Delta P}{24\mu \mathscr{R} T(R_2 - R_1)}$$

Since $P_{av} = (P_1 + P_2)/2$,

$$L = R_2 - R_1$$

$$\rho_{av} = \frac{P_{av}}{\mathscr{R} T}$$

and

$$\dot{M} = \frac{Wh^3 \rho_{av} \Delta P}{12 \mu L}$$

The preceding equation is written in incompressible form.

Leakage expressed as standard cubic meters per second: In order to have a meaningful assessment of leakage at a common base (standard conditions) to account for density variation with temperature, it is convenient to express the leakage in the following manner:

$$Q_{scfm} = \frac{\dot{M}}{\rho_{std}} = \frac{\dot{M} \mathscr{R} T_{std}}{P_{std}}$$

Therefore,

$$Q_{scfm} = \frac{Wh^3}{24 \mu L} \left(\frac{P_1^2 - P_2^2}{P_{std}} \right) \frac{T_{std}}{T_1}$$

and equation (123) becomes

$$P = P_1 \left[1 - \left(1 - \frac{P_2^2}{P_1^2} \right) \left(\frac{x}{R_2 - R_1} \right) \right]^{1/2} \tag{125}$$

where

$$x = r - R_1$$

(Mass flow is proportional to $P_1^2 - P_2^2$ for compressible flow but proportional to the pressure drop for incompressible flow. Also compare eq. (125) with its incompressible counterpart, eq. (31).) This is the classical form of the narrow-slot leakage equation; thus, hydrostatic radial flow can be approximated with a narrow-slot (plane flow) analysis with small error if $(R_2 - R_1) << R_1$. This approximation shall be known, hereinafter, as the "face-seal approximation."

Opening force: The net seal opening force is found by integrating equation (125). The result is

$$\frac{F}{W} = \frac{2P_1(R_2 - R_1)\left[1 - \left(\frac{P_2}{P_1}\right)^3\right]}{3\left[1 - \left(\frac{P_2}{P_1}\right)^2\right]} - P_{min}(R_2 - R_1) \tag{126}$$

By algebraic manipulation, it can be shown that the load factor

$$\overline{F} = \frac{F_{net}}{A_{SD}\,\Delta P} = \frac{1}{3}\left(1 + \frac{1}{1 + \frac{P_2}{P_1}}\right)$$

This equation is plotted in figure 29 and illustrates the strong variation of load factor with pressure ratio. Since $\overline{F} = \overline{F}(P_2/P_1)$, $\overline{F}$ can equal the geometric balance ratio only at one operating condition. This illustrates why it is impossible to completely balance a face seal for all sealed-gas pressure situations and that a slight unbalance at large pressure differential will greatly overload the seal.

Since equation (126) also describes the pressure profile for laminar and fully developed turbulent flows, the preceding load factor applies to turbulent flow as well. (The load factor equation is independent of film thickness and fluid properties.)

For pressure ratios close to 1 the gas should behave like an incompressible fluid. This is the case, since the load factor is 0.5. At very large pressure ratios,

$$\overline{F} = \lim_{P_2/P_1 \to 0}\left[\frac{1}{3}\left(1 + \frac{1}{1 + \frac{P_2}{P_1}}\right)\right] = \frac{2}{3}$$

However, this high-pressure-limiting situation is not physically correct. In reality, the governing equations break down, in that fluid inertial forces become important and the phenomenon of fluid choking can occur. This is discussed in the section Physics of compressible flow and concept of choking.

Center of pressure: The center of pressure can also be readily found from equation (126), which yields

$$X_c = \frac{W(R_2 - R_1)^2}{F}\left\{\frac{P_1\left[\frac{2}{5}\left(\frac{P_2}{P_1}\right)^5 - \frac{2}{3}\left(\frac{P_2}{P_1}\right)^3 + \frac{4}{15}\right]}{\left[1 - \left(\frac{P_2}{P_1}\right)^2\right]^2} - \frac{P_{min}}{2}\right\} \tag{127}$$

An alternate formulation of this classical compressible viscous flow case would have been to start with the compressible Reynolds lubrication equation (ref. 15).

Quasi-fully-developed flow. - Incompressible flow in long narrow spaces is characterized by a linear pressure drop and a velocity profile that does not change in the flow direction. This can be seen by examining the continuity equation for this parallel flow:

$$\frac{\partial u}{\partial x} = 0$$

Let us now examine the continuity equation for the same case but for a compressible fluid:

$$\frac{\partial(\rho u)}{\partial x} = 0$$

or

$$\frac{\partial(\rho u)}{\partial x} = \rho \frac{\partial u}{\partial x} + u \frac{\partial \rho}{\partial x} = 0$$

Hence, from the equation of state, $P \propto \rho$; that is, as the pressure drops the density also decreases, and the velocity is no longer constant in the flow direction but increases (fig. 30). Thus, the term "quasi-fully-developed flow" is used in compressible viscous flow.

A gas generally has a large specific volume increase associated with a pressure drop. (Liquids are, of course, incompressible.) Hence, for a given pressure drop across a seal, the less dense the sealed fluid, the lower the resultant mass flow rate. (Perhaps this is one of the reasons that a labyrinth seal is effective in sealing a gaseous fluid but would be ineffective for the same fluid in the liquid state.) This lower mass flow rate can be seen by comparing the leakage rates for the same gas and through the same geometry but obtained at two different temperatures (fig. 31, from ref. 16).

Pressure Distribution - Application Example

Figure 32 shows, for parallel sealing faces, the normalized pressure as a function of radial position within the sealing gap. The normalized pressure distributions for three operating design points representative of aircraft climb, cruise, and idle are shown for both compressible and incompressible fluids. Since the faces are parallel, the profile is independent of film thickness. However, the profiles shown are valid only below the choking points (Mach number, <0.845). The compressible pressure profile is parabolic rather than the linear profile as is found for incompressible fluids (and for flow between parallel surfaces).

Nonparallel surfaces can have been deliberately machined as a taper or can be caused by distortions. Distortions of the primary seal faces are inherently present in gas film face seals. Distortions present include radial and axial displacements due to the centrifugal force and are especially important under high rotational speeds as anticipated for advanced aircraft operation. A typical centrifugal distortion is shown in figure 33. Another common face distortion is thermal coning, which is caused by an axial thermal gradient along the shaft. The hotter end of the shaft causes a differential shaft radial displacement which results in the face coning illustrated in figure 34. Other distortions could be caused by (1) pressure - due to high pressure drops and improper seal balance diameter; (2) mechanical effects; (3) asymmetry of rotating seal seat; and (4) tolerance buildup due to fabrication and assembly. Generally, for internally pressurized seals, the distortions will cause seal faces to diverge.

For nonparallel sealing surfaces, the pressure gradients are dependent on film thickness. This is shown in figure 35 for the design point of 45 N/cm^2 abs (65 psia) and 311 K (100° F). The pressure gradients are plotted for mean film thicknesses of 5.1 and 10.2 μm (0.2 and 0.4 mil) and for a seal face deformation of ± 0.001 radian. (A negative (-) deformation indicates a converging film in the leakage-flow direction, and a positive (+) deformation indicates a diverging film.) The important point (fig. 35) is that for the convergent film, a decrease in film thickness results in greater area (larger opening force) under the pressure gradient curve; thus, the convergent film has a positive film stiffness. Conversely, as shown by figure 35, a divergent film has a negative film stiffness. This means that for a divergent film a decrease in film thickness (which always occurs dynamically) will cause a decrease in opening force.

Approximate Models of Compressible Flow

As was the case with liquids, approximate models can be formulated for gases to predict seal behavior where an exact model is impossible to solve or impractical for design analysis purposes. Such cases are turbulent flow, where exact physical knowl-

edge is unknown, and near-choked and choked flow, where nonlinear behavior characterizes the flow. Approximate integrated average methods can again be used.

First, quasi-fully-developed compressible flow models will be presented for both parallel and small linear deformed surfaces. Then a constant-area case will be formulated, which is especially useful for choked flow but also includes the quasi-fully-developed flow cases. A variable-area analysis is formulated for radial area expansion and small surface deformation in reference 17. This analysis includes both the quasi-fully-developed flow and constant-area cases, but the solutions are of the numerical Runge-Kutta type and will not be presented herein.

Quasi-fully-developed flow models. - Substitution of the perfect-gas law and mass flow definition into the viscous momentum equation (87) yields the following fundamental form:

$$P\,dP = \frac{-2\bar{f}\mathscr{R}T\dot{M}^2}{DA^2}\,dx \tag{128}$$

The leakage flow rate results for various special cases are shown in table III. The functional relations among the variables and the mass flow rate are similar to those for incompressible turbulent flow.

Constant-area case - critical and supercritical choked flow. - When the radial flow is close to choked or is choked at the exit, the viscous flow analysis is no longer valid. Fluid inertia, neglected in that analysis, becomes important. The rigorous inclusion of inertial terms necessitates the solution of nonlinear partial differential equations even for parallel surfaces and is therefore not practical for engineering calculations; hence, an approximate analytical model must be used.

It is assumed that the flow in the seal leakage-flow region behaves as a constant-area adiabatic flow with friction. A quasi-one-dimensional approximation is made wherein it is assumed that the flow properties can be described in terms of their cross-sectional averages.

The following assumptions are made in the analysis:

(1) The area expansion due to radius increase is neglected. (In many mainshaft face seals, the ratio of inside diameter to outside diameter is about 0.98.)

(2) The flow is adiabatic.

(3) No shaft work is done on or by the system.

(4) No potential energy differences are present, such as those caused by elevation differences.

(5) The fluid behaves as a perfect gas.

(6) The sealing surfaces are parallel.

With these assumptions, the flow is commonly known as Fanno line flow (ref. 18). The governing equations when area changes are neglected are as follows:

Conservation of mass:

$$\dot{M} = \rho u A = \text{Constant} \tag{129}$$

which reduces to

$$\frac{d\rho}{\rho} + \frac{1}{2}\frac{du^2}{u^2} = 0 \tag{130}$$

Conservation of energy:

$$e' + \frac{P}{\rho} + \frac{u^2}{2} = \text{Constant}$$

or

$$i + \frac{u^2}{2} = \text{Constant} \tag{131}$$

where i is the specific enthalpy. This can be written as

$$di = c_p\, dT = -\frac{1}{2}\, du^2 \tag{132}$$

This equation can be reduced to

$$\frac{dT}{T} + \frac{(\gamma - 1)}{2}\, M^2 \frac{du^2}{u^2} = 0 \tag{133}$$

where M is the Mach number, $u/\sqrt{\gamma \mathscr{R} T}$.

Equation of state:

$$P = \rho \mathscr{R} T \tag{134}$$

or

$$\frac{dP}{P} = \frac{d\rho}{\rho} + \frac{dT}{T} \tag{135}$$

Conservation of momentum:

$$-A\,dP - \tau_w\,dA_w = \dot{M}\,du \tag{136}$$

After the hydraulic diameter and Fanning friction factor are introduced, the set of equations (130), (133), (135), and (136) can be combined into a single equation in terms of the Mach number alone. Details of obtaining this equation are given in reference 11. The result is

$$\frac{4f}{D}\,dx = \frac{(1 - M^2)dM^2}{\gamma M^4\left(1 + \frac{\gamma - 1}{2}\,M^2\right)} \tag{137}$$

This equation can be integrated for subsonic, critical, and supercritical flow conditions. The equation is in an implicit form. Solutions are found by using a linear iteration scheme. Details and examples are given in reference 11.

Physics of compressible flow and concept of choking. - Compressible flow and choking occur in the following way: The static pressure drops to overcome flow friction. This pressure drop increases the specific volume of the fluid. Since the area change is negligible, the mean velocity must increase as the specific volume increases in order to maintain the same mass flow rate at each section of the leakage path. As the friction causes the velocity to increase, the fluid momentum change also becomes important. In order to accelerate the fluid to a greater velocity, a force is required which can be attained only through an additional pressure drop. This results in a still greater increase in specific volume. This process will continue until the end of the leakage path or until the fluid reaches the maximum (choking) condition. Choking occurs when the Mach number is 1 at the exit (i. e., exit velocity is sonic). Should the Mach number reach 1 somewhere along the leakage path interior, it is expected that behavior similar to duct flow will occur. For duct flow it can be shown that the flow process will adjust itself, until the point at which the Mach number reaches 1 is shifted to the exit of the leakage passage. The mass flow rate of the fluid is the maximum which can be handled for a given inlet density and passage cross-sectional area. This flow process is known classically as Fanno line flow.

The entrance velocity head loss is negligible in subsonic viscous flow compared to the total seal pressure drop; however, under choked conditions the entrance velocity head loss is no longer negligible. This results in an entrance pressure loss. Also, under choked flow conditions, the exit pressure is larger than the sump pressure and increases with film thickness. The pressure decreases through expansion waves to the sump pressure in the outer cavity. (However, this does not significantly affect the axial

force balance on a seal nosepiece.)

Application examples. - The computer program from reference 9 was used to carry out the quasi-one-dimensional flow analysis. By the use of this program, several problems have been solved. One such problem analyzed is a case which simulates advanced aircraft engine mainshaft seal conditions. The sealed-gas pressure and temperature were 45 N/cm^2 abs (65 psia) and 311 K (100^o F), respectively. The exit ambient pressure was 10.3 N/cm^2 abs (15 psia). The seal-face radial length (seal leakage passage length) was 0.127 cm (50 mils). Figure 36 shows the calculated sealed-gas leakage as a function of film thickness, which ranges from 3 to 51 μm (0.12 to 2 mils).

This approximate analysis agrees with the classical differential analysis for compressible viscous subsonic flow, which is used when the Mach number is less than $1/\sqrt{\gamma}$. As shown in figure 36, for film thicknesses less than 8 μm (0.3 mil), the Mach number is less than $1/\sqrt{\gamma} = 0.845$ and the leakage dependence on film thickness is the classical cubic dependence. The isothermal viscous flow model loses its validity when the Mach number exceeds $1/\sqrt{\gamma}$ (ref. 18). The present approximate model, however, is valid for both subsonic and choked flow. Figure 36 shows that for gaps larger than 8 μm (0.3 mil) the leakage has a lesser than cubic dependence on film thickness. (Choking occurs at a film thickness of 13 μm (0.52 mil).) The limiting case of orifice flow, in which the flow rate varies linearly with film thickness, would be achieved when the film thickness approaches the order of the seal-face radial length of 0.127 cm (50 mils).

As indicated in figure 36, the transition from laminar to turbulent flow occurs for a film thickness of approximately 33 μm (1.3 mils). A Reynolds number, based on hydraulic diameter, of 2300 has been chosen to be the critical transition Reynolds number. This appears to be a universal critical transition Reynolds number for flows in ducts, pipes, and bearings. For laminar flow a mean Fanning friction factor of $24/Re_{2h}$ was used. This friction factor is derived from the classical viscous compressible flow solution. For turbulent flow the Blasius friction factor - Reynolds number relation was chosen. The mean friction factor equals $0.079/Re^{1/4}$. For the transition flow regime the exact nature of the flow, and hence the friction factor, is complex and not fully understood. The friction factor used for this flow regime is derived in reference 9 by assuming a smooth transition from the laminar friction factor to the turbulent friction factor. The Reynolds number range of 2300 to 3000 is arbitrarily selected as the transition flow regime.

Correlation with experiment. - Experiments were conducted at the Lewis Research Center on a radial geometry representative of face seals to check the validity of the quasi-one-dimensional model for choked flow. Leakage flow was studied for two coaxial rings, 14 cm (5.50 in.) in inner diameter, 15.2 cm (6.00 in.) in outer diameter, and separated by a fixed parallel gap of 38 μm (1.5 mils). The reservior pressure of 41.8 N/cm^2 abs (60.6 psia) was held fixed, and the exit pressure varied. Figure 37 shows a comparison of this quasi-one-dimensional analysis, the classical differential analysis

for compressible viscous subsonic flow, and the radial flow experiment. The experiment shows that the flow does become choked. The maximum flow rate (choked) is 0.0080 kg/sec (0.0176 lbm/sec). The present analysis predicts a slightly higher mass flow, but agreement is within 19 percent over most of the range. On the other hand, classical compressible viscous flow theory overestimates the flow rate considerably at all pressure ratios except very near 1. The classical theory predicts a limiting mass flow of 0.02 kg/sec (0.040 lbm/sec), about 250 percent higher than the measured flow rate. However, if the limit is chosen as the mass flow when the Mach number is 1, predicted flows are about 80 percent higher than observed experimentally for choked flow.

Geometry Effect on Leakage

Figure 38 shows the effect of seal-face radial length on leakage flow for film thicknesses from 2.5 to 25 μm (0.1 to 1 mil). The four seal-face radial lengths used in the study were 0.0127, 0.051, 0.127, and 0.254 cm (5, 20, 50, and 100 mils). These are representative seal-face leakage flow lengths. From strictly a leakage point of view, the longest leakage path possible is most desirable. (However, the leakage path length must be compromised from a force-balance point of view when surface deformations occur.) Also shown in figure 38 is the relation of leakage flow rate to film thickness for a 0.00102-cm (0.4-mil) radial length. At film thicknesses greater than 6.35 μm (0.25 mil) the leakage coincides with the leakage obtained for a knife edge by using the theoretical orifice flow equation. (Knife-edge flow sees no frictional resistance from the walls.) Also, the linear variation of leakage flow with film thickness increases. For this narrow seal-face radial length, when flow behaves as knife-edge flow, the velocity entrance loss coefficient is the same as the flow discharge coefficient used in orifice flow analysis.

Figure 39 shows mass leakage flow rate as a function of pressure ratio for a fixed gap of 10.2 μm (0.4 mil) and a varying seal-face radial length. The knife edge, as expected, has the largest leakage flow rate. These values have been calculated from the theoretical orifice flow equation. The computer program result for a radial length of 10.2 μm (0.4 mil) agrees with the theoretical orifice flow equation. As the radial length increases, the critical pressure ratio for choking decreases, as indicated by the sonic line in figure 39. Again the advantage of longer seal faces is apparent.

Figure 40 shows the pressure profiles along the seal-face radial length found by using the quasi-one-dimensional computer program for parallel surfaces only. For film thicknesses equal to or less than 5.1 μm (0.2 mil), the profile does not depend on film thickness. The flow is subsonic, as is found from the isothermal viscous flow analysis and shown in figure 32. When the flow is choked and the mean film thickness

increases, the entrance pressure loss becomes significant. (The entrance pressure loss is negligible in subsonic viscous flow.) Also, under choked flow conditions, the exit pressure is larger than the sump pressure and increases with film thickness. As stated previously, the pressure decreases through expansion waves to the sump pressure in the outer cavity. (This does not significantly affect the axial force balance.)

Opening Force

The area under the pressure gradient curves represents a force which tends to open the seal. This opening force is found by an integration of the pressure distribution across the seal-face radial length. The marked effect of seal-face distortion can be shown by plotting the opening force as a function of mean film thickness (fig. 41). For illustration, the opening force is plotted for five angular face distortions α (0, $\pm$0.001, and $\pm$0.002 rad) for the design point of 45 N/cm^2 abs (65 psia) and 211 K (100° F). As shown in figure 41 the effect of angular distortion is more pronounced as the film thickness decreases; the larger distortion (0.002 rad) has a greater effect on opening force than the smaller distortion (0.001 rad). As stated previously, for parallel faces the opening force is independent of film thickness; for convergent faces the force increases as the film thickness decreases (positive film stiffness); and for divergent faces the opening force decreases as the film thickness decreases.

For classical viscous compressible flow, the opening force is independent of the fluid properties and the film thickness. This gives the well-known result that parallel surfaces yield no film stiffness. However, this is not the case when the classical compressible viscous flow theory is no longer valid. Figure 42 shows seal opening force as a function of film thickness obtained by using the computer program (ref. 9), for both isentropic and 0.6-entrance-loss-coefficient cases. For small film thickness (corresponding to $M < 1/\sqrt{\gamma}$), the force is constant, as predicted by classical analysis. However, as film thickness and Mach number increase, the force actually increases slightly for the isentropic entrance case. This is a condition of negative film stiffness. It would be undesirable to operate in this region unless an auxiliary film stiffness generating device, such as self-acting lift pads, could make the overall seal stiffness positive. Also, in figure 42 the opening force attains a peak value and then sharply decreases with increasing film thickness for the 0.6-entrance-loss-coefficient case.

Center of Pressure

Figure 43 illustrates the radial center-of-pressure variation obtained with the quasi-one-dimensional-flow computer program (ref. 9). At low values of film thickness

(subsonic flow), the center of pressure is the same as the value obtained from the isothermal viscous flow analysis (47.37 cm; 18.65 mils), which is valid for Mach numbers less than $1/\sqrt{\gamma}$. For film thicknesses larger than the critical choking film thickness, the center of pressure increases at a lesser rate and, eventually, at larger film thicknesses than shown, would be asymptotic to a dimensionless value of 0.500.

Continuum and Noncontinuum Flow

Generally, gas film seals operate in the continuum flow regime, where the gas is very dense; that is, the molecular mean free path is very small compared to the seal surface separation distance (film thickness) h. The parameter relating the mean free path with h is called the Knudsen number. The Knudsen number is defined as

$$Kn = \frac{\lambda}{h_m} \sim \frac{\text{Molecular mean free path}}{\text{Mean film thickness}} \sim \frac{\text{Constant} \times T}{h_m P}$$

The Chapman relation expresses the mean free path as a function of the pressure and gas properties

$$\lambda = \frac{\mu\left(\frac{2\pi kT}{m}\right)^{1/2}}{2P}$$

The relation of molecular flow rate to volumetric flow rate can be found from

$$\dot{N} = \frac{P}{kT} Q$$

where

$\dot{N}$ molecular flow rate, molecules/sec

k Boltzmann constant, $k = \mathscr{R}/N_o$

N_o Avogadro number, 6.027×10^{23} molecules/mole

Values of the Knudsen number indicate the regime:

(1) Continuum flow, $Kn < 0.01$

(2) Transition (slip) flow, $0.01 \leq Kn \leq 1$

(3) Molecular flow, $Kn > 1$

The equations just presented are for the continuum flow regime.

Noncontinuum flow (discussed in ref. 19) can occur in seals operating in a vacuum environment. Molecular mean free paths of liquids are sufficiently short that molecular flow need not be considered for most practical seals. The boundary lubricating mode predominates over mean-free-path fluid effects.

Flow Through Porous Media

Porous materials are used as sealing elements. (For example, the porosity of carbon is highly dependent on the process, type, treatment, and impregnation. Carbon manufacturers usually specify the porosity.) In high-temperature applications, porous materials are sometimes used for their abradability properties and/or because transpiration cooling can be used. The equation that governs horizontal, isothermal flow of a gas is

$$Q = \frac{kA}{\mu}\frac{dP}{dx}$$

where k is the permeability in darcys (length-squared units).

Permeability is a measure of the ease with which a fluid flows through the medium and is a statistical average of the fluid conductivities of the flow channels in the medium. Hence, permeability is empirically determined.

Porosity is defined as the void volume, or the volume of pore space divided by the total volume of the medium. The void volume is found by gravimetric techniques or by gas-expansion methods. The amount of liquid needed to saturate the dry medium is measured.

INVISCID FLOW EQUATIONS

Knowledge of orifice and nozzle flows is important in fluid sealing. Various modified forms of these equations are used in predicting flow in seals, such as labyrinth seals, and in entrance regions and as limiting cases of maximum theoretical leakage flows for a given cross-sectional area. The flow is analyzed as inviscid (neglects viscous friction forces); however, as will be seen, real flow effects such as those due to friction can be accounted for by various empirical coefficients.

The inviscid flow conservation-of-momentum equation for one-dimensional incompressible flow (eq. (136)) with the viscous friction term eliminated is

$$-A\,dP = \dot{M}\,du = \rho u A\,du \tag{138}$$

Integrating between any two points 1 and 2 gives

$$-\int_1^2 dP = \rho \int_1^2 u\,du \tag{139}$$

or

$$P_1 + \frac{\rho u_1^2}{2} = P_2 + \frac{\rho u_2^2}{2} \tag{140}$$

This is the classical incompressible Bernouilli equation.

Thin-Edge Orifice Flow

For orifice flows, the entrance velocity is generally negligible. Thus,

$$u_2 = \sqrt{\frac{2(P_1 - P_2)}{\rho}} \tag{141}$$

Thus,

$$Q_{ideal} = A_2 u_2 = A_2 \sqrt{\frac{2(P_1 - P_2)}{\rho}} \tag{142}$$

However, in real flow situations, this theoretical value is not achieved because of the "vena contracta" effect (fig. 44(a)). This effect is accounted for by an empirically determined discharge coefficient C_D which is a function of pressure ratio and Reynolds number. An ASME publication (ref. 20) contains data on many thin-edge orifice flow conditions. Thus, the mass flow rate is expressed as

$$\dot{M} = \rho C_D A_2 \sqrt{\frac{2(P_1 - P_2)}{\rho}} \tag{143}$$

where

$$C_D = \frac{\text{Actual flow rate}}{\text{Ideal flow rate}}$$

Figure 45 shows that the orifice discharge coefficient increases with larger pressure ratios. This can be partially explained by examining figure 46 (taken from ref. 21). Figure 46(a) shows a rounded orifice at low Reynolds number. The air molecules are able to "stream in" smoothly with a negligible vena contracta. In contrast, the sharp entrance edge shown in figure 46(b) results in a stream area that is about 60 percent of the orifice area. However, at high Reynolds numbers (high approach velocities) the stream area approaches the orifice area because of the momentum of the jet air (fig. 46(c)).

Gravitational-Head Orifice Flow

Orifice flow through a container with only a gravitational head driving the fluid can be found from Bernouilli's equation along a streamline. Refer to figure 47.

$$\rho gh = P_2 = \frac{1}{2}\rho u_3^2$$

The exit velocity is thus

$$u_3 = \sqrt{2gh}$$

This is known as Torricelli's law. The volume flow rate is

$$Q_{ideal} = A_3\sqrt{2gh}$$

Nozzle Flow

Nozzle flow is generally characterized by a decrease in area between entrance and exit (fig. 48). The continuity equation is

$$Q = A_1u_1 = A_2u_2 \tag{144}$$

Substituting the inlet velocity into the momentum equation, where $u_1 \neq 0$, yields

$$u_2^2 - u_1^2 = \frac{2}{\rho}(P_1 - P_2) \tag{145}$$

In terms of the ratio of exit area to inlet area, this is

$$u_2 = \frac{1}{\sqrt{1 - \beta^2}} \sqrt{\frac{2(P_1 - P_2)}{\rho}} \tag{146}$$

where

$$\beta = \frac{A_2}{A_1}$$

Thus,

$$Q = \frac{C_D A_2}{\sqrt{1 - \beta^2}} \sqrt{\frac{2(P_1 - P_2)}{\rho}} \tag{147}$$

The mass flow rate can be found from

$$\dot{M} = \rho Q$$

$$\dot{M} = \frac{C_D A_2 \rho}{\sqrt{1 - \beta^2}} \sqrt{\frac{2(P_1 - P_2)}{\rho}} \tag{148}$$

For compressible flow, it is common practice in flow measurements to generalize equation (148) by multiplying the right side by an expansion factor Y and specifying the specific density, $\rho = \rho_1$, as that at the inlet. Hence, both compressible and incompressible flow can be expressed by

$$\dot{M} = \frac{C_D A_2 \rho_1 Y}{\sqrt{1 - \beta^2}} \sqrt{\frac{2(P_1 - P_2)}{\rho_1}} \tag{149}$$

where C_D is the incompressible flow discharge coefficient. For an incompressible fluid, Y = 1. It is common to theoretically determine values of Y for flow nozzles and venturi meters and to use experimentally determined values of Y for orifice meters. Values can be found in reference 20. An example of a theoretical calculation for the

expansion function can be found in appendix C.

In fluid sealing, it is generally desirable to restrict or prevent leakage. Thus, a small discharge coefficient is desired, which is opposite to most fluid-flow applications. As shown in figure 45 the nozzle discharge coefficient is much higher than that of an orifice for the same conditions. This is due to a larger vena contracta, as illustrated in figure 44(b) compared with figure 44(a). Also the discharge coefficient in nozzle flow accounts for viscous friction of the nozzle wall as well as the vena contracta.

Equation (139) illustrates the desirability of using a low-density gas to reduce the mass flow rate:

$$\dot{M} \propto \sqrt{\rho}$$

A gas at a low pressure (e.g., approaching vacuum conditions) can have a low mass flow rate even though the gas volume flow rate may be high. This philosophy is used in some sealing applications where the gas is expanded to a low-pressure stage before it leaks out of the seal to ambient conditions.

Flow Function Approach

An alternate formulation of the leakage-flow equations is the flow function approach. This approach is extensively used in hydraulics and in sealing systems, especially for labyrinth seal flows. This formulation is based on the one-dimensional inviscid flow assumption but accounts for viscous and other effects by coefficients which are usually empirically determined.

For an orifice flow, equation (149) becomes (setting $\beta = 0$)

$$\dot{M} = C_D A \rho_1 \sqrt{\frac{2(P_1 - P_2)}{\rho_1}} \tag{150}$$

For a perfect gas, equation (150) becomes

$$\dot{M} = \frac{C_D A P_1}{\sqrt{\mathscr{R} T_1}} \left[\sqrt{2 \left(1 - \frac{P_2}{P_1} \right)} Y \right] \tag{151}$$

or

$$\frac{\dot{M}\sqrt{T_1}}{AP_1} = Y\sqrt{2\left(1 - \frac{P_2}{P_1}\right)\frac{C_D}{\sqrt{\mathscr{R}}}} \tag{152}$$

We define the flow function as

$$\varphi = \frac{\dot{M}\sqrt{T_0}}{AP_0}$$

The flow function is one dimensional and is a function of the pressure ratio and the particular overall geometric configuration. The pressurized fluid conditions are now designated by the subscript 0. The flow function is a measure of the flow effectiveness.

The dimensionless mass flow equation (152) can be rewritten in the following form:

$$G\frac{\sqrt{T_0}}{P_0} = \alpha\gamma\varphi C$$

where

$G = \dot{M}/A$	a convenient parameter for sizing orifices and knife edges
$\alpha = C_D$	discharge coefficient
γ	recovery factor, used for straight-through staged restrictions (e.g., in stages of orifices or labyrinth knife edges)
C	conversion constant (e.g., $\sqrt{\mathscr{R}}$)

The famous Egli formula (ref. 22) used in estimating labyrinth seal leakage is of such a form. The functions α, γ, and φ from that formula are plotted in figure 49.

The industrial gas compressor industry uses a formula

$$\dot{M} = KC_D A\rho u_m$$

where the coefficient K is empirically determined.

Labyrinth Seals

High friction losses due to turbulence are produced in throttling or restrictor seals such as labyrinths. The sealed gas expands as it passes through orifices or knife edges

formed by successive restrictions. An energy conversion process takes place. The stored gas (internal) energy (due to pressure and temperature) is converted into kinetic energy in the flow process. (The energy contained in the gas by its temperature and pressure state is called the gas enthalpy.) By designing the geometry within a given configuration, the kinetic energy is converted into heat; otherwise, a near full recovery would occur. A common way of dissipating the kinetic energy is by changing the flow direction between successive restrictions. A "stepped" labyrinth illustrates the use of this idea.

ENTRANCE FLOWS AND LOSSES

It is common in lubrication theory to neglect the entrance region entirely. This is reasonable for the slow viscous flows which characterize lubrication flows. Brodoia and Osterle (ref. 23) performed a numerical analysis of plane Poiseuille developing flows. They found that the entrance length X_L varied approximately as (fig. 50)

$$X_L \simeq 0.044\ hRe \tag{153}$$

Thus, it is seen that for low Reynolds number flows this region is negligible. Kawaguchi (ref. 24) studied entrance losses of flow between parallel disks and concluded that they were the same for low Reynolds numbers as for laminar flow. However, there are conditions when entrance losses are substantial, namely, when the flow is high Reynolds number (turbulent) and when the flow becomes choked in compressible flow.

There are several causes for pressure drops in the face-seal entrance region. An abrupt geometric change at the seal passage entrance can result in a nonuniform profile because of flow turning, separated flow, and the vena contracta effect. This nonuniform profile will cause an entrance pressure drop (fig. 51). Kawaguchi (ref. 24) found that the entrance loss for turbulent flow depends strongly on the ratio of film thickness to inlet radius and on the radius of inlet curvature but depends very little on the entrance Reynolds number. The pressure drop in the flow-development length is higher than that in the fully developed flow region because of two effects (ref. 25). The first effect is higher wall shear caused by higher transverse velocity gradients. The second effect is the momentum increase as the velocity distribution becomes less uniform. These entrance pressure losses can be accounted for by using entrance loss coefficients.

The role of the entrance velocity loss coefficient may be better understood by considering the incompressible Bernouilli equation relating the stagnation reservoir pressure with the static and dynamic pressure at the seal entrance:

$$P_0 = P_1 + \frac{1}{2}\rho_1 u_{1,\,ideal}^2 \tag{154}$$

The actual velocity at the seal entrance is less than ideal; it can be expressed as

$$u_1 = C_L u_{1,\,ideal} \tag{155}$$

where C_L is the entrance velocity loss coefficient (ref. 26) and is experimentally determined. Thus, the entrance pressure can be found from

$$P_1 = P_0 - \frac{1}{2}\rho_1 \frac{u_1^2}{C_L^2} \tag{156}$$

The head loss coefficient k' is commonly used in hydraulics and reported in the literature. The velocity loss coefficient can readily be related to the head loss coefficient by the following equation:

$$C_L = \frac{1}{\sqrt{k' + 1}} \tag{157}$$

(The head loss coefficient is sometimes also called the flow resistance coefficient.) Fleming and Sparrow have shown in reference 25 that the bulk of the entrance losses for duct flow occur in a small region very close to the duct inlet. Laminar incompressible entrance loss coefficients have been calculated and measured for a variety of duct shapes (e.g., refs. 25 and 27). Turbulent loss coefficients are not so widely reported; however, they may be calculated for parallel-plate channels from the information in reference 28. The values for head loss coefficients k' for turbulent flow are generally less than 20 percent of those for laminar flow. See the qualitative comparison shown in figure 50. Incompressible loss coefficients may be adequate for use with compressible flow (ref. 11).

The head loss approach is also used to analyze sealing systems. The head loss is

$$H = \frac{\Delta P}{\rho}$$

Thus, the inviscid flow velocity equation becomes

$$\bar{u} = C_L\sqrt{2H}$$

where C_L is the entrance loss coefficient and

$$H_1 = \frac{1}{2}\bar{u}^2\left(\frac{1}{C_L^2}\right)$$

The entrance loss coefficient is related to the head loss coefficient (or flow resistance coefficient) by

$$C_L = \frac{1}{\sqrt{k' + 1}}$$

$$H_1 = \frac{\bar{u}^2}{2}(k' + 1)$$

For viscous effects, equation (88)

$$D\frac{dP}{dx} = -2\rho\bar{u}^2\bar{f}$$

can be integrated to the form

$$\frac{P_1 - P_2}{\rho} = \frac{\bar{u}^2}{2}\frac{\bar{4fL}}{D} = H$$

Thus, the total head loss for both entrance and viscous losses is

$$H = \frac{\bar{u}^2}{2}\left(k' + 1 + \frac{\bar{4fL}}{D}\right)$$

where

$$u = \frac{1}{\sqrt{k' + 1 + \frac{\bar{4fL}}{D}}}\sqrt{\frac{2\,\Delta P}{\rho}}$$

Here

$$K = \frac{1}{\sqrt{k' + 1 + \frac{4\bar{f}L}{D}}} \tag{157a}$$

A head loss equation for labyrinth seals that is especially useful for seals with honeycomb-cell rub strips is

$$H = 1.5\,\frac{n\bar{u}^2}{2}$$

where n is the number of throttling stages.

FLOW REGIMES

As mentioned in the previous sections, the appropriate equations for seal analysis depend on the flow regime. There are many possible flow regimes because of the wide spectrum of seal operation. The most common ones will be discussed in this section.

The leakage flow regimes are defined by either the appropriate Reynolds number or, in the case of a gas, the molecular mean free path length. The flow regime must be established in order to determine the applicable theoretical leakage relation. Since the leakage flow is required for the Reynolds number calculation, it is necessary to assume a flow regime and to iterate the leakage and Reynolds number calculations.

Consider flow in a seal passage caused by a pressure differential. When the flow is laminar, the fluid flow is characterized by laminas, or layers (fig. 52). This flow is predictable analytically, as we have seen for flow in long passages. The chief characteristics of this viscous laminar flow are that the velocity is independent of the internal surface roughness and that the velocity distribution across the gap is parabolic in form with the maximum velocity at the midgap position. At flow velocities above a critical condition, the flow pattern changes to one of turbulence characterized by eddies and vortices (fig. 53). The energy losses now become affected by the surface roughness, and flow prediction requires the use of experimental data. Turbulent flow is characterized by velocity components which have random turbulent fluctuations imposed upon their mean values. A stream of dye or ink inserted in a laminar flow will streak out a thin line and will always be composed of the same fluid particles. However, in turbulent flow the dye line would quickly become tangled and mixed in with the fluid as it flows along, and we would see myriads of threads and clouds widening and dispersing as the fluid

flows along. Figure 54 qualitatively compares laminar and mean turbulent velocity distributions. The turbulent mean velocity profile is more elliptic (blunt nose) and is characterized by a much higher shear stress (due to the slope of the velocity profile at the wall). Further details can be found in any fundamental fluid mechanics textbook.

Figure 55 qualitatively shows how the pressure drop per unit flow length varies as the fluid velocity increases. There is a sharp increase in pressure drop when turbulent flow occurs. This sharp increase in pressure drop, which is a measure of the shear force, is characteristic of turbulent flow.

The exact transition point for any particular set of conditions is uncertain, but the limits of the laminar-turbulent flow transition regime can be defined by the value of the nondimensional parameter known as Reynolds number Re, where

$$Re = \frac{\rho \bar{u} D}{\mu}$$

The minimum transition Reynolds number for pressure flow is 2300. This has been observed to be the case for many geometries and experimental conditions in fluid mechanics and hydraulics. For flow between narrowly spaced plates and coaxial annular disks the hydraulic diameter is $D = 2h$.

For highly viscous liquids, such as oil, used in most sealing applications the flow will be laminar. Lower viscosity liquids, such as water and especially liquid metals, can operate in the turbulent flow regime at very high speeds. For gases, such compressibility effects as fluid choking appear to be important before the flow becomes turbulent. Hence, the Mach number, as well as the Reynolds number, will be important.

Shear flow. - If there is relative rotation of the seal surfaces, as in mechanical face seals, turbulence can be induced by this rotation. The rotational flow component of the velocity may be responsible for the flow becoming turbulent in the circumferential direction (shear flow direction), which means the entire flow field (radial pressure flow) will be turbulent.

For narrow gaps (close clearances, where the boundary layers are merged), the critical rotational Reynolds number for transition appears to be the simple Couette flow transition Reynolds number. Thus, $Re_r = r\Omega h/\nu \simeq 1900$ for transition (ref. 29); the smaller the gap, the longer the transition speed is delayed. Therefore, the wall has a stabilizing effect on the flow, and this should be considered in selecting the design gap (e.g., for a 30-cm- (1-ft-) diam air seal operating at room temperature, the transition speed would be 71 500 rpm for a 25-μm (1-mil) gap but would be 179 000 rpm for a 10-μm (0.4-mil) gap).

Some seals, such as vaneless slinger seals, operate at larger clearances in order to seal high pressures at high speeds. (Heat dissipation must be minimized, so clearances are relatively larger than with face seals.)

Daily and Nece (ref. 30) performed experiments on enclosed rotating disks. They identified four basic flow regimes:

(1) Regime I: laminar flow, close clearance

(2) Regime II: laminar flow, separate boundary layers

(3) Regime III: turbulent flow, close clearance

(4) Regime IV: turbulent flow, separate boundary layers

Similar experiments were performed by Ketola and McGrew (ref. 31), who identified the flow regimes for a partially engaged seal. A schematic of their seal is shown in figure 56. The approximate flow regimes are shown in figure 57. The characteristic length in the Reynolds number is the radius r instead of the gap h. This is the characteristic length for a rotating disk in an infinite fluid medium. For a highly polished disk the transition Reynolds number

$$\frac{r^2\Omega}{\nu} \simeq 3\times10^5$$

Since transition from laminar to turbulent flow depends on the disk radius, part of the seal (disk center region) will always be operating in the laminar flow regime. Whether or not the rotating boundary layers are merged can be estimated by applying von Kármán's formula (ref. 32). For laminar flow,

$$\delta \simeq 2.58\sqrt{\frac{\nu}{\Omega}}$$

Theoretical radial and circumferential velocity profiles are shown in figure 58 for various Reynolds numbers. These are taken from Lance and Rogers (ref. 33). For the boundary layer case (Re = 441), theoretical solutions are compared with experimental results in figure 59.

Annular flow between cylinders. - When inner and outer cylinders are very closely spaced, the flow remains laminar until the rotational transition Reynolds number is exceeded. However, if the gap is sufficiently large, a secondary flow regime called Taylor vortex flow can occur when the critical speed of rotation is reached. These vortices are ring shaped around a rotationary axis, about twice the gap size thick. Taylor vortex flow is illustrated in figure 60, and the vortices (paint pigment particles immersed in oil) are shown in figure 61 (ref. 34). Taylor (ref. 35) analyzed mathematically the critical speed of rotation at which these vortices are formed, and he confirmed it by his experiment. The criterion is that Taylor vortices occur when the Taylor number

$$Ta = \left(\frac{R_1 \Omega h_m}{\nu}\right)^2 \left(\frac{4h_m}{R_1 + R_2}\right) > 41.2$$

Kaye and Elgar (ref. 36) observed that Taylor vortices keep their shape until the speed of rotation is increased from a critical value to a certain value. Taylor vortex formation has been observed to be entirely different from turbulent flow formation. When the speed of rotation of the inner cylinder is increased by a large amount, the flow in the annulus becomes turbulent and vortices are superimposed on the turbulent fluctuations. When the speed of rotation is increased further, the Taylor vortices are observed to first distort and then completely disappear, and a purely turbulent flow results.

Kaye and Elgar (ref. 36) identified four modes of flow between coaxial rotating cylinders when there is a net axial flow:

(1) Purely laminar

(2) Purely turbulent

(3) Laminar plus Taylor vortex

(4) Turbulent plus Taylor vortex

These flow modes depend on the inner cylinder rotational speed and mean axial flow velocity. A schematic representation is shown in figure 62.

Pressure flow with rotational flow. - When there is both circumferential shear flow and radial pressure flow present (as in a face seal), the net flow is a spiral flow. In the laminar flow regime the shear flow and the pressure flow can generally be treated independently. This was concluded from experiments performed by Yamada (ref. 37), who studied axial flow through an annulus with the inner cylinder rotating. The rotational flow is always important for determining the power loss due to viscous shearing and for determining the transition to turbulent flow. Of course, it can be responsible for rotationally induced turbulence. As previously seen, the centrifugal component in the radial direction can contribute to the seal leakage, especially for liquids. Yamada also discusses various effects of rotation and the effect of the axial flow becoming turbulent.

Figure 63 illustrates a simplified envelope of possible seal-face compressible flow regimes when there is circumferential rotation as well as radial leakage flow (ref. 38). As previously stated, the Mach number is the radial flow parameter, and a simple Couette flow transition Reynolds number is used as the rotational flow parameter for very narrowly spaced disks representative of face seals. Theodorsen and Reigier (ref. 32) found that laminar-turbulent transition and drag were independent of compressibility for a disk rotating in an infinite medium. Although not verified, it is speculated that this is also the case in face seals.

MECHANISM OF FILM PRESSURE GENERATION BETWEEN RELATIVELY MOVING SURFACES

Full-fluid-film lubrication implies the existence of an interposed full film of fluid that physically separates the mating surfaces of the two members which traditionally comprise a bearing. However, fluid-film lubrication plays a key role in sealing as well.

Three generally recognized modes of lubrication are categorized as the sliding-surface bearing type (ref. 39):

(1) Hydrodynamic - in which fluid-film, load-carrying capacity is achieved by motion of the bearing members in the plane of the mating bearing surfaces

(2) Hydrostatic - in which fluid-film, load-carrying capacity is achieved by the introduction of externally pressurized flow

(3) Squeeze film - in which fluid-film, load-carrying capacity is achieved by motion of the bearing members normal to the plane of the mating bearing surfaces

These three modes of fluid-film lubrication are illustrated diagrammatically in figures 64(a) to (c). A possible fourth mode, termed "hybrid operation," is illustrated in figure 64(d) and derives its fluid-film, load-carrying capacity by a combination of two or more of the previously mentioned modes of lubrication.

Hydrodynamic Pressure Development

The classical lubrication equation is called the Reynolds equation. It is the differential equation which relates viscosity, film thickness, pressure, and sliding velocity. This equation is derived in many lubrication textbooks. In the section Flow Between Parallel Plates in Relative Motion, we have already used the same assumptions that are used in deriving the Reynolds equation. Appendix D contains a brief description of Reynolds equation taken from Bisson and Anderson (ref. 40).

The Reynolds equation is essentially a flow balance equation. The viscous flow assumption (that the viscous friction force is balanced with the pressure gradient force) is made. The momentum equation is then substituted into the mass conservation equation and integrated across the gap. The two-dimensional Reynolds lubrication equation is

$$\overbrace{\frac{\partial}{\partial x}\left(\frac{\rho h^3}{12\mu}\frac{\partial P}{\partial x}\right)}^{\text{x-Direction pressure flow}} + \overbrace{\frac{\partial}{\partial z}\left(\frac{\rho h^3}{12\mu}\frac{\partial P}{\partial z}\right)}^{\text{z-Direction pressure flow}} = \overbrace{\frac{1}{2}\frac{\partial(\rho U h)}{\partial x}}^{\substack{\text{Tangential shear flow} \\ \text{"Wedge film" or hydrodynamic term}}} + \overbrace{\frac{\partial(\rho h)}{\partial t}}^{\substack{\text{Flow due to wall motion normal to flow} \\ \text{Squeeze film term}}}$$

Physical explanation. - A physical understanding of pressure development in an oil film can be achieved by examining the pressure conditions that must prevail to maintain flow continuity with various film configurations.

Consider two parallel plane surfaces separated by a lubricant film. As shown in figure 65, the lower surface is stationary and the upper surface is moving with a velocity U in a direction parallel with the surfaces. The local flow velocity in the film u varies uniformly from zero at the stationary surface to U at the moving surface. If the plates are very wide in the direction perpendicular to the direction of motion, the rate of flow that crosses the left boundary AB will be equal to the flow that crosses the right boundary CD. The flows that cross these two boundaries result only from velocity gradients. Since they are equal, the continuity requirements are satisfied without any pressure buildup. Therefore, no pressure buildup will result when two parallel surfaces are moving relative to each other only in a direction parallel to the surface. This was shown in the section Flow Between Parallel Plates in Relative Motion.

Next, consider the two plane surfaces inclined slightly with respect to each other, with one of the surfaces in motion in a direction parallel to its surface (fig. 66(a)). Again, as with parallel surfaces, the local flow velocity u in the film varies uniformly from zero at the stationary surface to U at the moving surface. Assume that the plates are wide in the direction perpendicular to the direction of motion so that no flow occurs except in the direction of motion. Then the velocity flow that crosses the boundary AB will be greater than the flow that crosses the boundary CD. The requirements of flow continuity thus are not satisfied since no sources or sinks exist between the two boundaries. It can be surmised that there will be a pressure buildup in the oil film until the continuity of flow is satisfied.

The flow which results from the pressure buildup is sketched schematically in figure 66(b). The local flow velocity that results from pressure gradients is zero at both surfaces since no interfacial slip is assumed. The velocity is a maximum at a point halfway between the two surfaces. The velocity profiles are parabolic. Because pressure flow is always from a region of higher pressure to a region of lower pressure, the flow is out of the bearing at both boundaries.

The pressure flow at the boundary AB opposes the velocity flow, while the pressure flow at CD is in the same direction as the velocity flow. If the velocity and pressure flows are superimposed, the flow profiles that result are as shown in figure 66(c). The required equality of flow across AB and CD can now be maintained with the proper combination of velocity and pressure within the film. At some section EF within the film there is no pressure flow, and the velocity profile across the film is again linear. This is the point of maximum pressure or the point at which there is no pressure gradient.

It was deduced previously that some inclination of two plane surfaces in relative motion is required in order to achieve a pressure buildup. This deduction can be qualified further by requiring that the film be convergent in the direction of motion. A di-

vergent film will produce not a pressure buildup (eq. (60)) but a subambient pressure reduction. A convergent film in a hydrodynamic bearing is called a wedge film. A wedge film is one of two ways in which pressure or, equivalently, load capacity can be generated in a hydrodynamic bearing.

Narrow-seal approximation. - The narrow-seal approximation is commonly used in analyzing hydrodynamic face seals. This approximation neglects the circumferential pressure gradient contributions to the circumferential mass flow rate. This is analogous to Ocvirk and DuBois' short-journal-bearing theory (ref. 40):

$$\underbrace{\frac{\partial}{\partial X}\left(h^3 \frac{\partial P}{\partial X}\right)}_{0} + \underbrace{\frac{\partial}{\partial Z}\left(h^3 \frac{\partial P}{\partial Z}\right)}_{\substack{\text{z-Direction pressure flow rate,} \\ q_z}} = \underbrace{6\mu U \frac{\partial h}{\partial X}}_{\substack{\text{Viscous shear flow in x-direction}}}$$

$\underbrace{\qquad}_{\substack{\text{x-Direction pressure flow rate,} \\ q_x}}$

This assumption amounts to claiming that the majority of the circumferential mass flow is caused by tangential viscous shear (accounted for by the right side of the equation). For narrow seals with constant boundary pressure around the perimeter, it is usually unlikely that large circumferential pressure gradients can exist within the seal except possibly in narrow interior regions along the boundaries.

Step bearing. - A common configuration that generates hydrodynamic pressure is the step bearing configuration shown in figure 67. The main assumptions are that $h_1 \ll L_1$ and $h_2 \ll L_2$. The flow is assumed to be viscous, two-dimensional laminar flow. Attach a coordinate system to the slider, as shown in figure 67. Let the stationary bearing surface move with a velocity U in the negative x-direction. Hence, the boundary conditions are

$$u = 0 \qquad \text{at} \quad z = 0$$

$$u = -U \qquad \text{at} \quad z = h$$

and the gage pressure is

$$P = 0$$

at the inlet $x_2 = L_2$ and the exit $x_1 = 0$. The pressure at the step $x_1 = L_1$ or $x_2 = 0$ is unknown. This pressure must be found by invoking the continuity condition that $Q_1 = Q_2$.

Assuming that general Couette flow governs the flow along flow passages L_1 and

L_2 and using equation (87) give the continuity condition as

$$Q_1 = -\frac{h_1^3}{12\mu}\frac{P_s}{L_1} - \frac{Uh_1}{2}$$

$$Q_2 = \frac{h_2^3 P_s}{12\mu L_2} - \frac{Uh_2}{2}$$

The pressure in the land and the groove vary linearly with x, and a triangular pressure results. The peak pressure at the step P_s is found by equating Q_1 and Q_2. The result is

$$P_s = \frac{6\mu U(h_2 - h_1)}{\left(\frac{h_1^3}{L_1}\right) + \left(\frac{h_2^3}{L_2}\right)}$$

When this pressure is known, the entire distribution across the land and groove are known.

The total hydrodynamic load generated can be found by integrating the pressure distribution curve. The result is

$$F = \frac{P_s}{2} W(L_1 + L_2)$$

If the groove depth and film thickness were changed, the slider would rise or sink as the load was decreased or increased, respectively. Hydrostatic step seals and viscoseals use this life mechanism in their operation.

Compressibility effects. - Hydrodynamic lift concepts apply to gases as well as to liquids; however, compressibility effects (ref. 41) must be accounted for. The same assumptions apply as were stated for classical viscous compressible flow. Namely, isothermal, laminar, viscous flow of a continuous fluid with negligible inertia is assumed.

Since gas lubricant films are very thin and in contact with relatively large masses of metal, the films can be considered to be isothermal. Therefore, changes in local density in the film result primarily from changes in the local pressure as predicted by the perfect-gas law. This interdependence alters the pressure distribution from the

shape it would have if it were incompressible (fig. 68(a)). Consequently, the degree of gas compression affects the bearing performance.

The compressibility number Λ is a measure of the density variation importance. In the presentation for compressible flow the Mach number was stated to be the compressibility effect criterion. This parameter was an indication of when the inertia effects were important. In the viscous laminar flow regime, inertia effects are negligible and the Mach number is not used. Also the compressibility parameter can be interpreted as

$$\Lambda \cong \frac{\Delta\rho}{\rho}$$

For small Λ, the hydrodynamic effect is the same as for incompressible fluids. When Λ is large, figures 68(b) and (c) show that incompressible theory does not apply and that compressibility causes a deterioration in performance. Figure 68(c) illustrates a barrier which is imposed by compressibility on most types of gas bearings. The load capacity of the gas bearing does not indefinitely increase with increasing speed but levels off. In contrast, the load capacity of the liquid bearing is directly proportional to the speed.

Although this brief discussion applies to a basic fixed pad, the same effects are present in most other hydrodynamic bearing configurations. This includes spiral groove, herringbone, and tilted pad bearings. Further discussion is beyond the scope of this presentation. The solution procedures are similar to those already mentioned; however, compressibility does complicate the solution. For more information, refer to the textbook by Gross (ref. 15) or to reference 41.

Since gas viscosities are of the order of 1/1000th that of oil, hydrodynamic lift is much less for gases. The lift is also reduced because of compressibility effects. That is, as the pressure rises through the bearing, the density increases. The changing volume flow through the bearing modifies the pressure characteristic, giving lower load-carrying capacity. If the compression ratio P_{max}/P_a is close to 1, compressibility effects become insignificant and performance efficiency is imposed.

Squeeze-Film Concepts

Relative seal surface vibrations are inherent in all rotating seal systems. A typical vibration is one surface oscillated at a high frequency perpendicular to the plane of the surfaces. This phenomenon can best be investigated by studying a liquid in a narrow gap where one surface is oscillated at a high frequency. Figure 69 illustrates two parallel plane surfaces which are separated by a lubricant film, with the upper surface moving toward the lower. Lubricant is being squeezed out of the volume between the surfaces. Since the surfaces have no velocity in the direction of flow, the only cause of

this flow is a pressure gradient. Relative motion of two surfaces separated by a lubricant film toward each other will then result in a pressure buildup, as shown in figure 69. In a hydrodynamic bearing this film is called the squeeze film.

Hydrostatic cushioning. - Squeeze-film concepts play an important role in impact resistance. Generally, good impact loading resistance is obtained if the duration of impact is less than the squeeze-film duration. A viscous lubricant cannot be instantaneously squeezed from between two surfaces which are approaching each other. It takes time for these surfaces to meet. During that interval, because of the resistance of the fluid (lubricant) to extrusion, a pressure is built up and the load is actually supported by the fluid film. This is called hydrostatic cushioning, a special case of the squeeze-film concept. If the load is applied for a short enough period, the two surfaces may not contact. The governing form of the Reynolds equation for this case is

$$\frac{1}{r}\frac{\partial}{\partial r}\left(h^3 r\rho\frac{\partial P}{\partial r}\right) = 12\mu\frac{\partial(\rho h)}{\partial t} \tag{158}$$

For one circular disk approaching another, the flow rate for an incompressible fluid is

$$q = \pi r^2 v$$

where v is the relative velocity of the disk approach. If we assume laminar, viscous flow of the fluid effluxing out the boundary,

$$q = \frac{-2\pi r h^3}{12\mu}\frac{dP}{dr} = \pi r^2 v$$

or

$$dP = -\frac{6\mu v r\, dr}{h^3}$$

$$P = -\frac{3\mu v r^2}{h^3} + C$$

Applying the boundary condition that at $r = R$, $P = 0$ yields

$$P = \frac{3\mu v}{h^3}(R^2 - r^2)$$

This equation is for a paraboloid, for which

$$P_{av} = \frac{P_{max}}{2}$$

and $P = P_{max}$ when $r = 0$. Thus,

$$P_{av} = \frac{3}{2} \frac{\mu v R^2}{h^3}$$

The squeeze-film load can be found from

$$W = \pi R^2 P_{av} = \frac{3\pi\mu v R^4}{2h^3}$$

Observe the functional relations of the variables. Notice the inverse cubic dependence on film thickness.

The squeeze-film time can be found from the load equation after substituting

$$v = -\frac{dh}{dt}$$

Hence,

$$W = -\frac{3\pi\mu R^4}{2h^3} \frac{dh}{dt}$$

$$dt = -\frac{3\pi\mu R^4}{2W} \frac{dh}{h^3}$$

$$t = -\frac{3\pi\mu R^4}{2W} \int_{h_1}^{h_2} \frac{dh}{h^3}$$

$$t = \frac{3\pi\mu R^4}{4W} \left(\frac{1}{h_2^2} - \frac{1}{h_1^2} \right)$$

An example case (castor oil) is

$h_1 = 0.0004064$ cm (0.00016 in.) $\quad \mu = 2.43\times10^{-3}$ N-sec/in.^{2} (5.08×10^{-5} lbf-sec/in.^{2})

$h_2 = 0.0001270$ cm (0.00005 in.) $\quad W = 0.885$ N (0.199 lbf)

The calculated squeeze-film time is 71.6 minutes. This has been verified experimentally. Further discussion of hydrostatic cushioning can be found in references 41 and 42.

Relative sinusoidal vibration of surfaces. - Since the disk vibrates sinusoidally at a frequency ω,

$$h = h_m + e \cos \omega t \tag{159}$$

where e is one-half the amplitude of the movement about a mean film thickness h_m. Equation (159) can be written as

$$h = h_0(1 + \epsilon \cos \omega t) \tag{160}$$

where ϵ is called the excursion ratio,

$$\epsilon = \frac{e}{h_0}$$

To nondimensionalize, let

$$\tau = \omega t$$

$$h^* = \frac{h}{h_m}$$

$$r^* = \frac{r}{R_2}$$

$$P^* = \frac{P}{P_a}$$

Thus, equation (158) becomes

$$\frac{h^{*3}}{r^*}\frac{\partial}{\partial r^*}\left(P^* r^* \frac{\partial P^*}{\partial r^*}\right) = \sigma \frac{\partial (P^* h^*)}{\partial \tau} \tag{161}$$

where $\sigma = 12R^2\mu\omega/h_m^2 P_a$ is the squeeze number.

Salbu (ref. 43) has solved this equation for the pressure distribution and the generated squeeze-film forces. Figure 70 shows the dimensionless squeeze-film force for two excursion ratios ($\epsilon = 0.1$ and $\epsilon = 0.5$) and a squeeze number of 10. For the small excursion ratio ($\epsilon = 0.1$), the variation of the squeeze-film force with time is almost symmetrical, which results in a zero net load when integrated over a cycle of oscillation. At the larger excursion ratio ($\epsilon = 0.5$), the variation is asymmetrical, which gives a corresponding load. Thus, the behavior can be summarized in the following way: If the excursion ratio is small, the fluid is compressed very little and the pressures are almost symmetrical; hence, the net load is zero. However, when the excursion ratio is large, on the downstroke the air is compressed and resists the movement strongly. On the return and upstroke the gas becomes rarefied and offers less resistance. The squeeze-film force is thus highly asymmetrical, and a net load capacity exists over a cycle.

This behavior can be thought of in another way. At a low excursion ratio and/or low frequency the viscous forces predominate over the compressibility forces. Hence, gas moves radially to compensate for the normal motion. On the other hand, for a high excursion ratio and/or high frequency the gas moves very little radially, being compressed and rarefied. Under this condition the movement is very similar to a piston in a closed cylinder. Hence, Boyle's law, PV = Constant, applies.

Consider a simple, squeeze-film, thrust bearing. For high frequency, the film compresses and expands so quickly that there is very little leakage. If the very thin boundary layers near the boundaries are neglected, the P and V satisfy Boyle's law (PV = Constant). Hence,

$$P_+(V + \Delta V) = P_0 V = P_-(V - \Delta V) = \text{Constant}$$

or

$$P = P_+\left(1 + \frac{\Delta V}{V}\right) = P_-\left(1 - \frac{\Delta V}{V}\right)$$

where

$$P_+ = \frac{P_0}{1 + \frac{\Delta V}{V}}$$

and

$$P_- = \frac{P_0}{1 - \frac{\Delta V}{V}}$$

Hence, the average pressure due to expansion and contraction $2\,\Delta V$ is

$$\frac{P_+ + P_-}{2} = \frac{P_0}{2}\left(\frac{1}{1 + \frac{\Delta V}{V}} + \frac{1}{1 - \frac{\Delta V}{V}}\right)$$

$$= \frac{P_0}{2}\frac{\left(1 - \frac{\Delta V}{V} + 1 + \frac{\Delta V}{V}\right)}{\left[1 - \left(\frac{\Delta V}{V}\right)^2\right]}$$

$$= \frac{P_0}{1 - \left(\frac{\Delta V}{V}\right)^2} > P_0$$

and

$$\frac{1}{\left[1 - \left(\frac{\Delta V}{V}\right)^2\right]} = \left[1 - \left(\frac{\Delta V}{V}\right)^2\right]^{-1} = 1 + \left(\frac{\Delta V}{V}\right)^2 + \ldots$$

Thus,

$$P_{av} = P_0\left[1 + \left(\frac{\Delta V}{V}\right)^2 + \ldots\right]$$

This indicates a net pressure buildup to oscillation, which causes change in the volume ΔV. The buildup in mean pressure is a second-order effect in ΔV, as verified from the more sophisticated theory.

The net squeeze-film load can be estimated from (ref. 44)

$$\overline{W} = \frac{R_2^2 P_0 k\pi}{\omega}\left(\frac{1}{\sqrt{1-\epsilon^2}} - 1\right)$$

where $k \simeq 1.15$.

A net squeeze-film force exists for an isothermal gas. However, for a liquid (incompressible fluid), this is theoretically not the case. Since the sonic velocity is infinite, any disturbance of the fluid is instantaneously felt everywhere. Hence, theoretically the liquid will always move radially to compensate for the normal motion. However, squeeze-film bearings have operated successfully with alcohol and water. The reason for a net load is attributed to degasification and/or cavitation of the fluid - a characteristic of real liquids. With a two-phase system, the lowest pressure is not reached, because of the phase change or greater concentration of dissolved gas (fig. 71). Hence, a net load appears. This effect probably occurs in seals and may be a mechanism for obtaining seal-face separation.

Cavitation and Degasification

As seen in the section Flow Between Parallel Plates in Relative Motion, for viscous flow between apparently parallel surfaces, theory predicts no hydrodynamic film. This would indicate rubbing contact. With the formation of a film a load-carrying capability is developed, resulting in a positive separation of the surfaces. Lubricant cavitation has been offered as a possible cause for the generation of this hydrodynamic force.

The common explanation of the cavitation phenomenon is that it occurs when the dynamic conditions at some point in a flowing fluid produce a pressure lower than its vapor pressure. For some liquids, however, the vapor pressures are so low that this explanation of cavitation must be modified. "Cavitation" then results from dissolved gases separating from a solution, which is sometimes called "degasification." Experiments show that the amount of gas dissolved increases with increasing pressure and that the gas is released from the liquid when the pressure decreases. These situations are especially significant for seals as most oils have low vapor pressures. Hence, degasification will be seen to play a key role in generating a hydrodynamic lift force; however, the appearance of bubbles alters the performance of the lubricant as a whole by transforming it to a two-phase fluid. This, in turn, lowers the ability of the fluid to withstand shear stress and to transfer heat effectively. Degradation of the lubricant results. Hence, there is a trade-off. The exact role of cavitation and degasification is still not well understood.

Pressure Development due to Microroughness

Surface roughness on the microscale may be an important mechanism for generating an opening force when the film thickness is of the order of the surface irregularities. The surface irregularities are assumed to cause a pressure gradient in the oil film in the same manner as a pressure gradient is established across a tapered-shoe thrust bearing. The interface of the seal is assumed to have the form shown in figure 72. This is a simplification of the actual roughness pattern. Application of a simplified form of the Reynolds equation

$$\frac{d}{dx}\left(h^3 \frac{dP}{dx}\right) + 6\mu U \frac{dh}{dx} = 0$$

gives the pressure distribution across one of these microsurface wedges.

The sealing surfaces can be idealized into a smooth moving surface and a stationary surface with a roughness pattern, as shown in figure 73. Davis (ref. 45) states that if an idealized seal surface consists of a number of units B'AB (fig. 74) which are rigid, the pressure distribution would be skewed symmetrically about A and, if cavitation effects are neglected, the net lift would be zero. However he states that if the surface is elastic and deforms with pressure, a new form results (fig. 74) and the pressure distribution becomes asymmetrical. The surface now experiences a positive lift expressed by

$$\overline{W} = \frac{\mu U r f 2\pi \overline{R} L}{4h_m^3}$$

where L is the seal radial length, h_m is the mean clearance, $\overline{R}$ is mean seal radius, r is the maximum surface separation, and f is the convergent surface spacing (fig. 73). Davis makes an empirical allowance for the diverging clearance by supposing the lift is generated by the converging gap only.

Anno, Walowit, and Allen (ref. 46), in their experimental investigation of face seals with photoengraved microasperities on one of the faces, observed that a hydrodynamic film with small cavities was established between the seal surfaces (fig. 75). The small cavities began at the downstream side of each asperity and ended at the adjacent upstream asperity. As the formation of the cavities prevents the generation of a hydrodynamic pressure less than cavity pressure, the effect of the cavities on the face-seal flow lies in truncating the negative pressure buildup that otherwise would have balanced the positive pressure buildup in the vicinity of the asperity if the cavities were absent. This gives rise to an asymmetrical pressure distribution whose integrated effect is the development of a hydrodynamic force. Fluids that have low vapor pressures at atmospheric conditions will generally degas the entrained vapor; water may also cavitate.

Pressure Generation due to "Wavy" Surfaces

Hydrodynamic face separation can also be achieved from "wavy" seal surface effects in radial face seals. From lapping of carbon, typically, two or three peaks and valleys are present. The short-bearing form of the Reynolds equation is valid and in polar coordinate form is

$$\frac{\partial}{\partial r}\left(h^3 r \frac{\partial P}{\partial r}\right) = 6\mu r\Omega \frac{dh}{d\theta}$$

By assuming that cavitation occurs where the pressure is subambient and the surfaces are diverging, a net hydrodynamic lift force is calculated. This process has been studied and observed by Stanghan-Batch and Iny (ref. 47) and is illustrated in figure 76. Similar pressure generation can be obtained by diametrically misalined seal faces. Other methods of pressure generation appear in the literature on seals.

BOUNDARY LUBRICATING REGIMES

Many seals rub during operation or during startup and shutdown. The boundary lubricating regime entails rubbing of seal surfaces. Before this regime is discussed, it is advantageous to study some fundamental friction and wear concepts.

Fundamental Friction Concepts

Several basic friction and wear concepts that have been accepted by many investigators are important in understanding the phenomena that occur in lubrication of surfaces in solid contact (boundary lubrication). All surfaces have irregularities (or roughness); however, our common measures of roughness may only define whether a surface is rough on a macroscopic, a microscopic, or an atomic scale. These concepts are based on a microscopic consideration of surface character and usually are essentially independent of the gross geometry of the mechanical parts. References 48 to 50 discuss these concepts in detail.

A primary concept is that surface contact occurs between asperities (or protuberances). It follows that the real area of contact is a minute fraction of the apparent area of contact. (The apparent area of contact is defined as the gross geometry of the mating parts.) As surfaces come into solid contact under light load, very few of the asperities, or high points, may actually touch. With increasing loads, the initial points of contact deform elastically and then plastically, and additional asperities assume a portion of the total load. The local stress of the initial asperities in contact is then at the elastic limit (or yield stress in compression) of the weaker of the materials in contact. Thus, the maximum real surface stress will usually be the yield stress, and increased total load simply increases the real area of contact.

The common laws of friction (Amonton's laws) are usually valid because plastic formation determines the real area of contact. However, they are not valid when deformation is primarily elastic or when the load, materials, and geometry are such that the real and apparent areas of contact are equal. The latter case gives rise to gross plastic flow and results in a "plowing" friction force.

The most widely accepted expression for these concepts has been advanced by Bowden and Tabor (ref. 50). This expression shows that friction coefficient η, which is defined as the ratio of friction force F_η to normal load $\overline{W}$, is equal to the shear strength S of the softer metal in contact divided by the yield strength $\overline{P}$ of the weaker metal in compression. Figure 77 illustrates solid surfaces in contact. Where A_o is the real area of contact, these simple concepts may be related as follows:

$$\eta = \frac{F_\eta}{\overline{W}} = \frac{A_o S}{\overline{W}} = \frac{A_o S}{A_o \overline{P}} = \frac{S}{\overline{P}}$$

Film transfer and reactive coatings. - Thin surface films, such as lubricants or other deposited or reactive coatings, reduce friction by lowering effective shear strength. The important bulk yield strength factor, which determines shear area, is a function only of the base metal substrate so long as the film is very thin. Among the most common surface films important to lubrication are the surface oxides. The type, thickness, and character of such films are a function of the thermal history, chemical kinetics, and thermodynamics of the system; surface temperature is especially important. Figure 78 illustrates the influence of contamination on the friction coefficients for various material combinations.

Nonmetals, such as carbon, can transfer to the mating metal surface. This occurs when a residual surface oxide is present on the metal surface. The carbon bonds to the oxygen of the metal oxide, and transfer occurs during sliding. The end result is carbon sliding on a carbon film and a very desirable compatible situation of low friction and wear exists. (A mechanical lead pencil is a simple example of this transfer film.)

The "wearing in" of a carbon face seal can be thought of as the process in which the carbon transfers a thin film to the mating hard surface. Also a smearing or smoothing of the carbon surface microroughness may be occurring. However, if the mating surface is composed of a metal oxide which is thermodynamically unstable and dissociates, the metal can transfer to the carbon surface. This is generally a function of the temperature and load. The result is metal sliding on a metal film, an undesirable situation. This may be the mechanism involved in cases where carbon does not wear but the mating harder metal surface does.

The energy consumed in friction during sliding of solid surfaces must be dissipated as frictional heat. When the real area of contact is a small fraction of the total surface area, the heat flux at the surface asperities may be extremely high. It has been demon-

strated that surface temperatures of 500° to 1000° C (932° to 1832° F) above the ambient temperature can easily be experienced. With chemical activity a function of temperature, it is apparent that surface reactions will occur preferentially at the local high-temperature areas on the surface asperities. Excessive reactions result in chemical attrition or corrosive wear, so that an optimum chemical activity of the surface must be sought to obtain effective surface protection from both adhesive and corrosive wear.

Reactive coatings play an important role. Many sealed fluids act as lubricants. A typical solid surface in contact with a lubricant is shown in figure 79. Most solid surfaces in an air atmosphere contain films of oxides and adsorbed water. The physical and chemical nature of these films influence the interactions between the lubricant and the solid surface.

Lubricating fluids, such as mineral oils, contain small amounts of materials, such as fatty acids, which have attached polar (head) and hydrocarbon (tail) groups. Some hydrocarbon groups may contain chemically active atoms like sulfur, oxygen, and nitrogen. Also, mineral oils will contain small amounts of dissolved air and water. Additive oils may contain a variety of other elements which can participate in chemical reactions. These active components of lubricating fluids and their interactions with their environment determine lubrication performance.

An ideal mechanism for lubrication by adsorbed films is shown in figure 80, where the interface between two opposing films provides a low-friction shear plane between the sliding surfaces. The actual lubricating film, however, may not be made up entirely of the surface active material but may be a mixture of a surfactant (e.g., fatty acid) and a hydrocarbon of the base fluid. Evidence of the influence the base fluid solvent has on the performance of adsorbed boundary films is shown in figure 81. The lubricating ability is greatest when the polar component and the hydrocarbon carrier have equal chain lengths.

High temperatures from the heat generated by plastic deformation and fluid shear cause the boundary film to desorb, disorient, or melt. This can lead to local adhesion between solid surfaces, as shown in figure 82. Lubricating ability is therefore frequently measured by the temperature at which the coefficient of friction rises (transition temperature). In general, physically and chemically adsorbed boundary films are effective primarily at low and moderate temperatures.

Stick-slip friction. - Stick slip is a phenomenon of friction which is characterized by "jerky" motion and "squealing" noise as one surface is moving relative to the other. Although this phenomenon is not fully understood, it is believed to be a result of small, local, dry, asperity contacts which are subsequently sheared.

Fundamental Wear Concepts

Wear, like friction, can be very complex; however, for the purpose of this discus-

sion, it can be described in a relatively straightforward manner. Perhaps the most useful survey of wear mechanisms was published by Burwell (ref. 51) although other pertinent publications are typified by that of Archard and Hirst (ref. 52). The various types of wear are frequently included in the self-description categories (table IV) of adhesive, corrosive, abrasive, fatigue, erosion, impact chipping, and miscellaneous (e.g., electrical attrition). Usually, adhesive, corrosive, and abrasive wear phenomena are of predominant importance. However, in some applications a seal can experience all these wear modes. Adhesive wear phenomena are particularly dependent on the same factors important to the adhesive concept of friction. This should not necessarily infer, however, that we should expect a direct correlation between wear and friction. Very frequently there is no correlation whatever. The adhesive and abrasive wear mechanisms are illustrated in figure 83.

Difficulties in maintaining an effective lubricating film suggest that adhesive wear is of primary importance. The high ambient and higher interface temperatures achieved in the presence of active materials from either the lubricant or the operating environment also suggest that corrosive wear can present a major problem. Since wear mechanisms are not well understood, wear models are not usually sufficiently general to predict quantitative values.

Wear can be correlated on the basis of the simple theory of adhesive wear as suggested by Burwell, Archard, and others. In this model,

$$\overline{V} = c_w \overline{W} \overline{L}$$

and

$$V = \frac{C_w \overline{W} \overline{L}}{3H}$$

where $\overline{V}$ is the volume of material removed, $\overline{W}$ is the applied load, $\overline{L}$ is the total rubbing distance, c_w is the specific wear rate, C_w is the wear coefficient, and H is the indentation hardness of the softer material in contact. The wear coefficients are found empirically.

Thus, the wear rates are proportional to load and inversely proportional to the hardness or yield stress of the worn material. Generally, wear is more severe in the softer material. Also wear usually increases with temperature. Some speculate that this is due to the decrease in hardness with temperature. Surface contamination also influences the wear coefficients (fig. 84).

Rubbing contact - ultra-thin-film operation. - A broad group of seals operate under non-full-film conditions and fall into the classifications of boundary-lubricated, thin (mixed)-film-lubricated, or dry seals. Operation under these conditions does not lend itself to the straightforward treatment possible with full-film seals. This is because

boundary and thin-film lubrication phenomena involve the physical-chemical properties of the lubricant and the sliding parts. These properties are far more difficult to treat than the purely physical properties considered in full-film lubrication.

Pressure-velocity criteria. - In the absence of any simple accurate analysis, operation under boundary lubricating conditions is frequently analyzed by the P_fV (pressure times velocity) or rubbing-factor method. This method is also used as a performance limit measure for fully lubricated face-seal operation. Although this treatment leaves much to be desired, it is useful if its limitations are kept in mind.

This rubbing-factor analysis generally is not intended to answer the question of how a seal will perform at any given operating condition. It is intended primarily to provide the limiting conditions under which the seal will operate satisfactorily.

The rubbing factor is useful because it is related to two important criteria which can be used to establish limits for acceptable seal performance. These are the allowable operating temperature and the allowable wear rate.

Pressure-velocity-limiting criterion based on heat generation: If a reference temperature such as the ambient temperature is taken as a base, the allowable operating temperature can be expressed in terms of the allowable temperature rise above ambient. This highly simplified approach for temperature rise calculation is aided by referring to figure 85.

The heat generated under steady conditions is given by

$$\tilde{Q}_g = \frac{F_\eta V}{J}$$

Assume heat dissipation depends on the interface temperature rise above ambient:

$$\tilde{Q}_d = kA(T - T_a) = kA\,\Delta T$$

Balance the heat generated with the heat dissipated and solve for the temperature rise:

$$\Delta T = \frac{F_\eta V}{JkA}$$

Note

$$\frac{F_\eta}{A} = \eta P_f$$

Thus,

$$\Delta T = \frac{\eta P_f V}{Jk}$$

Letting ΔT be the maximum allowable temperature rise and assuming a constant coefficient of friction η yield

$$P_f V = \frac{Jk\ \Delta T}{\eta} = \text{Constant}$$

Pressure-velocity-limiting criterion based on wear: From the relation for adhesive wear, the volume of material worn from the contacting surface in figure 86 is given by

$$\overline{V} = C_w A_o \overline{L}$$

Since A_o is related to the hardness by the relation

$$\text{Real area of contact} = A_o = \frac{\overline{W}}{H}$$

$$\overline{V} = \frac{C_w \overline{W}\,\overline{L}}{H}$$

Dividing by A and t and noting that $\overline{V} = Ah'$ and $\overline{L}/t = V$ yield

$$\frac{\overline{V}}{At} = \frac{Ah'}{At} = \frac{C_w \overline{W}\,\overline{L}}{HAt} = \frac{C_w P_f V}{H}$$

If h'/t is the maximum allowable wear rate specified for a particular design and C_w and H are assumed to be constant,

$$P_f V = \frac{h'H}{tC_w} = \text{Constant}$$

Generally, the constant based on allowable wear rate will have a lower value than the corresponding limiting constant based on heat generation. This is generally true for carbon seals.

Pressure-velocity values for various materials: Although manufacturers of bearing and seal materials rate their products in terms of pressure times velocity PV (usually in psi and ft/min), the various PV values are difficult to compare because the exact conditions under which they were obtained are usually not given. The advertised PV ratings of a wide range of materials are plotted against the heat-generation parameter $k\,\Delta T/\eta$ in figure 87. This figure is taken from reference 41.

Permissible values of P_fV may vary with boundary-lubricated, mixed-, and full-film operation. It is important to check and be assured that these values have not been exceeded in an application.

Application of pressure-velocity criteria: Applying the PV approach to a seal usually means that the velocity can be replaced by its equivalent in terms of rotational speed $V = \pi DN$ and the temperature rise can be expressed as

$$\Delta T = \frac{\pi D \eta P_f N}{Jk}$$

If k is assumed to be a constant, the temperature rise of a given-diameter seal will be directly proportional to η and P_fN. This relation is graphically illustrated in figure 88. The larger the friction coefficient, the steeper the surface and the greater the temperature rise for a given value of P_fN (or PV). The maximum temperature rise depends on the material. If the limit is exceeded, surface and internal structural damage may result. This is especially true for elastomeric lip seals.

If the allowable operating temperature is assumed to be fixed, the allowable temperature rise above ambient will be constant and is represented by the line AB. The projection of AB on the base gives CD, which is the P_fN = Constant in P_f and N coordinates.

SEAL MATERIALS

There is a great deal of information available on seal materials from both the technical literature and seal material suppliers. The actual material choice depends on the specific seal type and environment. (Generally, seal types are characterized as contact and clearance seals.) In selecting seal materials such factors as the fluid cleanliness (infiltration of particles, abrasives), the temperature and chemistry of the fluid environment, the lubricating properties of the materials, the lubricating ability of the sealed fluid, and the expected or necessary life of the seal must be considered. An excellent survey of seal materials for specific contact- and clearance-type seals operating in specific environments can be found in reference 53.

Carbon and carbon-graphite combinations are widely used seal materials. Carbon is found in two forms - amorphous and graphitic. Graphitic carbon has excellent boundary lubricating properties (self lubricating) but relatively low strength (low friction but high wear at high loads, and poor abrasion resistance). Amorphous carbon has high strength and hardness but is only a fair lubricant (low wear but higher friction). Hence, a combination of amorphous and graphitic carbon is a useful compromise of self-lubricating properties and relatively high compressive strength. The coefficient of friction at room temperature is about 0.10 to 0.75, and comprehensive strengths are 103 to 276 MN (15 000 to 40 000 psi). Additional useful properties are low density, low elastic modulus (conformability), and resistance to thermal shock and corrosion. Most physical properties of carbon improve with temperature. Experimenters have observed that oxygen and/or water vapor play an important role in the physical behavior of carbon and graphite. The absorbed gases act to reduce friction between the crystallites of the carbon body and those crystallites of the carbon adhering to the mating surface. It is this ability to develop transfer films on opposing materials that gives carbon its excellent friction and wear properties. The overall conclusion (generalizing results) is that the mating material and its surface finish play a major role in the frictional behavior of a carbon. Also load level, speed, and ability to dissipate heat from the mating surface are important.

Since the carbon surface is porous, it can be impregnated with oxidation inhibitors (oxidation being a problem at high temperatures) or treated to prevent air from permeating into the carbon. Treatments are also used to improve the friction and wear properties and the chemical resistivity.

Because carbon has a low modulus of elasticity (about 27 580 MN (4×10^6 psi)), it readily conforms to the mating surface. This property, along with its excellent friction and wear properties, has led some people to call carbon a very "forgiving" material. More information on carbon and graphite is given in reference 54.

CONCLUDING REMARKS

Some fundamentals of fluid sealing have been presented. General fluid-flow equations were developed that are applicable for many fluid seals. Included in this report are seal performance parameters and seal operating regimes. Also discussed are geometry effects, surface deformations, rotation, pressure balancing, mechanisms of seal surface separation, fundamental friction and wear concepts applicable to seals,

seal materials, and pressure-velocity criteria. These fundamentals should enhance understanding of various sealing devices and enable more in-depth investigation of specific seals.

Lewis Research Center,
National Aeronautics and Space Administration,
Cleveland, Ohio, October 2, 1975,
505-04.

APPENDIX A

SYMBOLS

A	cross-sectional area or apparent area of contact, cm^2; $in.^2$
A_o	real area of contact
a	speed of sound, m/sec; ft/sec
B	friction parameter, $4\bar{f}L/D$
C	conversion constant
C_D	flow discharge coefficient
C_L	velocity entrance loss coefficient
C_w	wear coefficient
c_p	specific heat at constant pressure, J/(kg)(K); Btu/(lbm)(^oR)
c_v	specific heat at constant volume, J/(kg)(K); Btu/(lbm)(^oR)
c_w	specific wear rate, cm^3/cm-N; $in.^3$/in.-lbf
D	hydraulic diameter, 2h
D/Dt	material derivative, $\partial/\partial t + u(\partial/\partial x) + v(\partial/\partial z) + w(\partial/\partial y)$
d	diameter, cm; in.
e	eccentricity; or amplitude of normal movement, cm; in.
e'	specific internal energy
F	seal opening force, N; lbf
$\bar{F}$	pressure profile load factor, dimensionless
f	Fanning friction factor, $\tau_w/(\rho u^2/2)$
$\bar{f}$	mean Fanning friction factor
G	flow parameter, $\dot{M}/A$, kg/min/m^2; lbm/sec/m^2
g	acceleration of gravity, m/sec^2; ft/sec^2
H	indentation hardness; or total head loss coefficient
HP	horsepower
h	film thickness (gap), cm; in.
Δh	change in film thickness, μm, mil
h'	mean depth of surface worn away, cm; in.

h_{char}	characteristic film thickness, $\left(h_1^2 h_2^2 / h_m\right)^{1/3}$
h_m	minimum film thickness, cm; in.
i	specific enthalpy
J	heat equivalent of mechanical work conversion factor, 4.184 J/cal (778 ft-lb/Btu)
K	expression defined by eq. (157a); or axial film stiffness
Kn	Knudsen number, λ/h
k	thermal conductivity; or Boltzmann constant
k'	head loss coefficient
L	flow length from entrance to point of choking
$\overline{L}$	total rubbing distance, cm; in.
L_1	length of recess region in step bearing
L_2	length of land region in step bearing
M	Mach number
$\dot{M}$	mass leakage flow rate, kg/min; lbm/min
$\Delta\dot{M}$	change in mass flow
m	molecular weight of gas, kg/kg-mole; lbm/lbm-mole
N	rotational speed, rpm; or number of flow restrictors
$\dot{N}$	molecular flow rate, molecules/sec
N_o	Avogadro number, 6.027×10^{23} molecules/mole
P	static pressure, N/m^2; psi
ΔP	pressure differential, N/m^2; psi
$\overline{P}$	yield strength of material, N/m^2; psi
P_{min}	smaller pressure of two pressure boundary conditions, N/m^2; psi
P_r	normal force, N; lbf
Q	volumetric leakage flow rate, scms; scfm
$\tilde{Q}_d$	heat dissipated, J/sec; Btu/sec
$\tilde{Q}_g$	heat generated, J/sec; Btu/sec
q	volumetric flow rate per unit width, $m^3/sec/m$; $ft^3/min/ft$
R	radius, cm; in.

$\mathscr{R}$ gas constant, $\underline{R}/m$, m-N/(kg)(K); in.-lbf/(lbm)(^{o}R)

$\underline{R}$ universal gas constant, 8.3143 N-m/(mole)(K); 1545.4 ft-lbf/(lbm-mole)(^{o}R)

$\overline{R}$ mean radius, $(R_1 + R_2)/2$, cm; in.

ΔR seal face length

Re leakage-flow Reynolds number in radial direction, $\rho Uh/\mu$

Re_r shear-flow Reynolds number in circumferential direction, $\rho \overline{R} \Omega h/\mu$

r radial direction coordinate

S shear strength of material, N/m^2; psi

s labyrinth knife-edge spacing, cm; in.

T temperature, K; ^{o}F

$\mathscr{T}$ linear tilt factor, $h_2^2(2h_1 + \alpha x)/2h_m(h_1 + \alpha x)^2$

ΔT temperature rise in fluid film, K; ^{o}F

Ta Taylor number

t labyrinth knife-edge thickness, cm; in.; or time, sec

U leakage-flow reference velocity, m/sec; ft/sec

U_1 lower moving surface velocity, m/sec; ft/sec

U_2 upper moving surface velocity, m/sec; ft/sec

u velocity in r-direction or x-direction, m/sec; ft/sec

V reference flow velocity across gap, $U(h/\Delta R)$; or seal rubbing velocity, m/sec; ft/sec

$\overline{V}$ volume of wear, cm^3; $in.^3$

v velocity in z-direction, m/sec; ft/sec

W flow width, cm; in.

$\overline{W}$ normal load, N; lbf

W' reference shear-flow velocity (surface speed due to rotation), m/sec; ft/sec

w velocity in θ-direction or y-direction, m/sec; ft/sec

X body force in x-direction, N/cm^3; $lbf/in.^3$

X_c center of pressure in radial or x-direction, cm; in.

x coordinate in pressure gradient direction

x_e entrance length, cm; in.

Y body force in y-direction, N/cm^3; lbf/cm^3; or expansion function

y distance normal to flow, cm; in.

Z body force in z-direction, N/cm^3; $lbf/in.^3$

α seal-face distortion (relative inclination angle of surface), rad

$\overline{\alpha}$ fluid acceleration

β radial flow factor, W/r; or ratio of nozzle-inlet- to nozzle-exit-flow cross-sectional area in section INVISCID FLOW EQUATIONS; or ratio of exit to inlet film thickness in section Flow Between Flat Converging or Diverging Plates, h_2/h_1

γ specific-heat ratio, c_p/c_v

δ boundary layer thickness, cm; in.

ϵ excursion ratio, e/h_m

η coefficient of Coulomb friction

θ circumferential coordinate

Λ bearing or compressibility number, $6\mu U \Delta R/h^2 P_a$

λ molecular mean free path, cm; in.

μ absolute or dynamic viscosity, $N\text{-}sec/cm^2$; $lbf\text{-}sec/in.^2$

ν kinematic viscosity, m^2/sec; ft^2/sec

ρ density, $N\text{-}sec^2/cm^4$; $lbf\text{-}sec^2/in.^4$

σ squeeze number, $12\mu R^2 W/h_m^2 P_a$

τ shear stress, N/cm^2; psi; or characteristic dimensionless time

φ ratio of inlet to exit film thickness

Ω angular rotational velocity, rad/sec

ω normal relative surface oscillation frequency, Hz

∇^2 Laplacian operator

Subscripts:

a ambient conditions

av average

c cavitation or degasification

char characteristic

F frictional

f	net face contact
HS	hydrostatic
h	based on film thickness
I	inertial
inc	incompressible
L	entrance length
m	mean
max	maximum
min	minimum
r	based on rotational velocity
ref	reference condition
S	spring
SD	sealing dam
s	step location
std	standard conditions
w	wetted surface
x	x-direction
z	z-direction
η	shear force (friction) component
0	sealed (reservoir) conditions
1	entrance conditions
2	exit conditions
3	ambient sump conditions

Superscript:

*	dimensionless quantity; or reference to Mach 1 condition (critical flow)

APPENDIX B

VISCOSITY OF FLUIDS

Viscosity is the property of a substance by which it offers resistance to shear stresses. In a Newtonian fluid, the viscosity is in linear proportion to the ability of the fluid to resist such shear stresses.

All substances, both liquids and gases, have viscosity. Because of this, the property should be explained by one or more physical properties common to all fluids, such as molecular activity. Because of molecular activity, there is a constant interchange of molecules, and therefore of momentum, between adjacent layers of the fluid. If adjacent layers are moving with different velocities, this constant interchange of momentum sets up a resistance to any relative motion of the two layers (fig. 89). As a result of this resistance, energy is transformed into heat; and to maintain the velocity, a steady force is required.

The viscosity of a liquid decreases with an increase in temperature. Unlike other material properties which change slightly with temperature, viscosity is somewhat unique in that, for a liquid, it can change several orders of magnitude with temperature. The temperature range seen by a liquid in a hydrodynamic environment is usually very large; thus, predicting the variations of viscosity with temperature is important. The interchange of momentum is accelerated with an increase in temperature, but the viscosity of a liquid must be regarded as the combined effect of cohesion and interchange of momentum.

Cohesion is the force with which like molecules of a substance attract each other. A change in temperature has opposite effects on cohesion and molecular activity, with the effect of cohesion being more pronounced so that in a liquid as temperature is decreased, viscosity is increased. Because of low cohesive forces in gases, the viscosity of a gas increases with temperature. The viscosities of some liquids and gases are compared in figure 90.

Note the analogy with solids, where Hooke's law relates normal stress with normal strain; for example, Young's modulus is a material property. For fluids the stress is proportional to the strain rate. (When the fluid is not in motion, the shear stresses vanish.)

The simple linear dependence of shear stress on velocity gradient is known as the Newtonian relation. Fluids which behave this way are called Newtonian fluids. Many oils at moderate shearing rates, water, air, and many gases are essentially Newtonian. Thus, the theory is highly developed for these fluids. (All equations and formulas in this text are for Newtonian fluids.)

Seals may use fluids that are not Newtonian. Some fluids are a function not only of velocity gradient but of ordinary strain as well. These fluids are termed "viscoelas-

tic." (Polymer-fortified oils are viscoelastic, especially at high shear rates.) Some fluids are not Newtonian because there may be a rather complicated nonlinear shear stress - strain rate relation. Some greases and sludges behave as solids until an apparent yield stress is exceeded; then they behave as viscous fluids. This is known as plastic behavior. Various shear stress - strain rate relations are depicted in figure 91. Further information on non-Newtonian behavior in seals can be found in reference 2. Understanding of Newtonian behavior can shed light on the physical behavior of non-Newtonian fluids.

APPENDIX C

COMPRESSIBLE FLOW - AN ALTERNATE THEORETICAL APPROACH TO FINDING THE ORIFICE EXPANSION FUNCTION

Consider the adiabatic one-dimensional energy conservation equation. (Again for compressible flow the energy equation must be considered.)

$$e' + \frac{P}{\rho} + \frac{u^2}{2} = \text{Constant}$$

or

$$i_1 + \frac{u_1^2}{2} = i_2 + \frac{u_2^2}{2} = \text{Constant} \qquad \text{(C1)}$$

For an ideal gas,

$$i = c_p T$$

And by neglecting u_1, equation (C1) becomes

$$u_2 = \sqrt{2c_p(T_1 - T_2)}$$

Now

$$c_p = \frac{\gamma \mathcal{R}}{\gamma - 1}$$

Thus,

$$u_1 = \sqrt{\frac{2\gamma \mathcal{R} T_1}{\gamma - 1}\left(1 - \frac{T_2}{T_1}\right)}$$

Since

$$\frac{T_2}{T_1} = \left(\frac{P_1}{P_2}\right)^{(1-\gamma)/\gamma}$$

the exit velocity is

$$u_2 = \sqrt{\frac{2\gamma \mathscr{R} T_1}{\gamma - 1}\left[1 - \left(\frac{P_2}{P_1}\right)^{(\gamma-1)/\gamma}\right]}$$

$$= \sqrt{\frac{2\gamma \mathscr{R} T_1}{\gamma - 1}\left[1 - \left(\frac{P_2}{P_1}\right)^{(\gamma-1)/\gamma}\right]\frac{(P_1 - P_2)}{P_1\left(1 - \frac{P_2}{P_1}\right)}}$$

$$= \sqrt{\frac{2\gamma}{\gamma - 1}\left[1 - \left(\frac{P_2}{P_1}\right)^{(\gamma-1)/\gamma}\right]\frac{\rho_0(P_1 - P_2)}{\rho_0^2\left(1 - \frac{P_2}{P_1}\right)}}$$

$$= \sqrt{2\rho_1(P_1 - P_2)\left(\frac{P_2}{P_1}\right)^{2/\gamma}\left(\frac{\gamma}{\gamma - 1}\right)\frac{\left[1 - \left(\frac{P_2}{P_1}\right)^{(\gamma-1)/\gamma}\right]}{\left(1 - \frac{P_2}{P_1}\right)}}$$

Let

$$Y = \sqrt{\left(\frac{P_2}{P_1}\right)^{2/\gamma}\left(\frac{\gamma}{\gamma - 1}\right)\frac{\left[1 - \left(\frac{P_2}{P_1}\right)^{(\gamma-1)/\gamma}\right]}{\left(1 - \frac{P_2}{P_1}\right)}}$$

Thus, the orifice expansion function is found theoretically. However, in practice, it has been found to generally underpredict the flow rate when a constant discharge coefficient is assumed.

APPENDIX D

DERIVATION OF REYNOLDS LUBRICATION EQUATION[1]

As stated in the main text, load capacity can be built up in a hydrodynamic bearing from both the wedge-film and the squeeze-film actions.

The differential equation that describes hydrodynamic bearing operation relates viscosity, film thickness, pressure, and sliding velocity. This equation was first developed by Osborne Reynolds and is named for him. In the derivation of the Reynolds equation, the following assumptions (also used in deriving the equations in the section Mechanism of Film Pressure Generation Between Relatively Moving Surfaces) were used:

(1) The flow is laminar.

(2) The fluid is Newtonian (Newton's definition of viscosity, Viscosity = Shear stress/Shear rate, holds), and the viscosity is constant across the film.

(3) Inertial forces are small as compared with viscous shear forces and are neglected. (Reynolds number is low.)

(4) The weight of the fluid is negligible compared with other forces.

(5) No slip exists at the fluid-solid interface.

(6) The film thickness is small compared with any radii of curvature.

(7) The pressure across the film is constant.

(8) The inclination of one surface relative to the other is so small that the sine of the angle of inclination can be set equal to the angle and the cosine can be set equal to unity.

Figure 92 shows that the moving member has a tangential velocity U and a normal velocity V.

The coordinate axes are directed as shown, with the origin in the moving member. An infinitesimal volume of fluid, with dimensions dx, dy, and dz in the film, is shown. Pressure forces act on four faces and shear forces act on two faces. There is no net pressure force in the y-direction (assumption 7). Let the fluid particle have velocities u, v, and w in the x-, y-, and z-directions.

If the forces in the x-direction are equated with negligible fluid accelerations,

$$P\,dy\,dz + \left(\tau_x + \frac{\partial \tau_x}{\partial y}\,dy\right)dx\,dz - \left(P + \frac{\partial P}{\partial x}\,dx\right)dy\,dz - \tau_x\,dx\,dz = 0 \tag{D1}$$

$$\frac{\partial P}{\partial x} = \frac{\partial \tau_x}{\partial y} \tag{D2}$$

[1]Appendix is partially derived from ref. 40.

From the definition of viscosity,

$$\mu = \frac{\tau_x}{\frac{\partial u}{\partial y}} \tag{D3}$$

$$\frac{\partial P}{\partial x} = \mu \frac{\partial^2 u}{\partial y^2} \tag{D4}$$

Similarly, in the z-direction

$$\frac{\partial P}{\partial z} = \mu \frac{\partial^2 w}{\partial y^2} \tag{D5}$$

Equations (D4) and (D5) can be integrated with respect to y since pressure P is independent of y. Integrating twice yields

$$u = C_1 + C_2 y + \frac{1}{2\mu} y^2 \frac{\partial P}{\partial x} \tag{D6}$$

$$w = C_3 + C_4 y + \frac{1}{2\mu} y^2 \frac{\partial P}{\partial z} \tag{D7}$$

Specific boundary conditions are used to determine the constants C_1, C_2, C_3, and C_4. In the x-direction, C_1 and C_2 are determined by

$$u = U \quad \text{at} \quad y = 0$$

$$u = 0 \quad \text{at} \quad y = h$$

where h is the thickness of the film at any point. Then

$$u(y) = \frac{(h - y)}{h} U - \frac{y(h - y)}{2\mu} \frac{\partial P}{\partial x} \tag{D8}$$

The variation of the velocity u across the film as given in equation (D8) is the sum of two terms. The first is the linear variation in velocity from the stationary surface at $y = h$ to the surface moving with velocity U at $y = 0$. It is independent of viscosity and

is constant throughout the film. The second term in the velocity distribution is that due to the pressure gradient in the x-direction. The distribution across the film is parabolic and is dependent on viscosity.

In the z-direction, C_3 and C_4 are determined by

$$w = 0 \qquad \text{at} \quad y = 0$$

$$w = 0 \qquad \text{at} \quad y = h$$

Then

$$w(y) = -\frac{y(h - y)}{2\mu} \frac{\partial P}{\partial z} \tag{D9}$$

In the z-direction, the velocity distribution is parabolic and results from the pressure gradient in that direction.

Because the Reynolds equation is essentially a continuity equation, the next step in its derivation is the calculation of flow rates in the film. When a unit width is considered, the flows in the x- and the z-directions, q_x and q_z, are obtained by integration of the velocities u and w over the film thickness:

$$q_x = \int_0^h u \, dy = \frac{Uh}{2} - \frac{h^3}{12\mu} \frac{\partial P}{\partial x} \tag{D10}$$

$$q_z = \int_0^h w \, dy = -\frac{h^3}{12\mu} \frac{\partial P}{\partial z} \tag{D11}$$

If a volume of fluid of cross section dx dz extends across the film of thickness h and an expression is written for the net mass flow out of the volume in the x- and z-directions, this expression must equal the rate of change of mass in the volume (fig. 93):

$$\frac{\partial(\rho q_x)}{\partial x} dx \, dz + \frac{\partial(\rho q_z)}{\partial z} dx \, dz = -\frac{\partial(\rho h)}{\partial t} dx \, dz \tag{D12}$$

where $\partial h/\partial t = V$ is positive when away from the other surface. Substituting for q_x and q_z from equations (D10) and (D11) gives

$$\frac{\partial}{\partial x}\left(\frac{\rho h^3}{12\mu}\frac{\partial P}{\partial x}\right)+\frac{\partial}{\partial z}\left(\frac{\rho h^3}{12\mu}\frac{\partial P}{\partial z}\right)=\frac{1}{2}\frac{\partial(\rho U h)}{\partial x}+\frac{\partial(\rho h)}{\partial t} \tag{D13}$$

Equation (D13) is a general form of the Reynolds equations. It applies for full-film lubrication in many bearing configurations for both compressible and incompressible fluids when the assumptions made in its derivation are valid. Solution of the Reynolds equation for a particular bearing configuration results in an expression for the pressure throughout the film as a function of viscosity, film shape, and velocity. Integration of the pressure over the film area yields the total load supported by the film.

No exact solution of the generalized form of the Reynolds equation given by equation (D13) has been obtained. Approximate solutions for specific conditions have been obtained by the use of infinite series and relaxation techniques, and accurate numerical solutions have been obtained through the use of digital computers. While all these approximate solutions are valuable, they fall far short of a general solution.

The Reynolds equation is readily solvable if it is assumed that the bearing is wide relative to its length (the so-called infinite bearing) or that the bearing is short enough that the pressure-induced circumferential flow is negligible (the short-bearing solution). Dowson (ref. 56) has developed a generalized Reynolds equation for fluid-film lubrication.

REFERENCES

1. Mayer, E. (B. S. Nau, trans.): Mechanical Seals. 2nd ed., Elsevier Pub. Co., 1973.

2. Seals Design Guide: Study of Dynamic and Static Seals for Liquid Rocket Engines. (S-70-1028, General Electric Co.; NAS7-434) NASA CR-109646, 1970.

3. A Glossary of Seal Terms. Publication SP-1, American Society of Lubrication Engineers, 1969.

4. Kay, J. M.: Introduction to Fluid Mechanics and Heat Transfer. Cambridge Press, 1957.

5. Dynamic Sealing: Theory and Practice. Koppers Co., Inc.

6. Pape, J. G.: Fundamental Aspects of Radial-Face Seals. WTHD-17, Technische Hogeschool, Delft (Netherlands), 1969.

7. Schweiger, F. A.: The Performance of Jet Engine Contact Seals. Lubrication Eng., vol. 19, no. 6, June 1963, pp. 232-238.

8. Thomas, R. L.; Parks, A. J.; and Slayton, R. M.: Development of Mainshaft Seals for Advanced Airbreathing Propulsion Systems. (PWA-2996, Pratt & Whitney Aircraft; NAS3-7609) NASA CR-85908, 1967.

9. Zuk, John; and Smith, Patricia J.: Quasi-One-Dimensional Compressible Flow across Face Seals and Narrow Slots. II - Computer Program. NASA TN D-6787, 1972.

10. Tao, L. N.; and Donovan, W. F.: Through-Flow in Concentric and Eccentric Annuli of Fine Clearance with and without Relative Motion of the Boundaries. ASME Trans., vol. 77, no. 11, Nov. 1955, pp. 1291-1301.

11. Zuk, J.: Fluid Mechanics of Noncontacting Gas Film Seals. Ph. D. Thesis, Case-Western Reserve Univ., 1972.

12. Sneck, H. J.: The Effects of Geometry and Inertia on Face Seal Performance - Turbulent Flow. J. Lubr. Tech., ASME Trans., vol. 90, ser. F, no. 2, Apr. 1968, pp. 342-350.

13. Snapp, R. B.: An Analytical Study of Thin Fluid Films in Face Type Seals. U. S. Naval Engineering Experiment Station, 1962.

14. Snapp, R. B.: Theoretical Analysis of Face-Type Seals with Varying Radial Face Profiles. ASME 64-WA/LUB-6, Nov. -Dec. 1964.

15. Gross, William A.: Gas Film Lubrication. John Wiley & Sons, Inc., 1962.

16. Paladini, W.: Static and Rotating Air/Gas Seal Evaluation. CW-WR-70-024F, Curtiss-Wright Corp. (AD-730361; USAAMRDL-TR-71-28), 1971.

17. Zuk, J.: Analysis of Face Deformation Effects on Gas Film Seal Performance. Presented at American Society of Lubrication Engineers, Annual Meeting, Houston, Tex., May 1-4, 1972.

18. Shapiro, Ascher H.: The Dynamics and Thermodynamics of Compressible Fluid Flow. Vol. I, Ronald Press Co., 1953.

19. Milligan, M. W.: Viscoseal Performance with Rarefied-Gas Sealant. (AE-71-023-9; Tennessee Univ., Grant NGR-43-001-023.) NASA CR-120911, 1971.

20. Fluid Meters; Their Theory and Applications. 5th ed., American Society of Mechanical Engineers, 1959.

21. The Aircraft Gas Turbine Engine and Its Operation. Instr. 200, Pratt & Whitney Aircraft Oper., 1960.

22. Egli, A.: The Leakage of Steam through Labyrinth Seals. ASME Trans., vol. 57, no. 3, 1935, pp. 115-122.

23. Brodoia, J. R.; and Osterle, J. F.: Finite Difference Analysis of Plane Poiseuille and Couette Flow Developments. Applied Scientific Research, Sec. A, vol. 10, 1961, pp. 265-276.

24. Kawaguchi, T.: Entrance Loss for Turbulent Flow without Swirl between Parallel Discs. JSME Bulletin, vol. 14, no. 70, Apr. 1971, pp. 355-363.

25. Fleming, David P.; and Sparrow, E. M.: Flow in the Hydrodynamic Entrance Region of Ducts of Arbitrary Cross Section. J. Heat Transfer, vol. 91, no. 3, Aug. 1969, pp. 345-354.

26. Sabersky, Rolf H.; and Acosta, A. J.: Fluid Flow. Macmillan Co., 1964.

27. Lundgren, T. S.; Sparrow, E. M.; and Starr, J. B.: Pressure Drop due to the Entrance Region in Ducts of Arbitrary Cross Section. J. Basic Eng., vol. 86, no. 3, Sept. 1964, pp. 620-626.

28. Deissler, Robert G.: Analysis of Turbulent Heat Transfer and Flow in the Entrance Regions of Smooth Passages. NACA TN 3016, 1953.

29. Hinze, J. O.: Turbulence: An Introduction to Its Mechanism and Theory, McGraw-Hill Book Co., Inc., 1959, p. 27.

30. Daily, J. W.; and Nece, R. D.: Chamber Dimension Effects on Induced Flow and Frictional Resistance of Enclosed Rotating Disks. J. Basic Engr., Trans. ASME, ser. D, vol. 82, no. 1, Mar. 1960, pp. 217-232.

31. Ketola, H. N.; and McGrew, J. M.: Theory of the Partially Wetted Rotating Disk. Proc. Third Intern. Conf. on Fluid Sealing, B. S. Nau, H. S. Stephens, and A. L. King, eds., British Hydromechanics Research Assoc., 1967, pp. H4-69 to H4-94.

32. Theodorsen, Theodore; and Reigier, Arthur: Experiments on Drag of Revolving Disk, Cylinders, and Streamline Rods at High Speeds. NACA Rep. 793, 1944.

33. Lance, G. N.; and Rogers, M. H.: The Axially Symmetric Flow of a Viscous-Fluid between Two Infinite Rotating Disks. Proc. Roy. Soc., vol. 266, ser. A, no. 1324, Feb. 1962, pp. 109-121.

34. Vohr, J. H.: Analysis of Turbulent Lubrication. Volume 2: An Experimental Study of Vortex Flow and Turbulence in Concentric and Eccentric Annuli. (MTI-64TR20; MTI-24(1-63), Mechanical Technology, Inc.; (NASw-771) NASA CR-54034, 1964.

35. Taylor, G. I.: Stability of a Viscous Liquid Contained between Two Rotating Cylinders. Phil. Trans. Roy. Soc. (London), ser. A, vol. 223, 1923, pp. 289-344.

36. Kaye, Joseph; and Elgar, E. C.: Modes of Adiabatic and Diabatic Fluid Flow in an Annulus with an Inner Rotating Cylinder. Trans. ASME, vol. 80, 1958, pp. 753-765.

37. Yamada, Yutaka: Resistance of a Flow through an Annulus with an Inner Rotating Cylinder. JSME Bulletin, vol. 5, no. 18, 1962, pp. 302-310.

38. Zuk, J.; and Ludwig, L. P.: Analysis of Rotational Effects on Compressible Viscous Flow across Shaft Face Seals. Lubrication Eng., vol. 28, no. 3, March 1972, pp. 82-92.

39. NASA Contributions to Fluid-Film Lubrication. NASA SP-5058, 1969.

40. Bisson, E. E.; and Anderson, W. J.: Advanced Bearing Technology. NASA SP-38, 1964.

41. Standard Handbook of Lubrication Engineering. McGraw-Hill Book Co., Inc., 1968.

42. Fuller, Dudley D.: Theory and Practice of Lubrication for Engineers. John Wiley & Sons, Inc., 1956.

43. Salbu, E. O. J.: Compressible Squeeze Films and Squeeze Bearings. Basic Eng., ASME Trans., ser. D, vol. 86, no. 1, Mar. 1964, pp. 355-366.

44. Cameron, Alastair: The Principles of Lubrication. John Wiley & Sons, Inc., 1966.

45. Davis, M. G.: The Generation of Lift by Surface Roughness in a Radial Face Seal. Proc. First Intern. Conf. on Fluid Sealing, British Hydromechanics Research Assoc., 1961, paper C4.

46. Anno, J. N.; Walowit, J. A.; and Allen, C. M.: Microasperity Lubrication. ASME Paper 67-WA/Lub-1, Nov. 1967.

47. Stanghan-Batch, B.; and Iny, E. H.: A Hydrodynamic Theory of Radial-Face Mechanical Seals. J. Mech. Engr. Sci., vol. 15, no. 1, Feb. 1973, pp. 17-24.

48. Buckley, D. H.: Friction, Wear, and Lubrication in Vacuum. NASA SP-277, 1971.

49. Rabinowicz, E.: Friction and Wear of Metals. Metals Eng. Quart., May 1967, pp. 4-8.

50. Bowden, Frank P.; and Tabor, D.: Friction and Lubrication of Solids. Oxford University Press, 1954.

51. Burwell, John T., Jr.: Survey of Possible Wear Mechanisms. Wear, vol. 1, no. 2, Oct. 1957, pp. 119-141.

52. Archard, J. F.; and Hirst, W.: The Wear of Metals under Unlubricated Conditions. Proc. Roy. Soc. (London), ser. A, vol. 236, no. 1206, Aug. 2, 1956, pp. 397-410.

53. Ruthenberg, M. L.: Mating Materials and Environment Combinations for Specific Contact and Clearance-Type Seals. ASLE Preprint Paper 72AM-23, May 1972.

54. Paxton, R. R.: Carbon and Graphite Materials for Seals, Bearings, and Brushes. Electrochem. Tech., vol. 5, no. 5-6, May-June, 1957, pp. 174-182.

55. Compressed Gas Handbook, NASA SP-3045, 1969.

56. Dowson, D.: A Generalized Reynolds Equation for Fluid-Film Lubrication. Intern. J. Mech. Sci., vol. 4, 1962, pp. 159-170.

TABLE I. - OTHER NAMES FOUND IN THE LITERATURE FOR GEOMETRIC BALANCE RATIO (OR MODULUS) AND PRESSURE PROFILE LOAD FACTOR

(a) Geometric balance ratio (or modulus), which is the ratio of hydrostatic closing area to seal-face area

Alternative name	Reference
Area ratio	1
Balance factor[a] (used by some seal manufacturers)	6
Pressure balance ratio (or modulus)	---

(b) Pressure profile load factor $\overline{F}$, which is the ratio of sealed-pressure opening force to sealed-pressure force; or pressure profile factor, which is the ratio of net or average seal-face pressure to sealed-pressure differential

Balancing modulus	---
Flow coefficient	7
Load ratio	6
Pressure form factor	8
Dimensionless form	9

[a]Ref. 6 also defines a complement to unity which is called the degree of balance.

TABLE II. - COMPARISON OF FUNCTIONAL DEPENDENCE OF MASS LEAKAGE FLOW RATE FOR LAMINAR AND TURBULENT FLOW

Laminar flow	Turbulent flow
h^3	$h^{12/7}$
W	W
μ^{-1}	$\mu^{-1/7}$
ρ	$\rho^{4/7}$
L^{-1}	$L^{-4/7}$
$P_1 - P_2$	$(P_1 - P_2)^{4/7}$

TABLE III. - MASS LEAKAGE FLOW RATE EQUATIONS FOR VARIOUS QUASI-FULLY-DEVELOPED (SUBSONIC) FLOW RATE SITUATIONS

Case	Laminar flow	Turbulent flow
Constant area, parallel surfaces	$\dot{M} = \frac{Wh^3\left(P_1^2 - P_2^2\right)}{24\mu\mathscr{R}T(R_2 - R_1)}$	$\dot{M} = \frac{Wh^{12/7}\left(P_1^2 - P_2^2\right)^{4/7}}{2^{3/7}(0.079)^{4/7}\mathscr{R}^{4/7}T^{4/7}\mu^{1/7}(R_2 - R_1)^{4/7}}$
Radial flow	$\dot{M} = \frac{h^3\left(P_2^2 - P_1^2\right)}{12\mu\mathscr{R}T \ln \frac{R_1}{R_2}}$	$\dot{M} = \frac{3^{4/7}h^{12/7}\left(P_1^2 - P_2^2\right)^{4/7}}{2(0.079)^{4/7}\mu^{1/7}\mathscr{R}^{4/7}T^{4/7}\left(\frac{1}{R_1^{3/4}} - \frac{1}{R_2^{3/4}}\right)^{4/7}}$
Small linear deformations ($h = h_1 + \alpha x$) and constant width	$\dot{M} = \frac{Wh_{char}^3\left(P_1^2 - P_2^2\right)}{24\mu\mathscr{R}T(R_2 - R_1)}$	$\dot{M} = \frac{Wh_{char}^{12/7}\left(P_1^2 - P_2^2\right)^{4/7}}{2^{3/7}(0.079)^{4/7}\mu^{1/7}\mathscr{R}^{4/7}T^{4/7}(R_2 - R_1)^{4/7}}$

TABLE IV. - TYPES OF WEAR (FROM REF. 40)

Type of wear	Example
Adhesive	Interface welds
Corrosive	Chemical surface reactions
Abrasive	Rough surface and free-particle cutting
Fatigue	Subsurface repetitive-shear-stress failure
Erosion	Impact displacement by fluid (possible with entrained solids)
Impact chipping	Solid-surface-impact stress failure
Miscellaneous	Electrical attrition and other phenomena

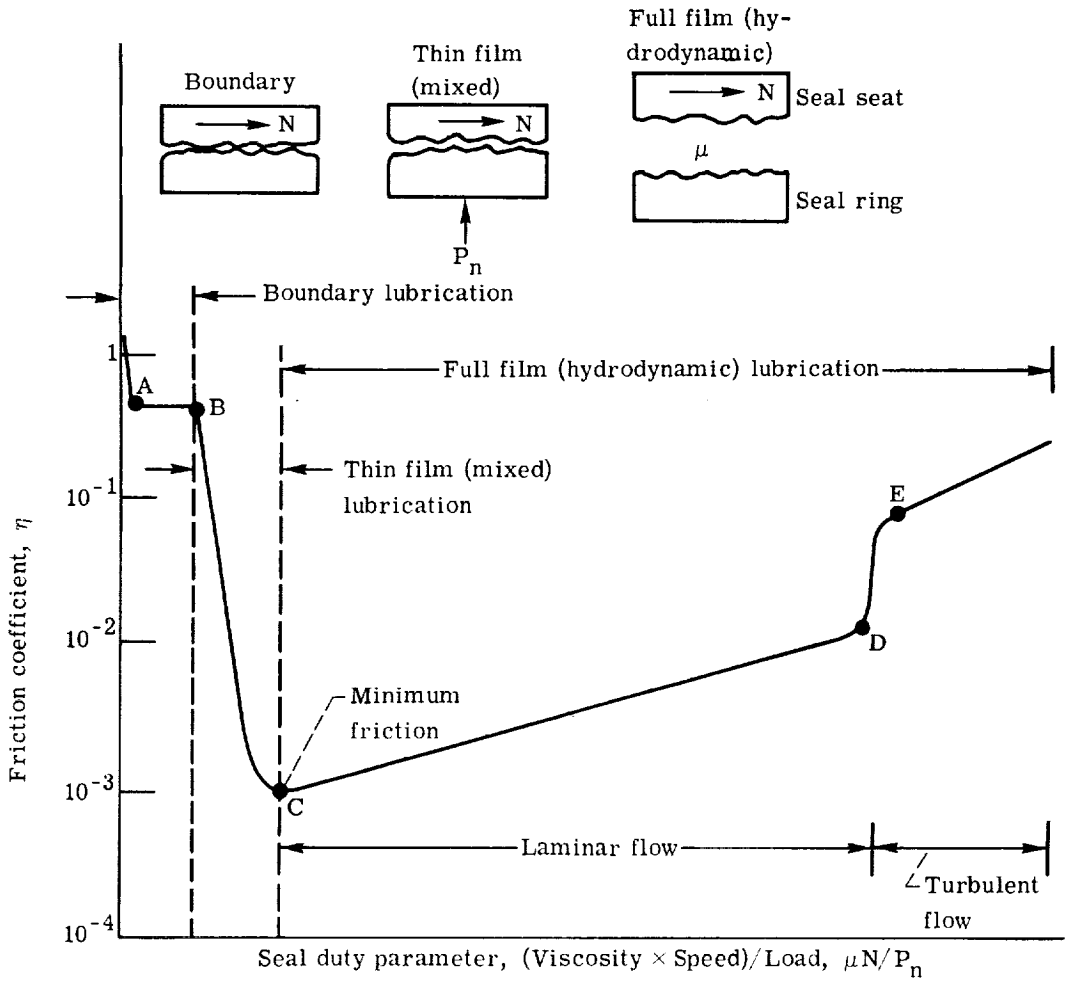

Figure 1. - Variation of friction coefficient with liquid lubrication.

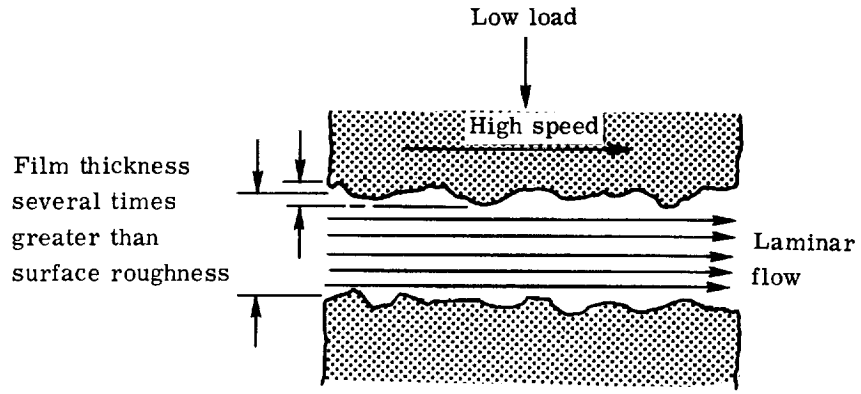

(a) Full-film (hydrodynamic) lubrication.

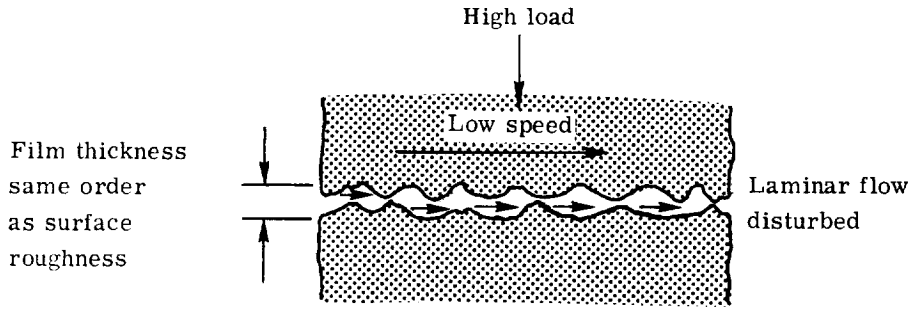

(b) Thin-film (mixed-film) lubrication.

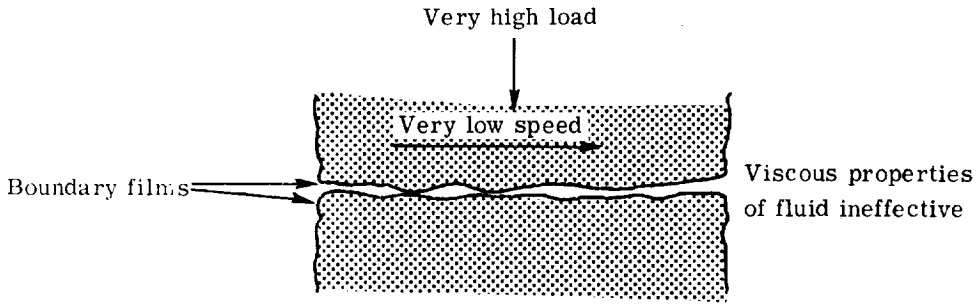

(c) Boundary lubrication.

Figure 2. - Hydrodynamic, thin-film, and boundary lubrication modes.

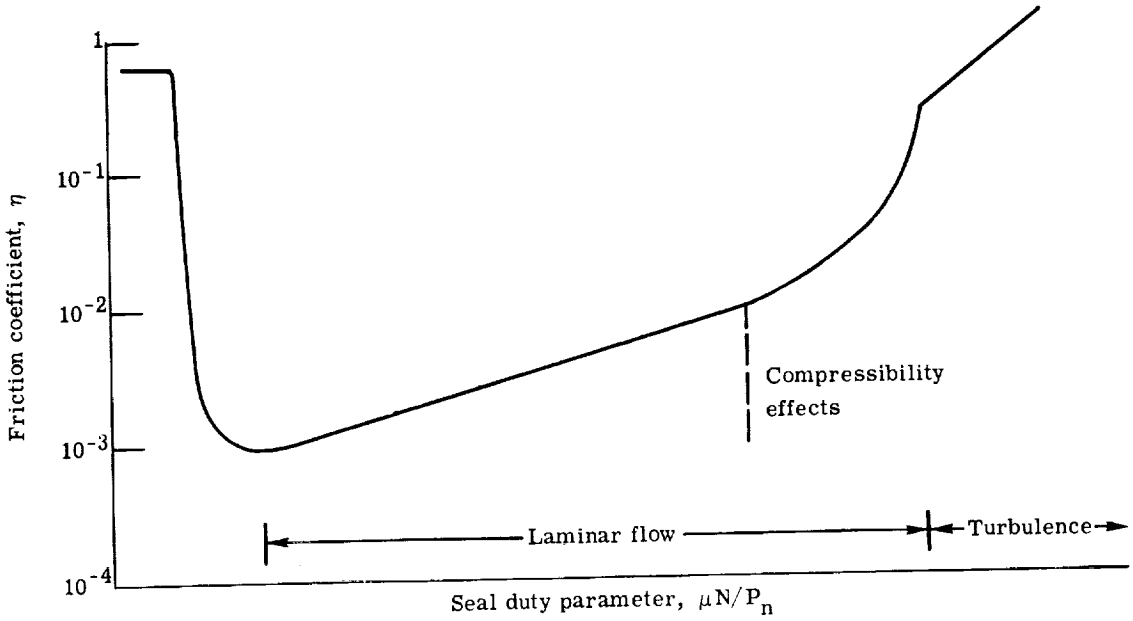

Figure 3. - Variation of friction coefficient for gas lubrication, compared with liquid lubrication.

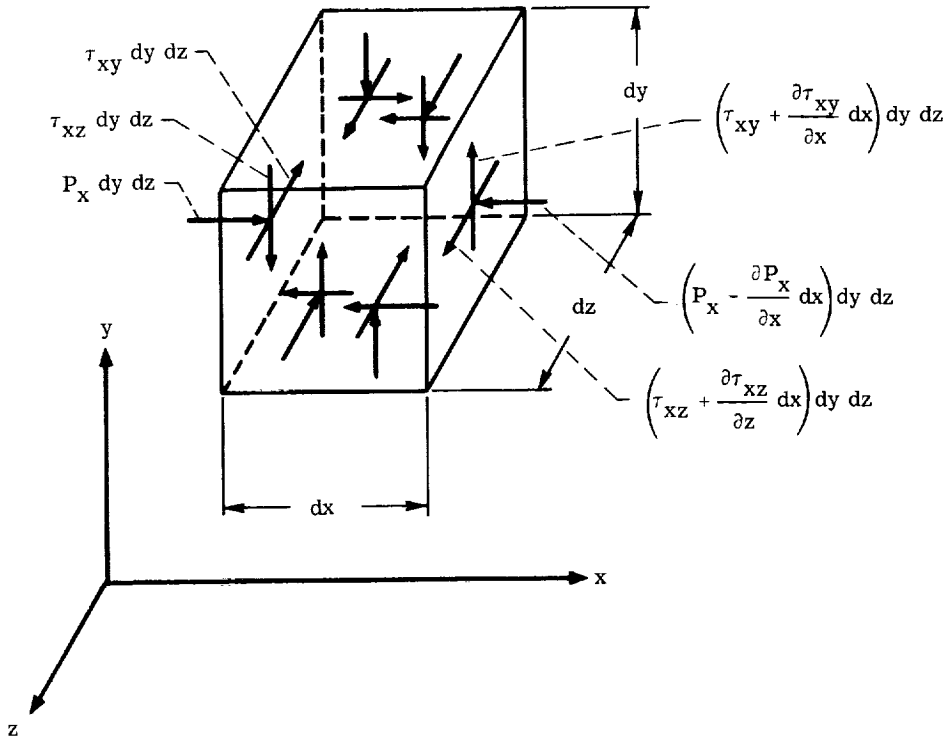

Figure 4. - Stressed element in fluid film. (From ref. 5.)

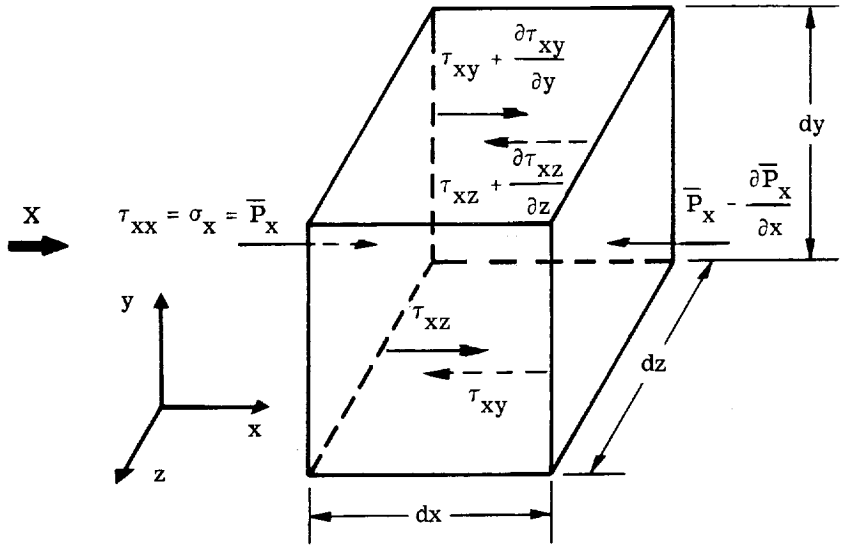

Figure 5. - Elemental volume forces acting in x-direction, where symmetry of stress tensor is denoted by $\tau_{zx} = \tau_{xz}$ and $\tau_{yx} = \tau_{xy}$.

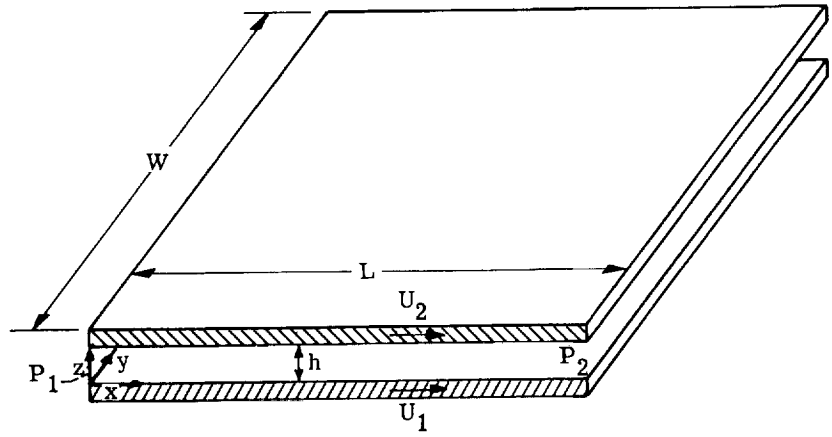

Figure 6. - Model of flow between narrowly spaced parallel plates, where $L >> h$.

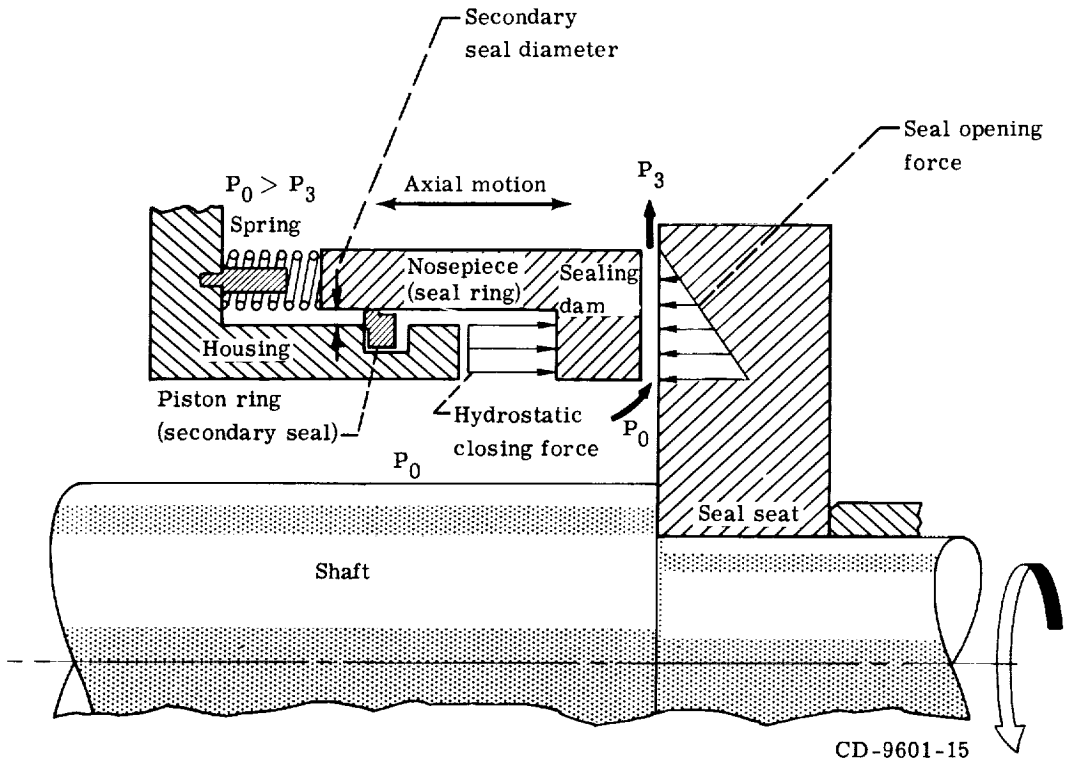

Figure 7. - Pressure-balanced face seal (no axial film stiffness).

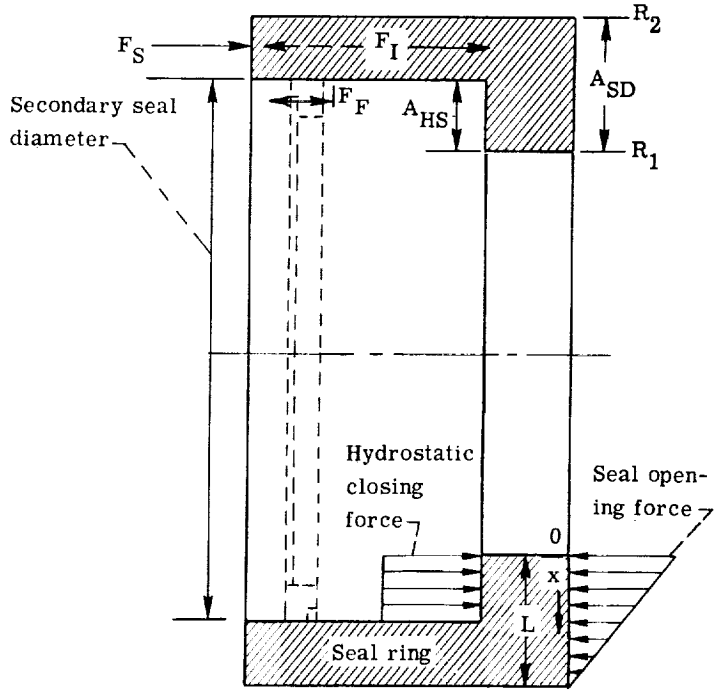

Figure 8. - Radial face seal, identifying nomenclature.

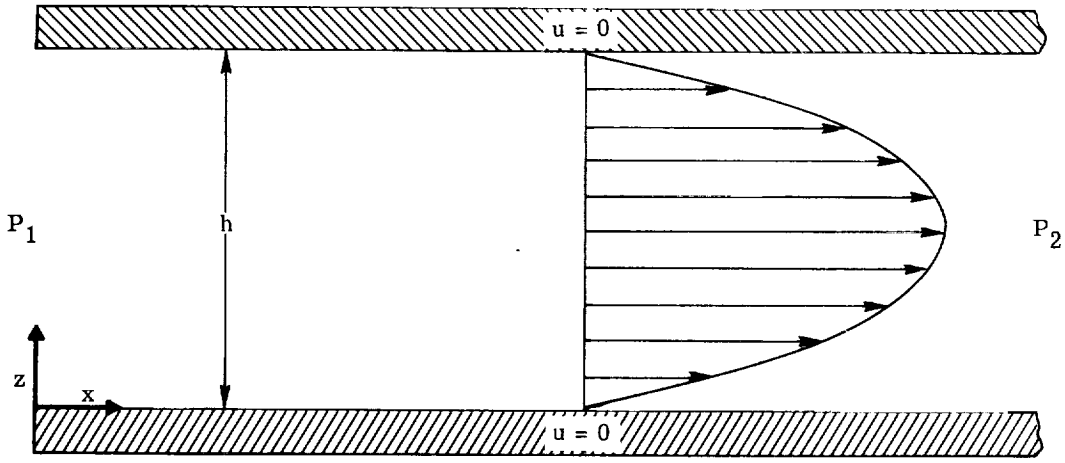

Figure 9. - Plane Poiseuille flow velocity profile, where $u = \frac{1}{2\mu}\frac{dP}{dx}(z^2 - hz)$.

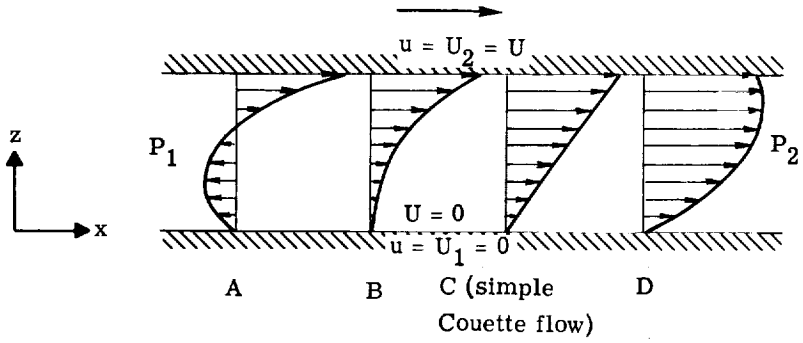

$$\frac{dP}{dx} > 0 \qquad \frac{dP}{dx} > 0 \qquad \frac{dP}{dx} = 0 \qquad \frac{dP}{dx} < 0$$

$$\left.\frac{du}{dz}\right|_{z=0} < 0 \qquad \left.\frac{du}{dz}\right|_{z=0} = 0 \qquad \left.\frac{du}{dz}\right|_{z=0} > 0 \qquad \left.\frac{du}{dz}\right|_{z=0} > 0$$

Figure 10. - General Couette flow velocity profiles, where $u = \frac{1}{2\mu}\frac{dP}{dx}(z^2 - hz) + \frac{Uz}{h}$.

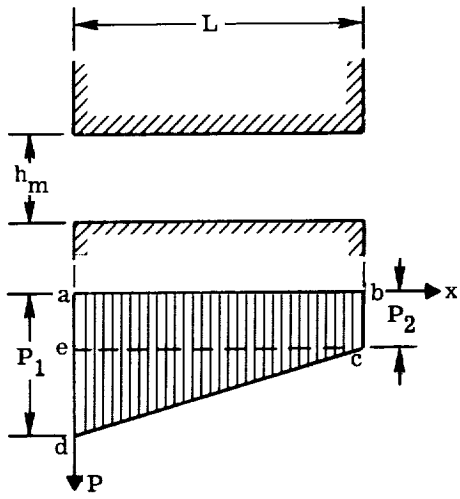

Figure 11. - Pressure profile due to flow between parallel plates.

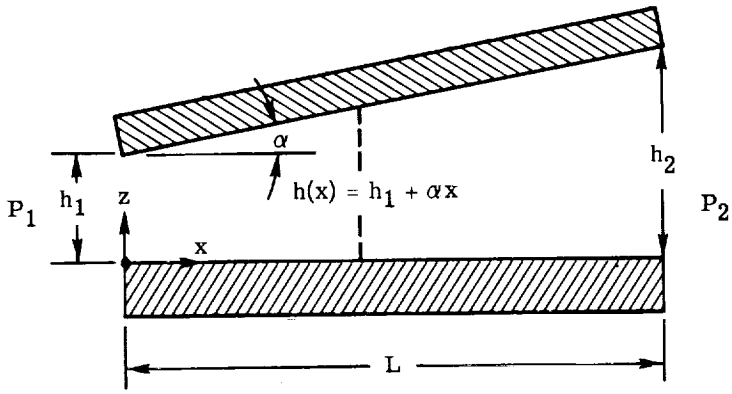

Figure 12. - Model of tapered seal face. (Taper is exaggerated).

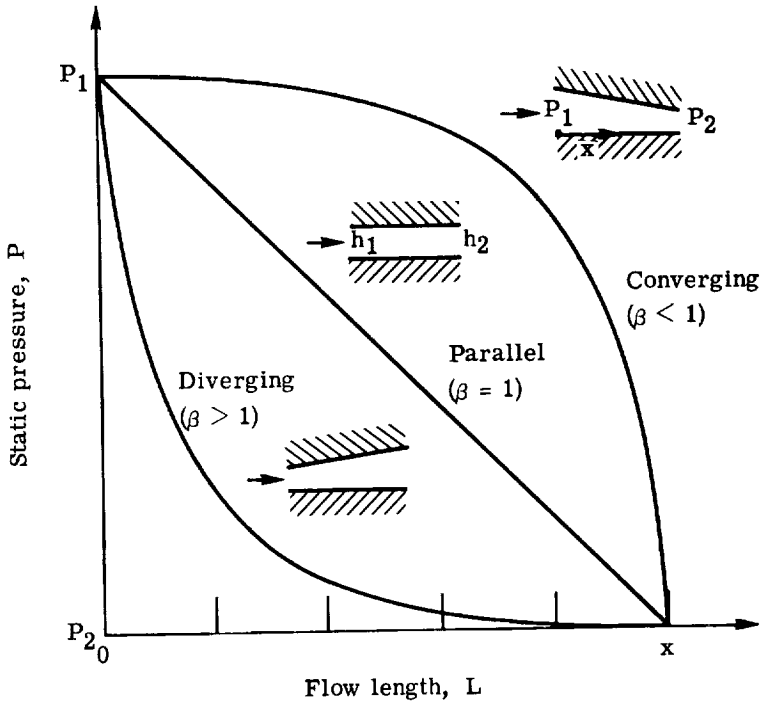

Figure 13. - Representative pressure profiles for various surface conditions, where β is ratio of exit to inlet film thickness, h_2/h_1.

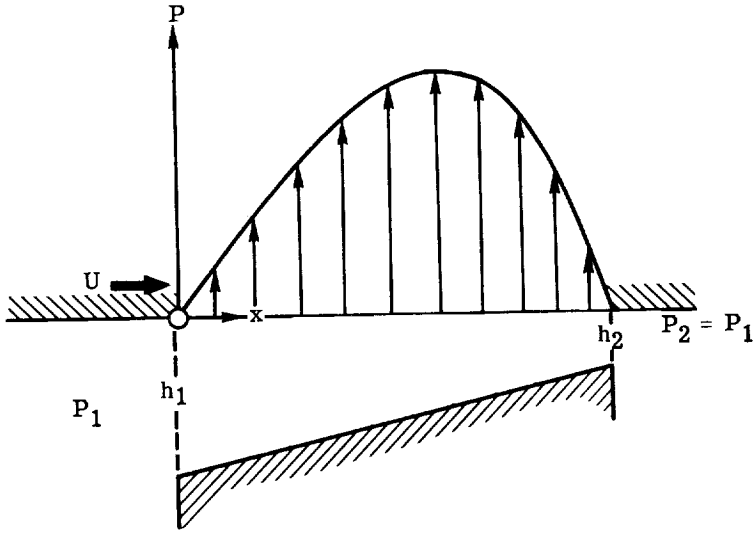

Figure 14. - Linear converging surfaces of a simple slider bearing in relative motion, illustrating pressure distribution.

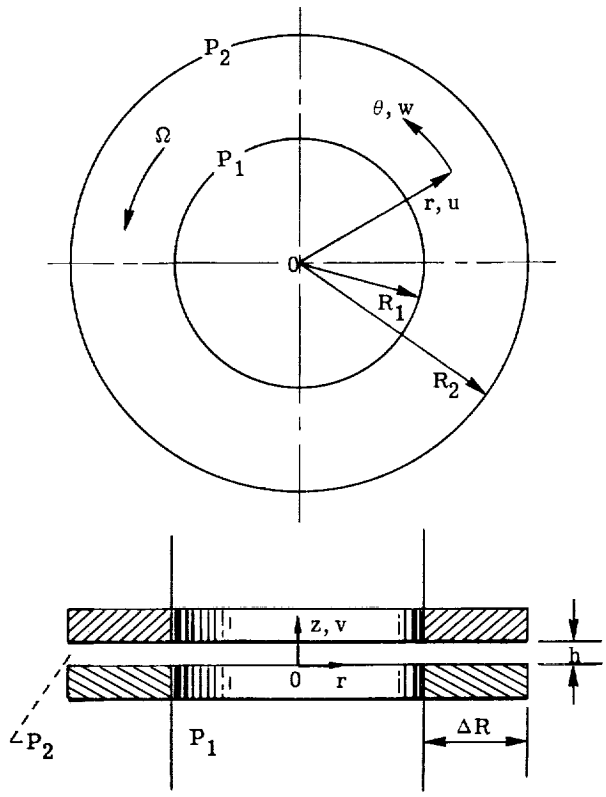

Figure 15. - Model of flow between annular disks.

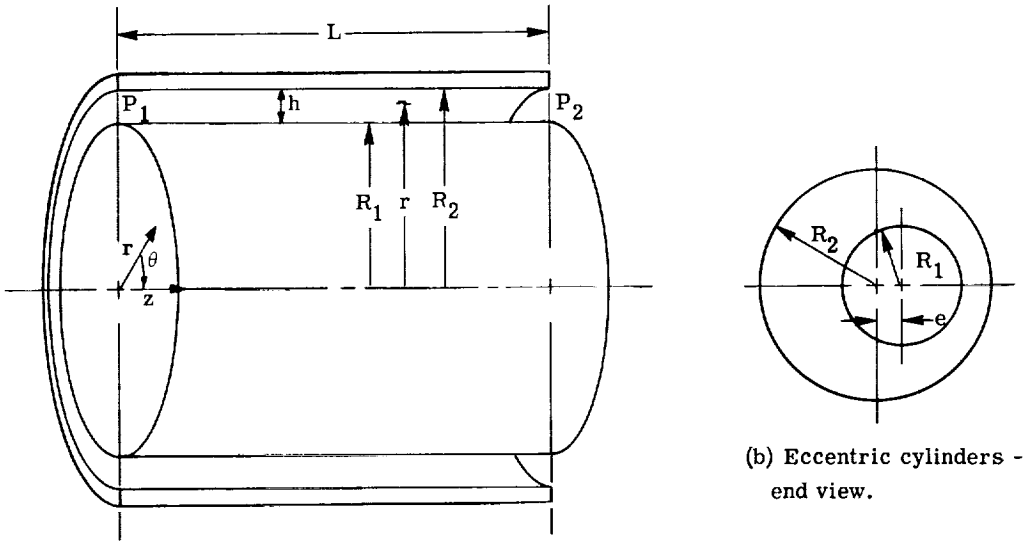

(a) Concentric cylinders.

(b) Eccentric cylinders - end view.

Figure 16. - Model of flow between annular cylinders.

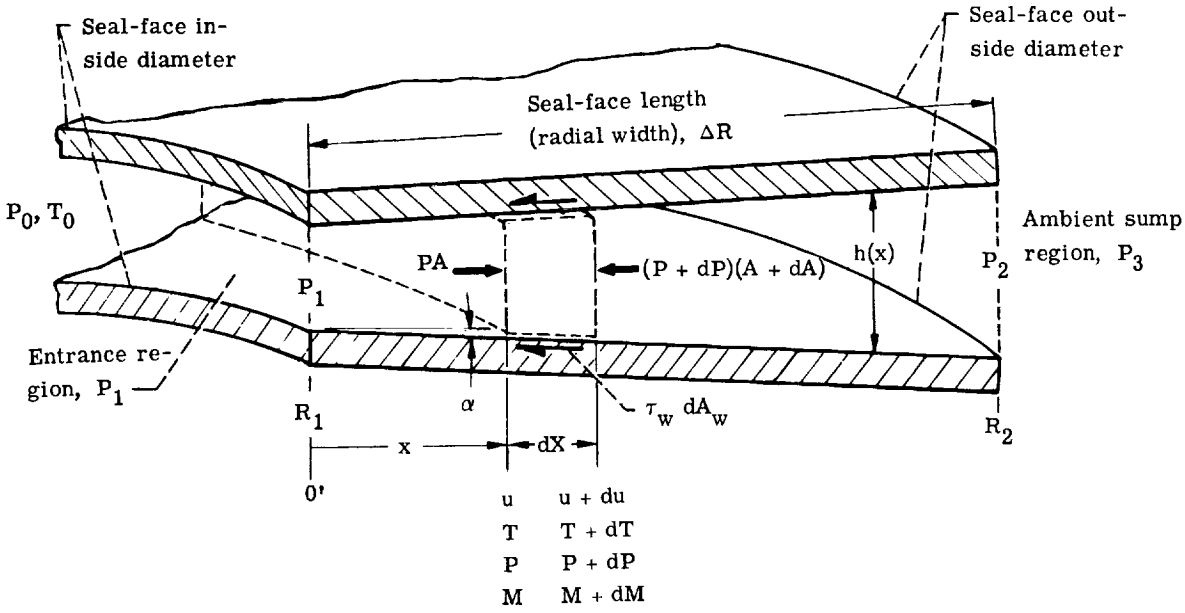

Figure 17. - Model of seal faces, showing notation and including control volume for quasi-one-dimensional flow with area change.

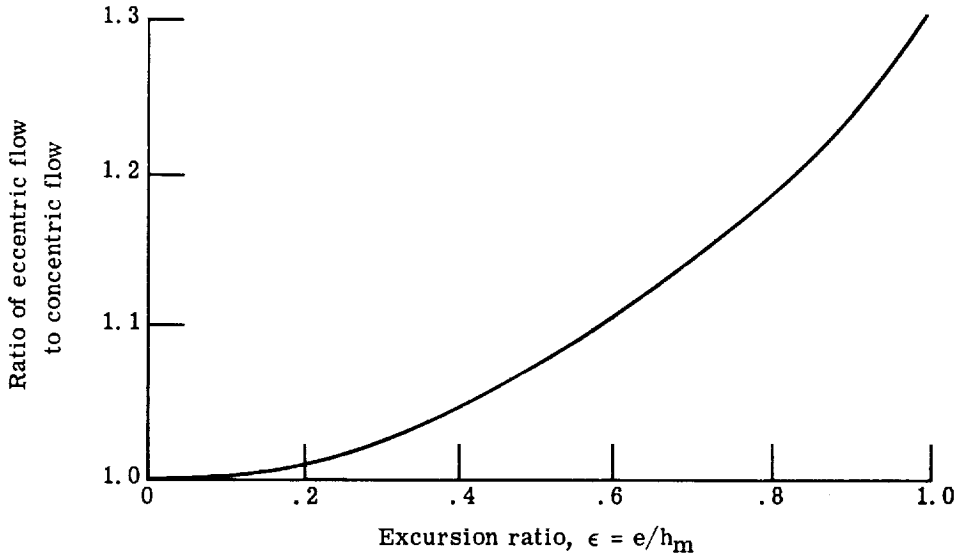

Figure 18. - Effect of eccentricity on turbulent flow. (From ref. 10).

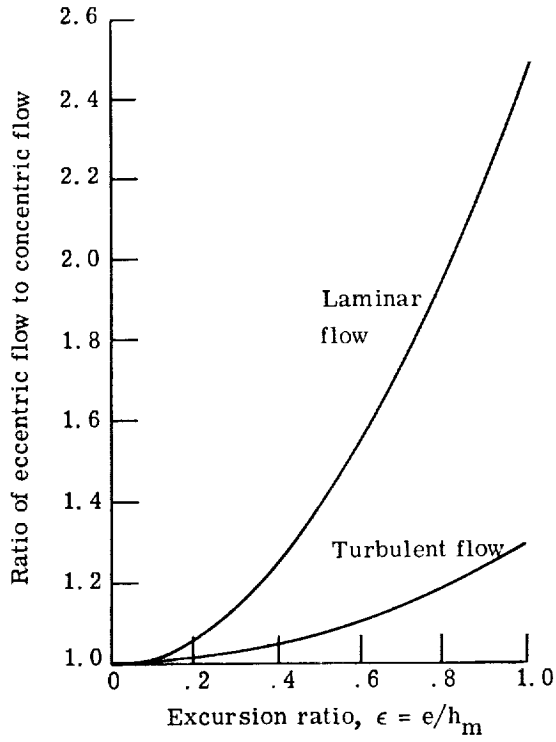

Figure 19. - Comparison of effect of eccentricity on laminar and turbulent flow. (From ref. 10.)

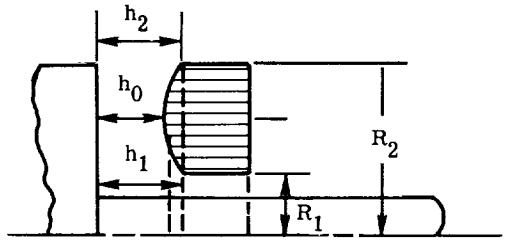

(b-1) Symmetrical ($\Delta h = h_1 - h_0 = h_2 - h_0$; $h_{min} = h_0$).

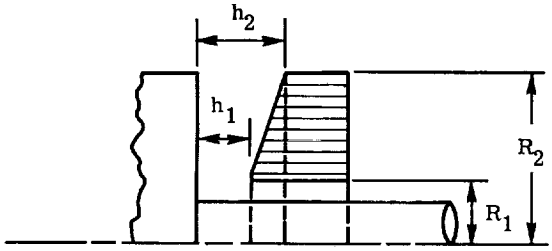

(a-1) Converging ($\Delta h = h_2 - h_1 > 0$; $h_{min} = h_1$).

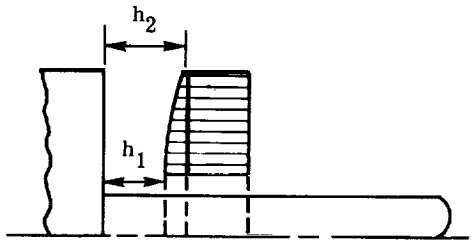

(b-2) Convex ($\Delta h = h_2 - h_1$; $h_{min} = h_1$).

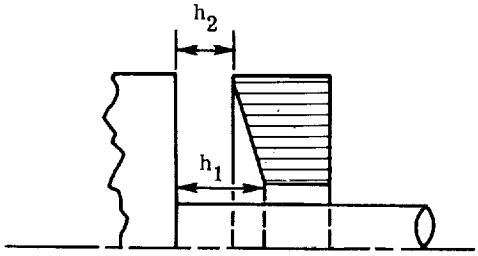

(a-2) Diverging ($\Delta h = h_2 - h_1 < 0$; $h_{min} = h_2$).

(a) Linear face contours.

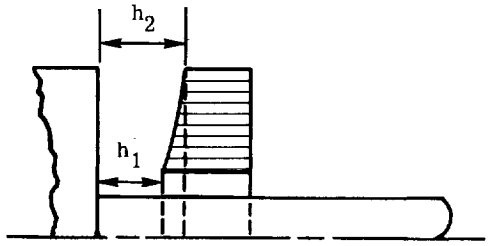

(b-3) Concave ($\Delta h = h_2 - h_1$; $h_{min} = h_1$).

(b) Parabolic face contours.

Figure 20. - Seal-face contours studied by Snapp (ref. 14). (Analytical film thickness expressions are given in ref. 14.)

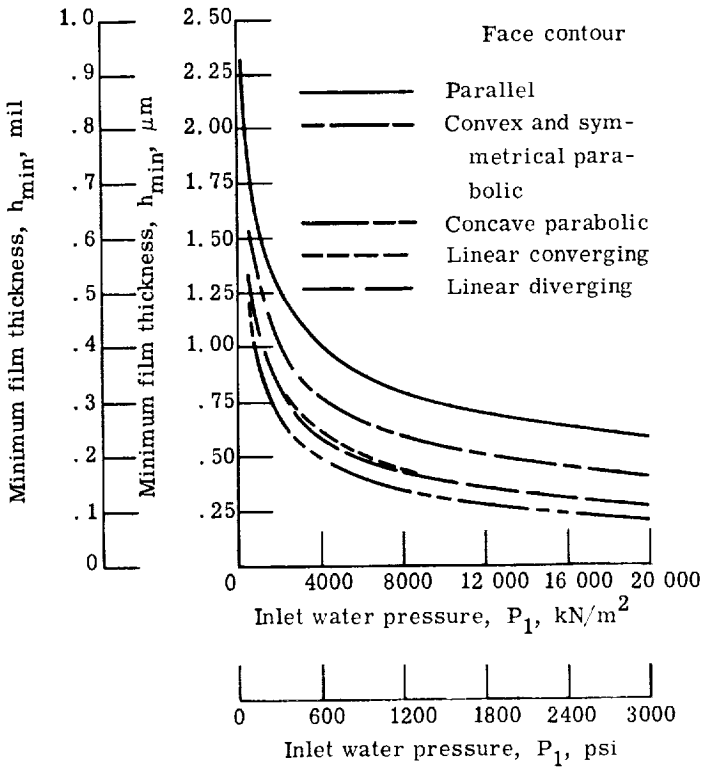

Figure 21. - Minimum film thickness as function of inlet water pressure for various face contours. Leakage flow rate, Q, 0.0019 m^3/min (0.5 gal/min); change in film thickness, Δh, 12.7 μm (0.0005 in.). (From ref. 14; revised.)

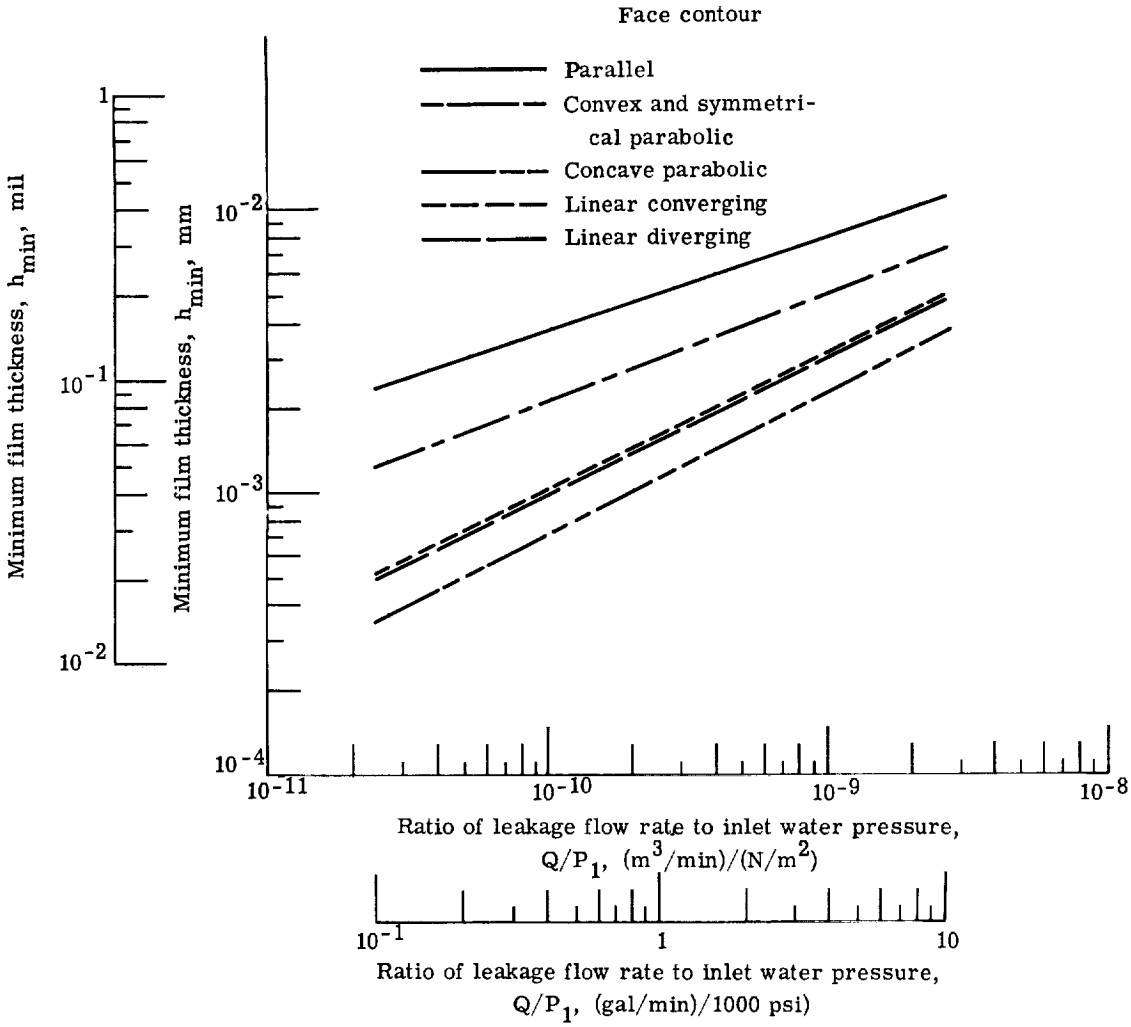

Figure 22. - Minimum film thickness as function of ratio of leakage flow rate to inlet water pressure for various face contours. (From ref. 14; revised.)

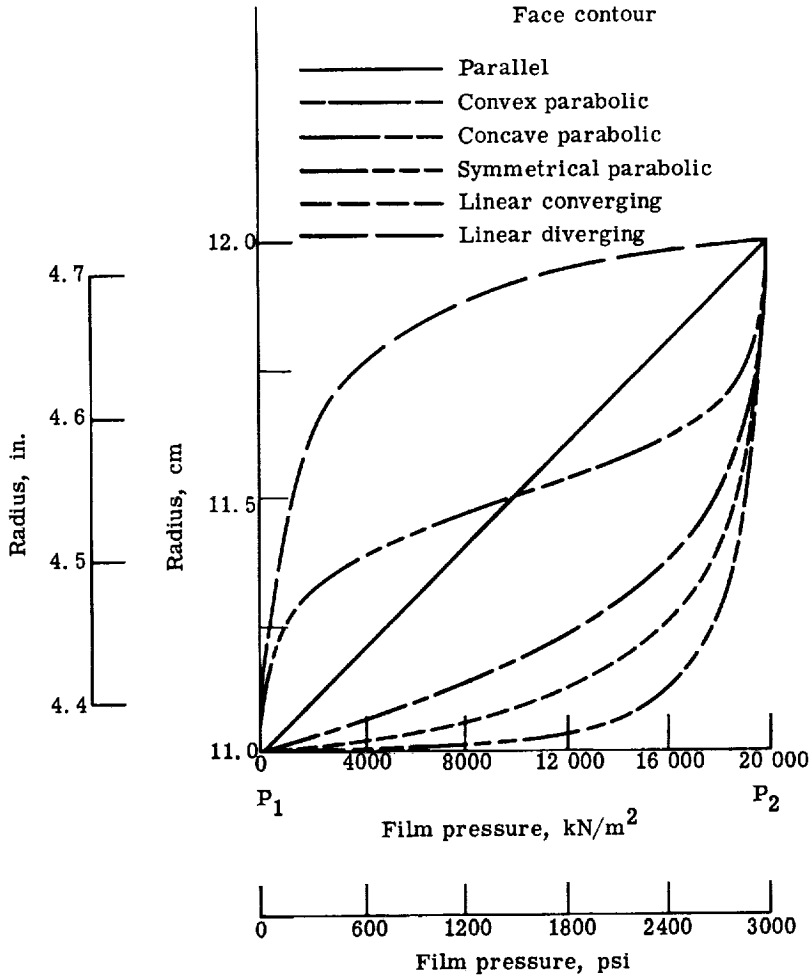

Figure 23. - Radial pressure profiles for various face contours. (From ref. 14; revised.)

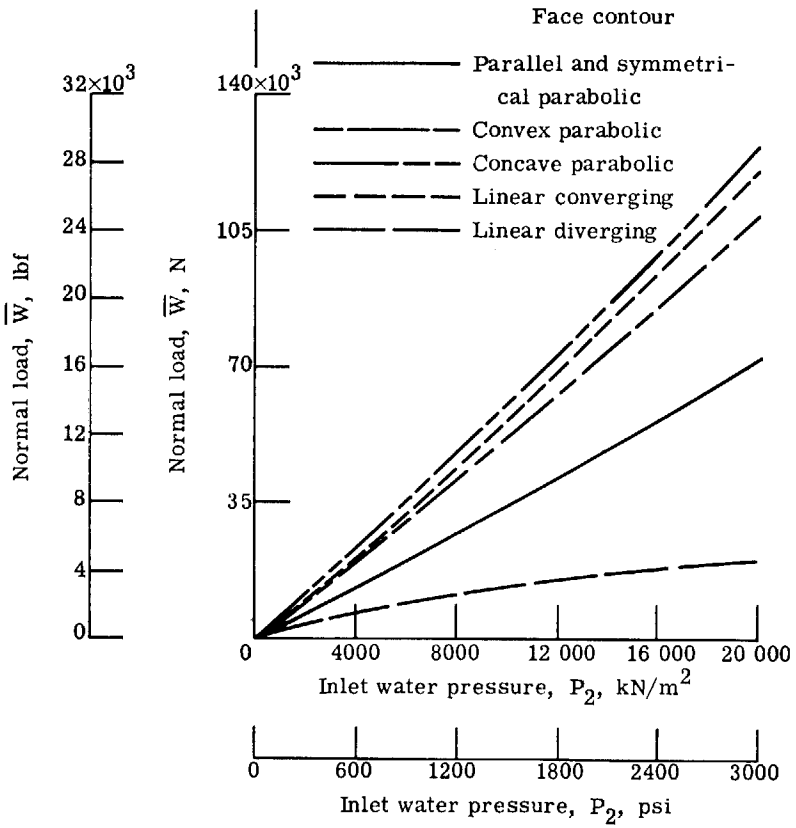

Figure 24. - Seal-face load as function of inlet water pressure for various contours. Constant leakage flow rate and constant film thickness. (From ref. 14; revised.)

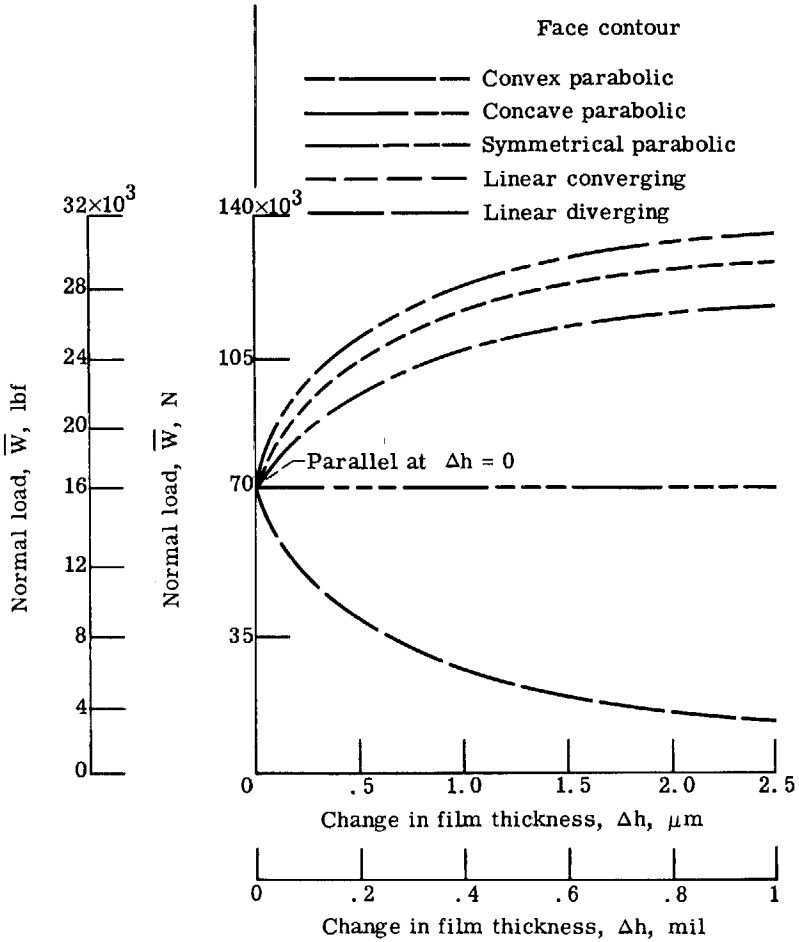

Figure 25. - Seal-face load as function of change in film thickness for various face contours. Constant exit pressure; constant leakage flow rate. (From ref. 14; revised.)

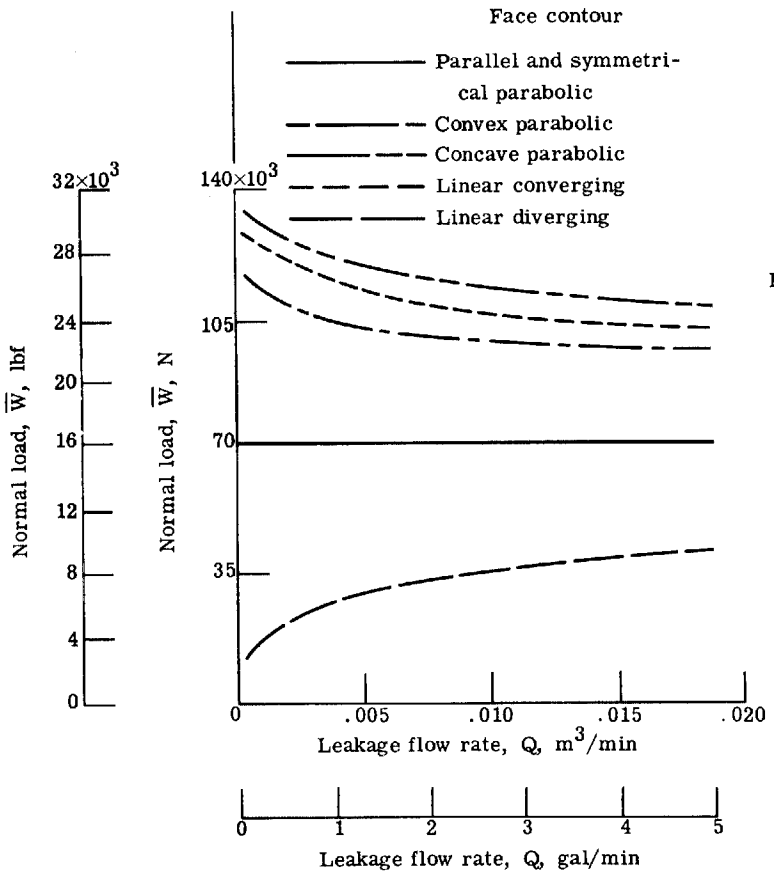

Figure 26. - Seal face load as function of leakage flow rate for various face contours. Constant exit pressure; constant film thickness. (From ref. 14; revised.)

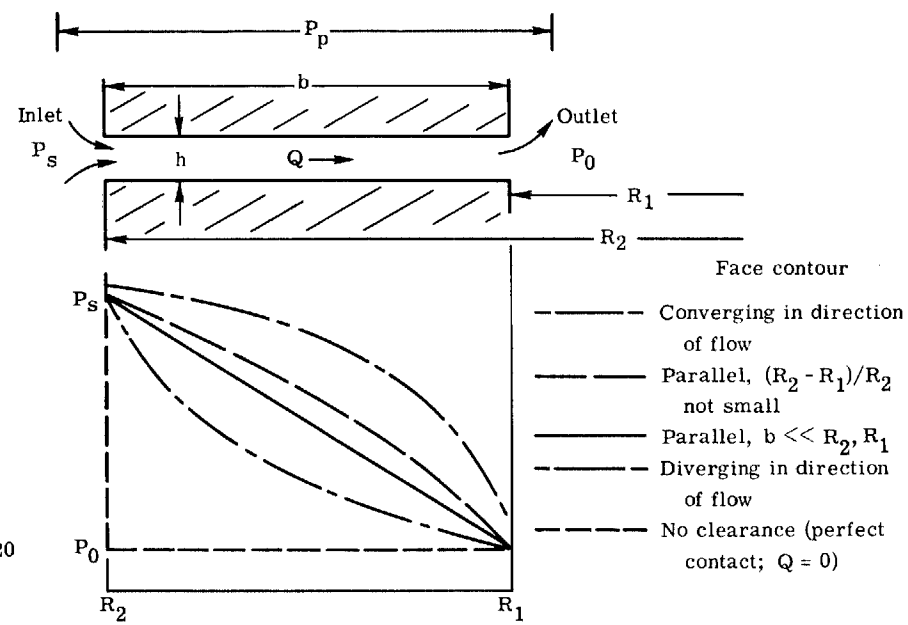

Figure 27. - Pressure between seal faces as function of leakage flow rate for various face contours. (From ref. 2.)

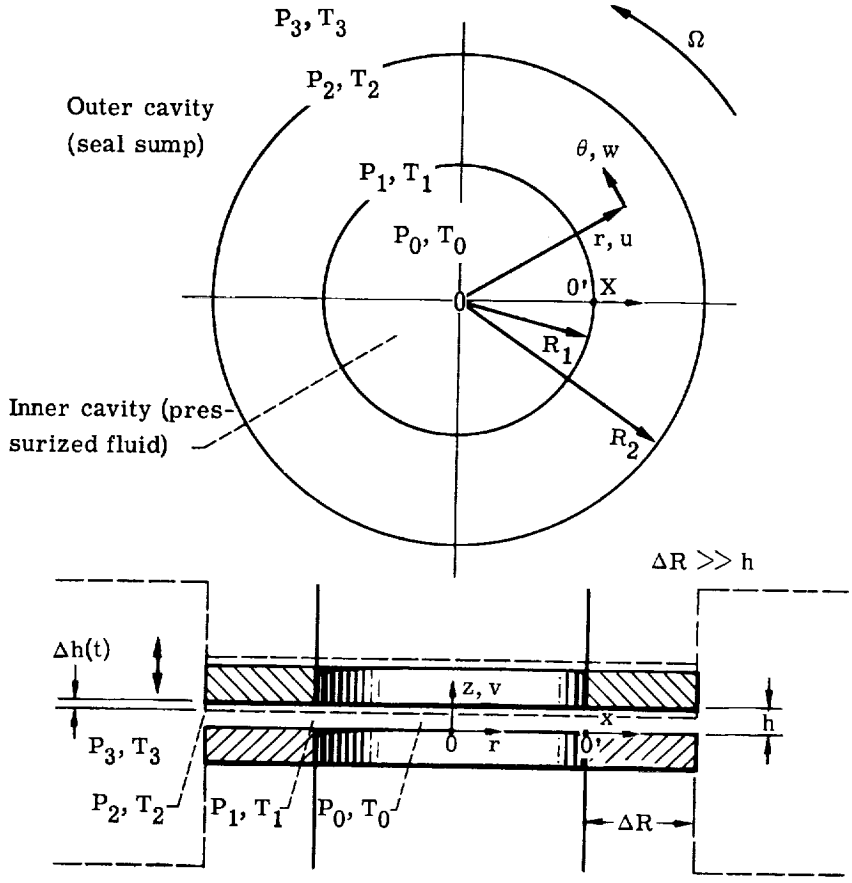

Figure 28. - Model of seal face for compressible fluids.

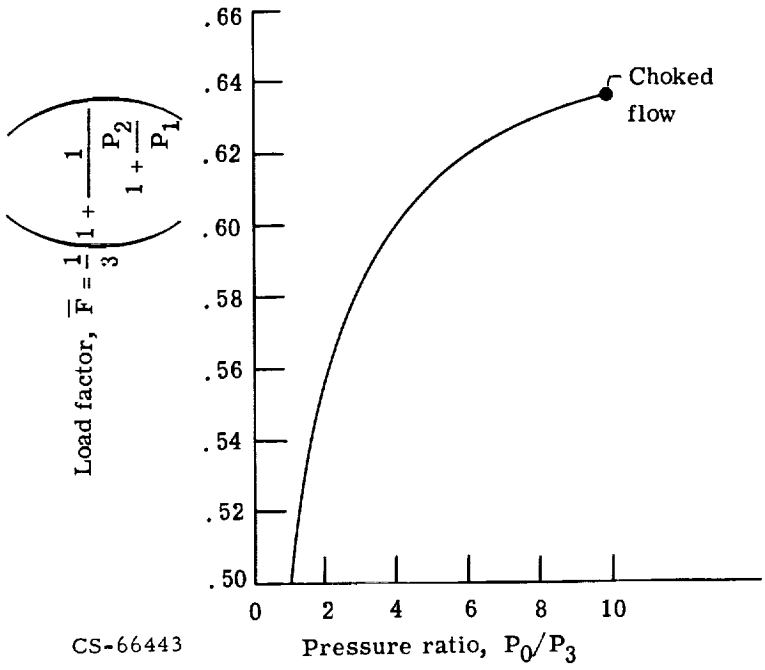

Figure 29. - Load factor as function of pressure ratio in subsonic flow regime for parallel sealing surfaces.

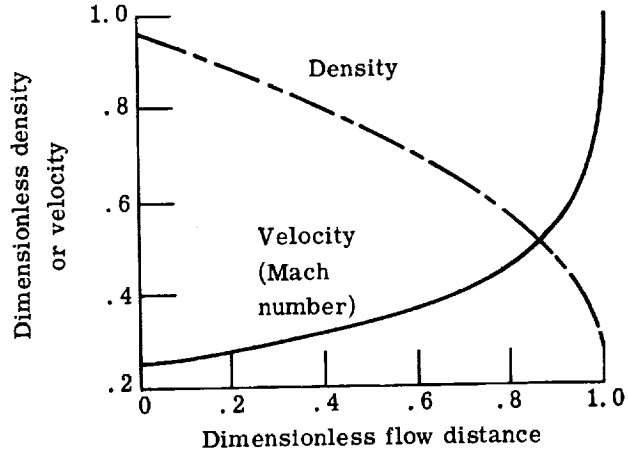

Figure 30. - Density and velocity as function of flow distance.

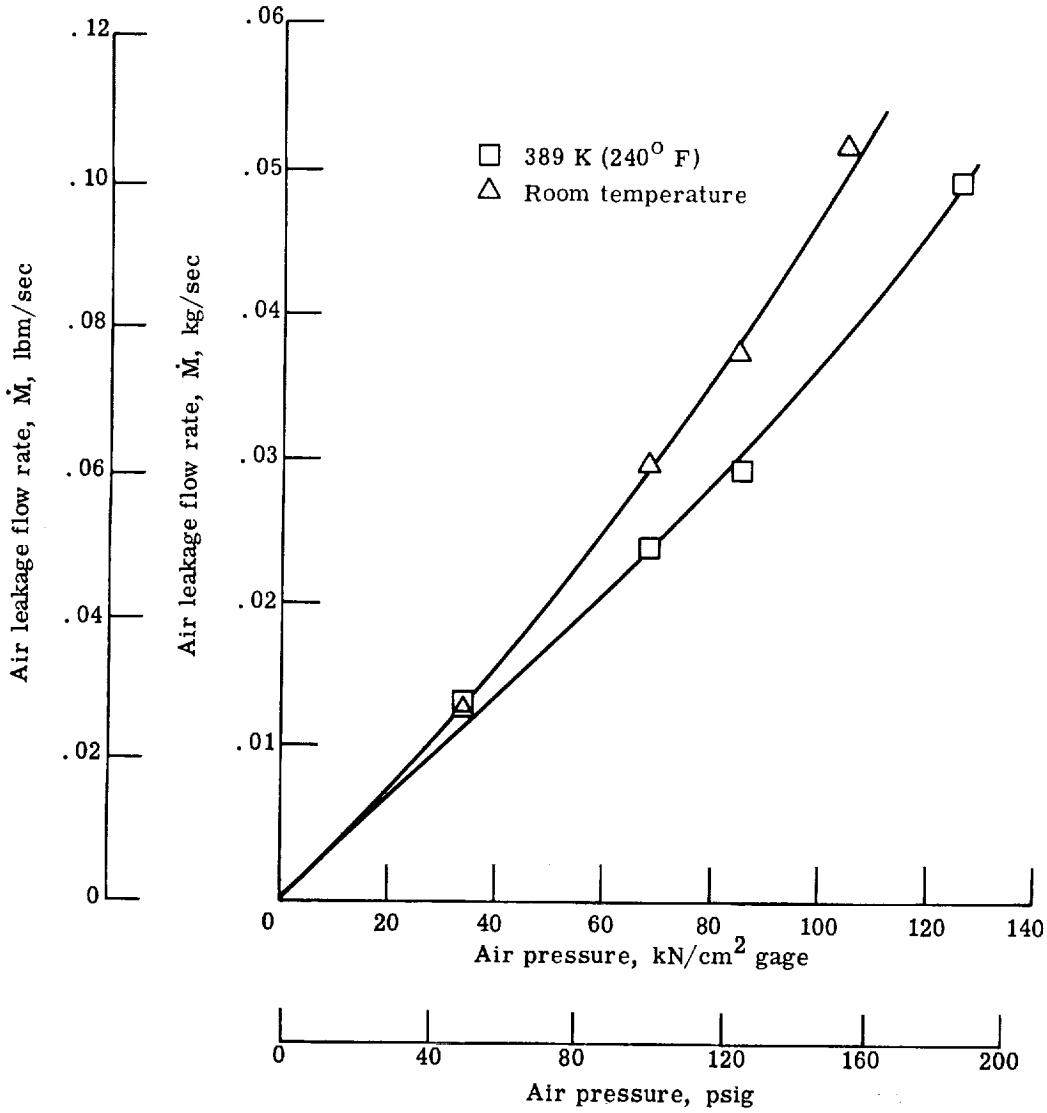

Figure 31. - Labyrinth seal leakage as function of air pressure. (From ref. 16.)

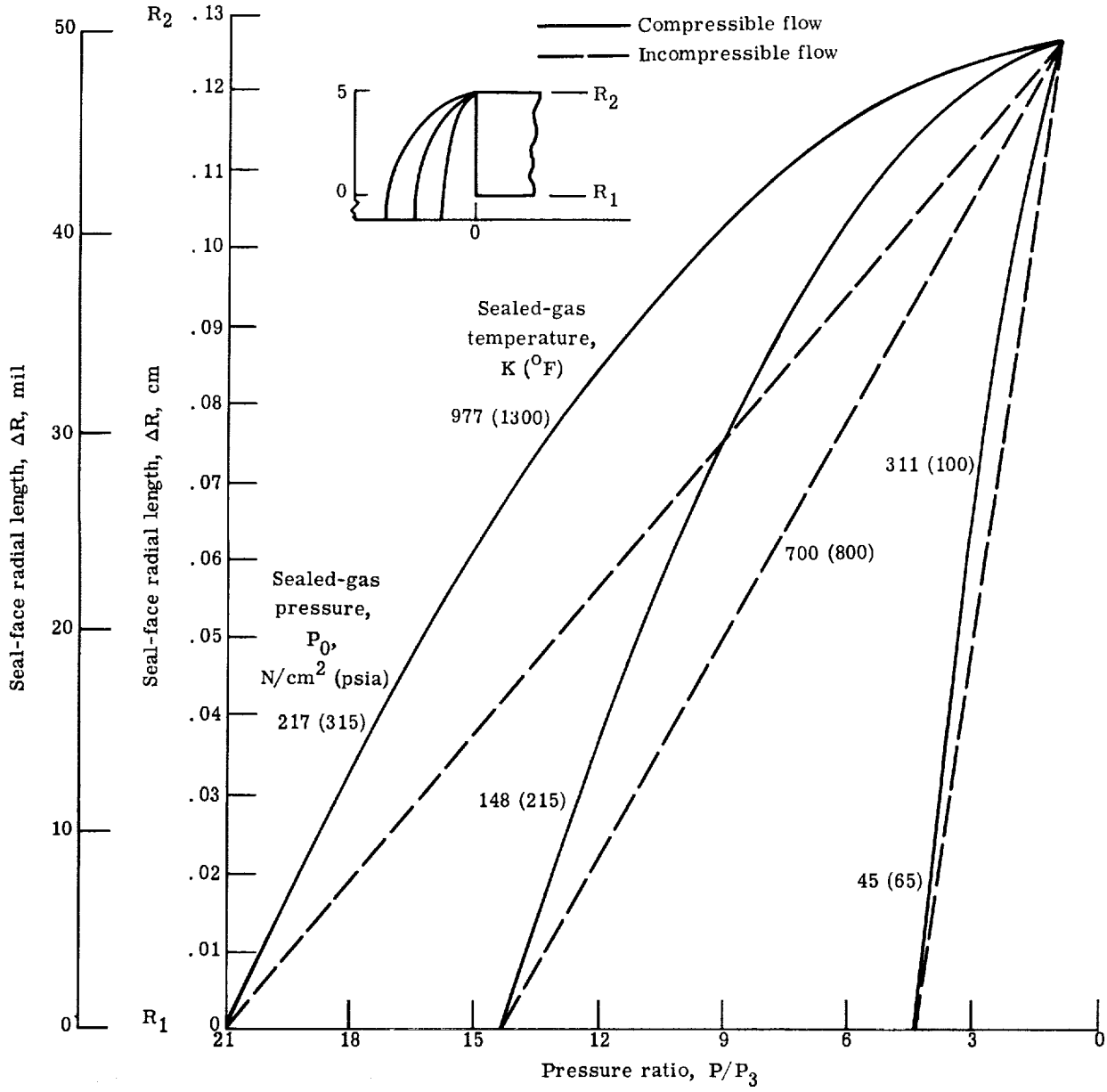

Figure 32. - Pressure profiles of gas within parallel seal faces. Sump pressure, P_3, 10.3 N/cm^2 abs (15 psia); subsonic flow (Mach number < 0.845).

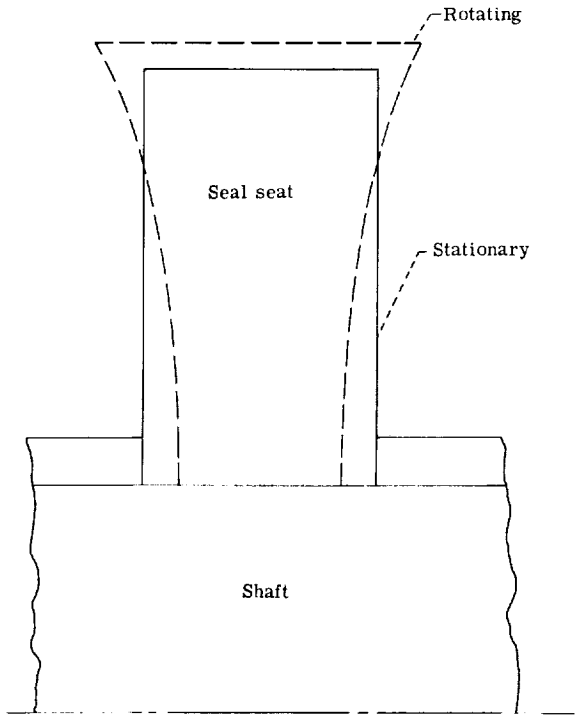

Figure 33. - Typical distortion of seal seat due to centrifugal force.

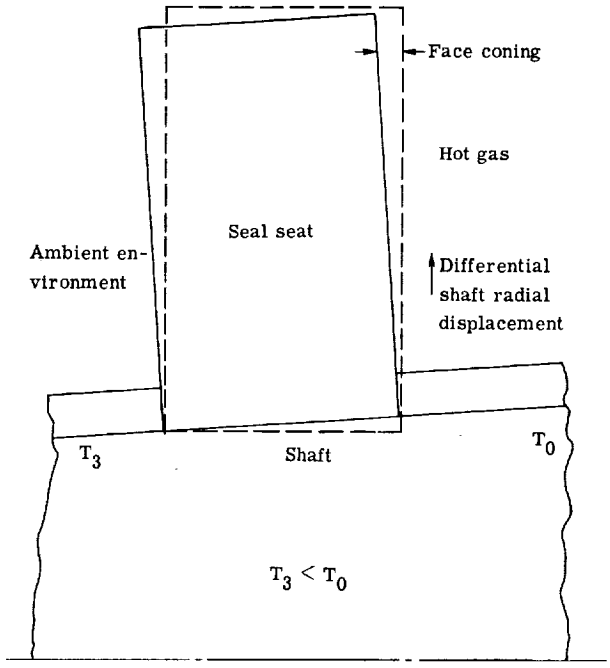

Figure 34. - Typical thermal distortion of seal due to shaft axial thermal gradient.

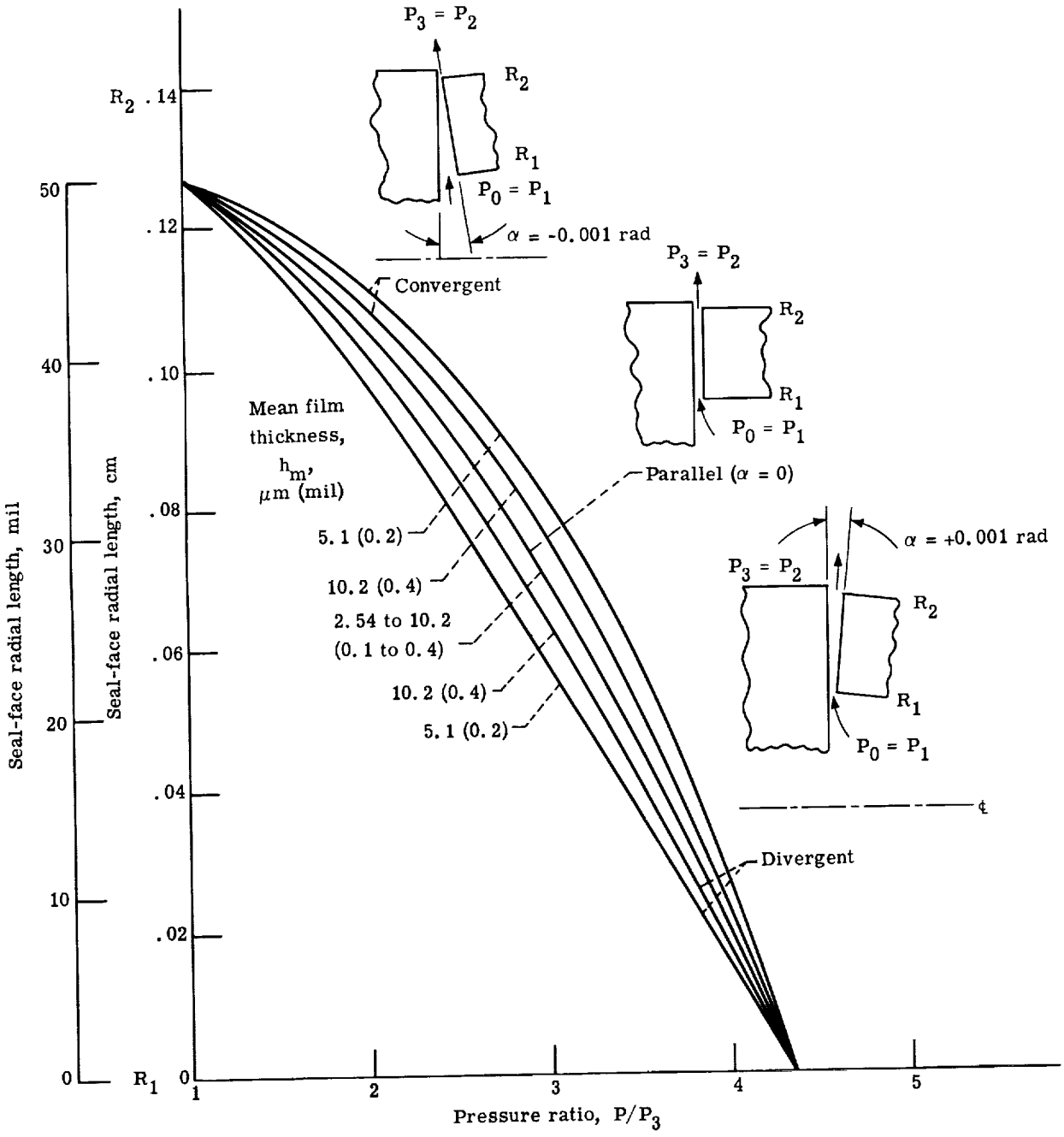

Figure 35. - Pressure ratio as function of mean film thickness. Sealed-gas pressure, P_0, 45 N/cm^2 abs (65 psia); sealed-gas temperature, T_0, 311 K (100° F); sump pressure, P_3, 10.3 N/cm^2 abs (15 psia); seal-face radial length, ΔR, 0.127 cm (50 mils).

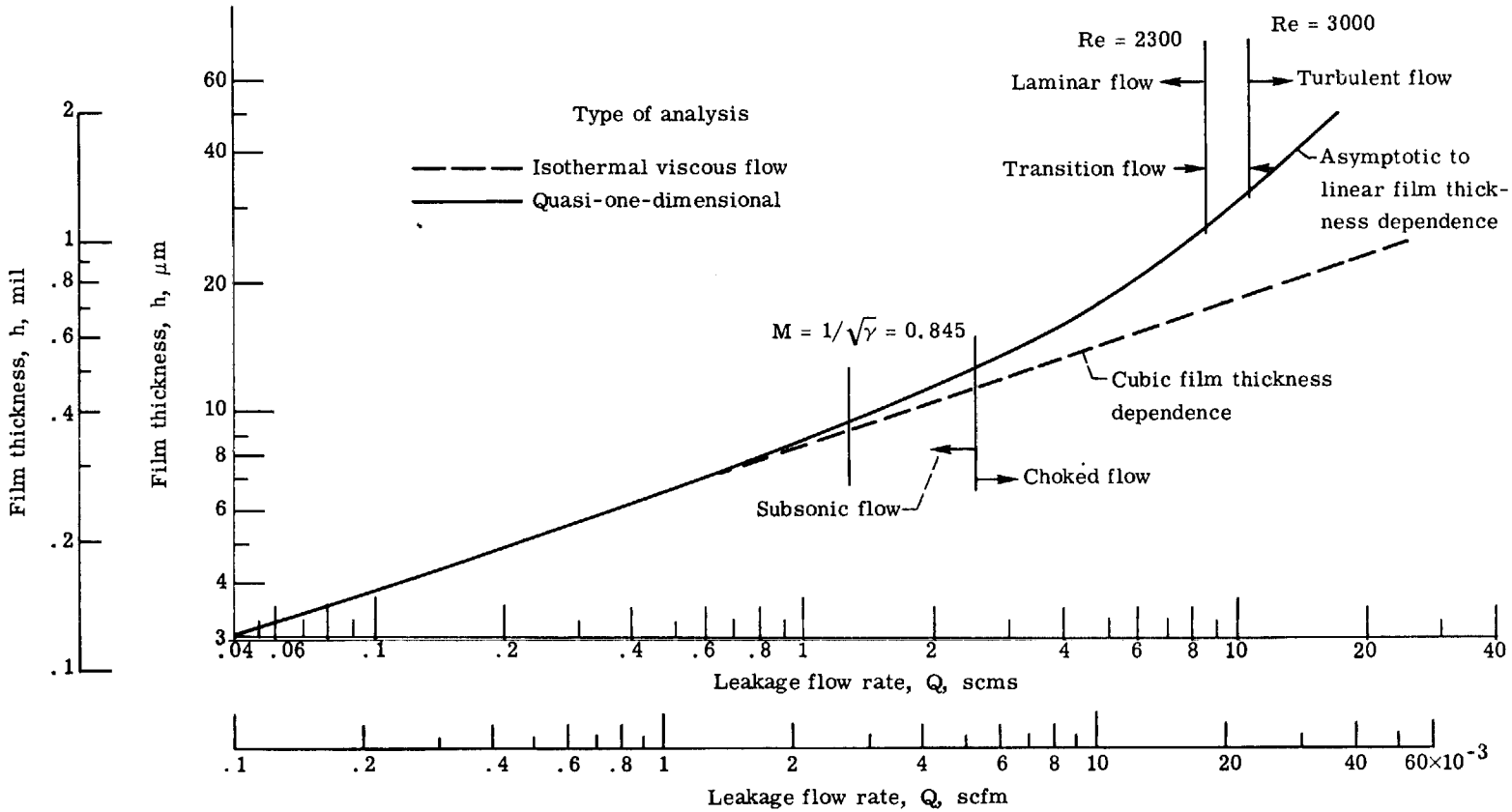

Figure 36. - Sealed-gas leakage flow rate as function of film thickness for parallel sealing-dam faces. Sealed-gas pressure, P_0, 45 N/cm^2 abs (65 psia); sealed-gas temperature, T_0, 311 K (100° F); sump pressure, P_3, 10.3 N/cm^2 abs (15 psia); seal-face radial length, ΔR, 0.127 cm (50 mils).

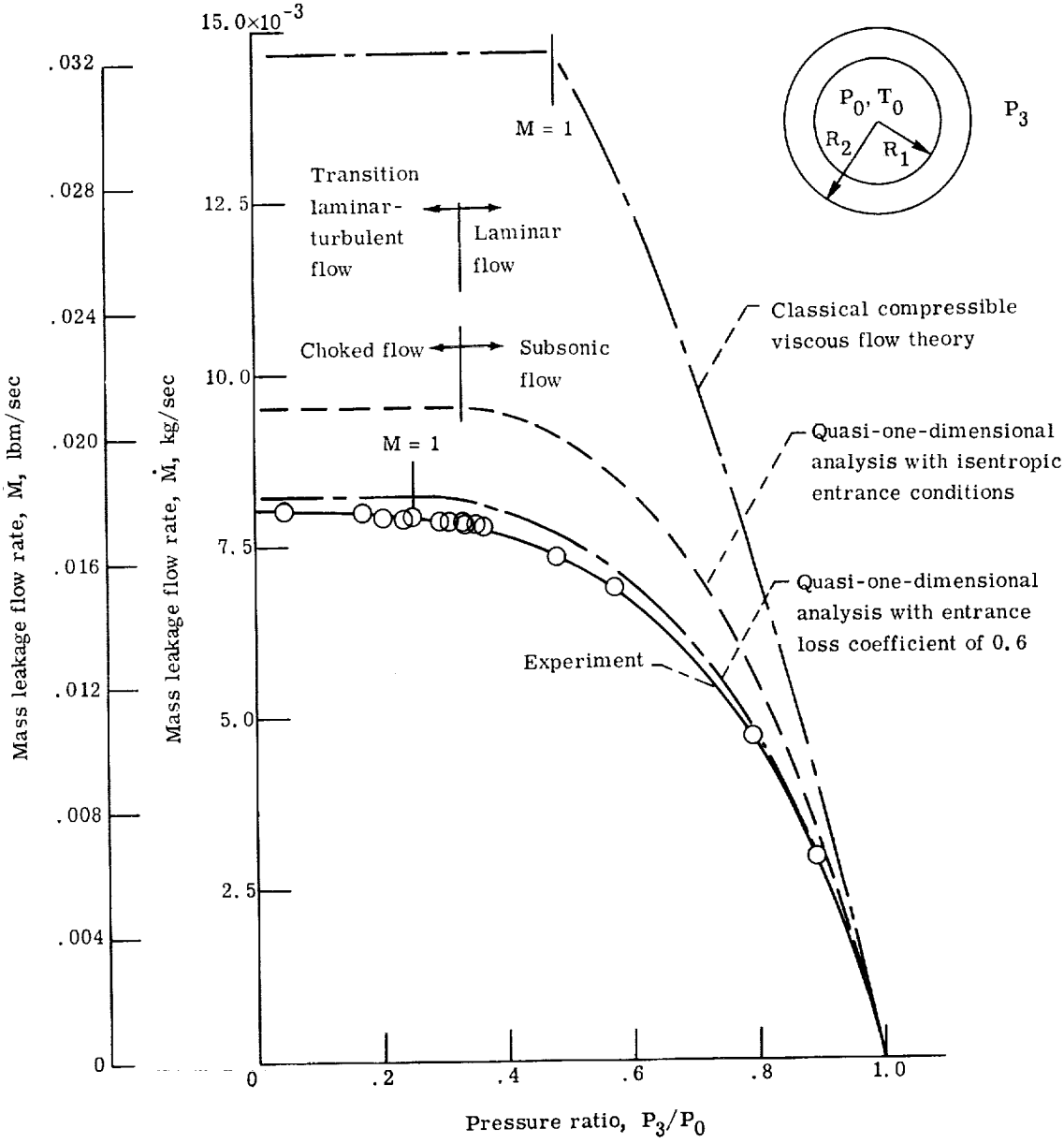

Figure 37. - Comparison of classical viscous flow theory and quasi-one-dimensional analysis with radial flow experimental results. Sealed-gas pressure, P_0, 41.8 N/cm^2 abs (60.6 psia); sealed-gas temperature, T_0, 300 K (80° F); sump pressure, P_3, varied; film thickness, h, 38 μm (1.5 mils); entrance radius, R_1, 6.98 cm (2.75 in.); exit radius, R_2, 7.62 cm (3 in.).

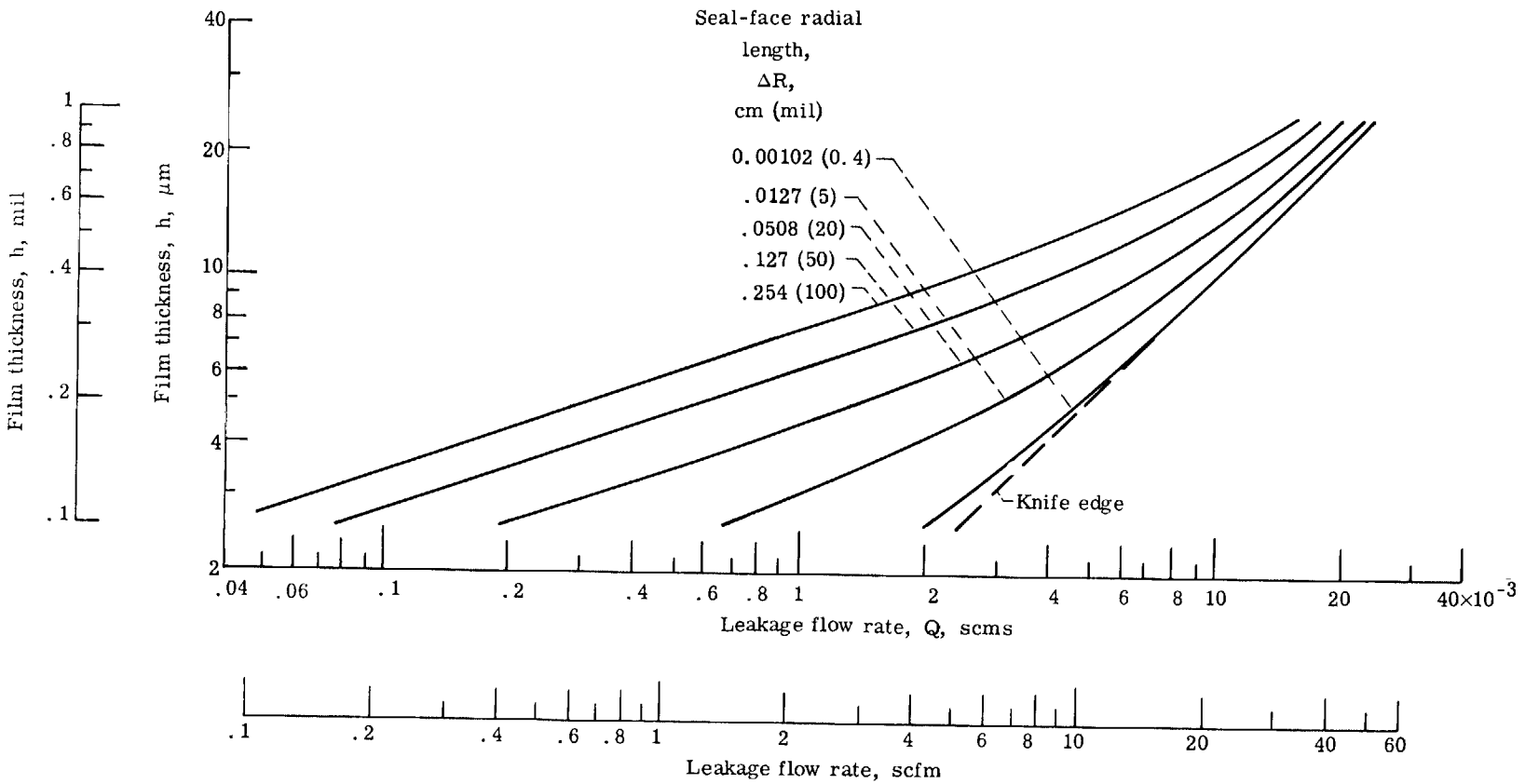

Figure 38. - Seal leakage flow rate as function of seal-face radial length. Sealed-gas pressure, P_0, 148 N/cm^2 abs (215 psia); sealed-gas temperature, T_0, 700 K (810^o F); sump pressure, P_3, 10.3 N/cm^2 abs (15 psia); parallel sealing faces.

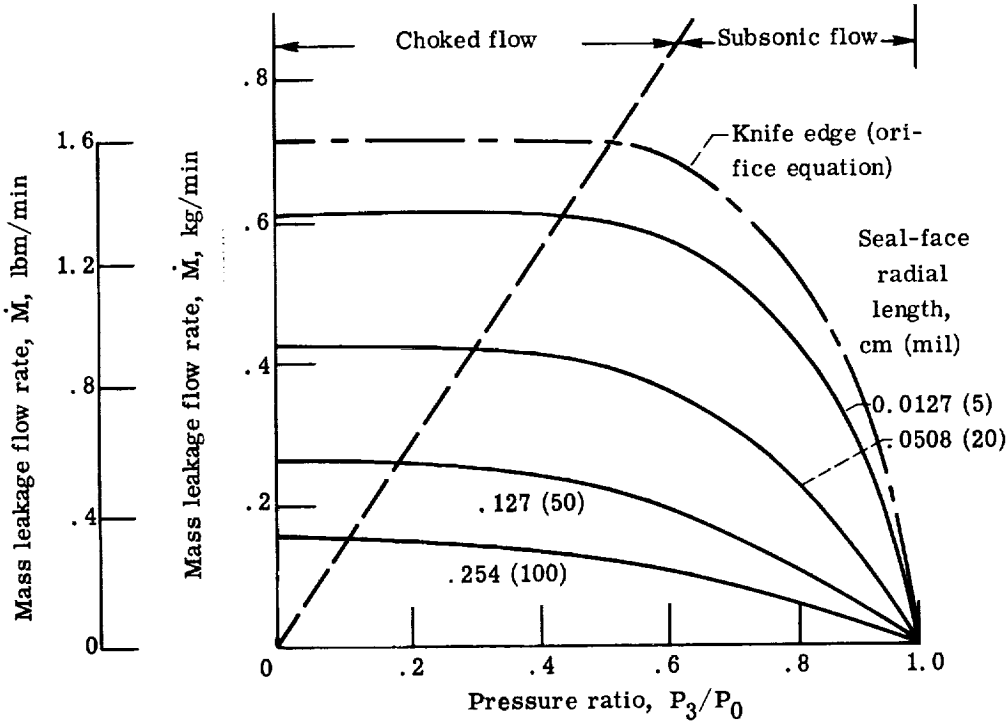

Figure 39. - Mass leakage flow rate as function of pressure ratio for various seal-face radial lengths. Sealed-gas pressure, P_0, 148 N/cm^2 abs (215 psia); sealed-gas temperature, T_0, 700 K (800° F); film thickness, h, 10.2 μm (0.4 mil); entrance radius, R_1, 8.293 cm (3.265 in.).

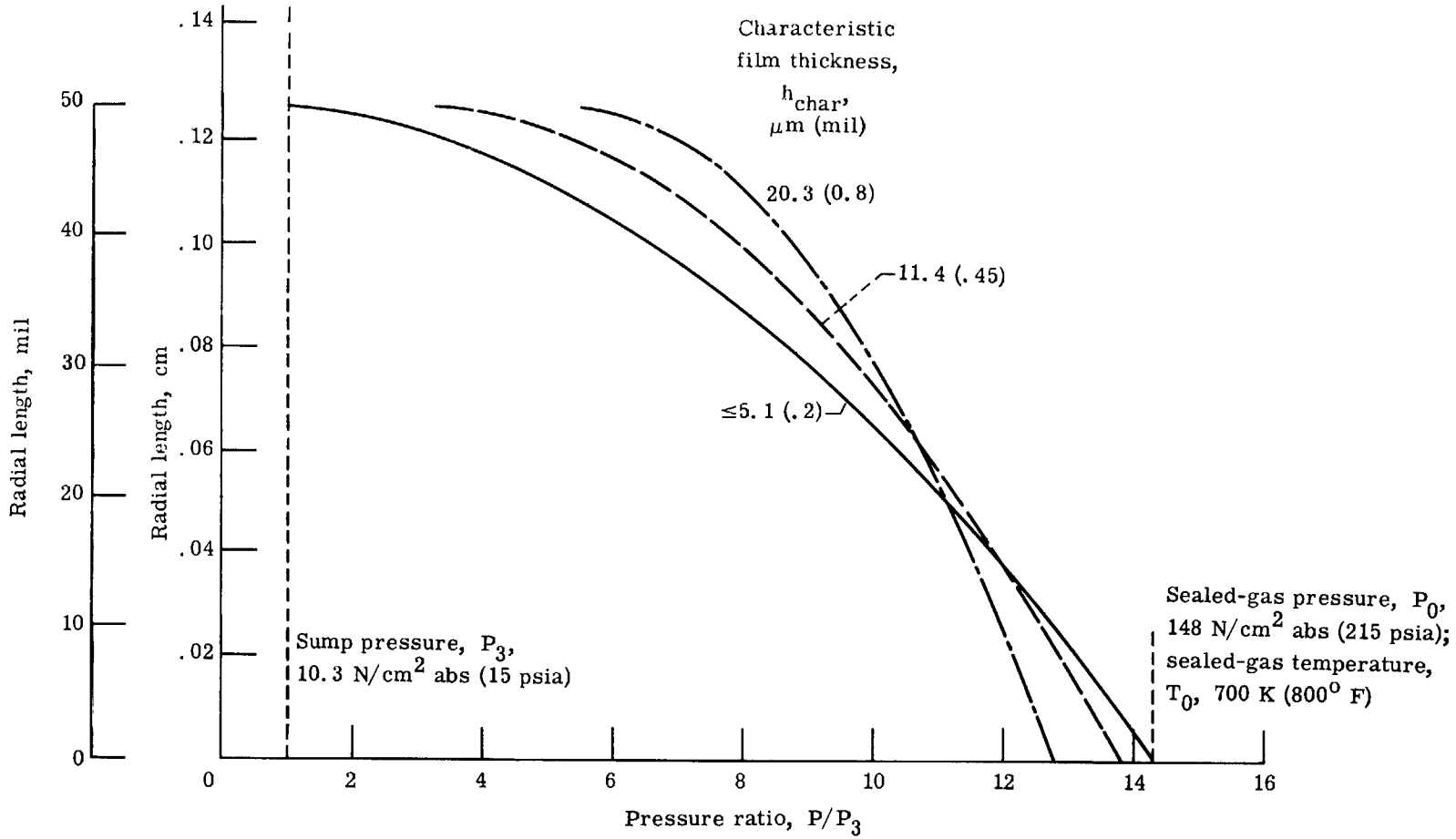

Figure 40. - Pressure ratio as function of seal-face radial length for various characteristic parallel-face film thicknesses representing subsonic and choked flow conditions.

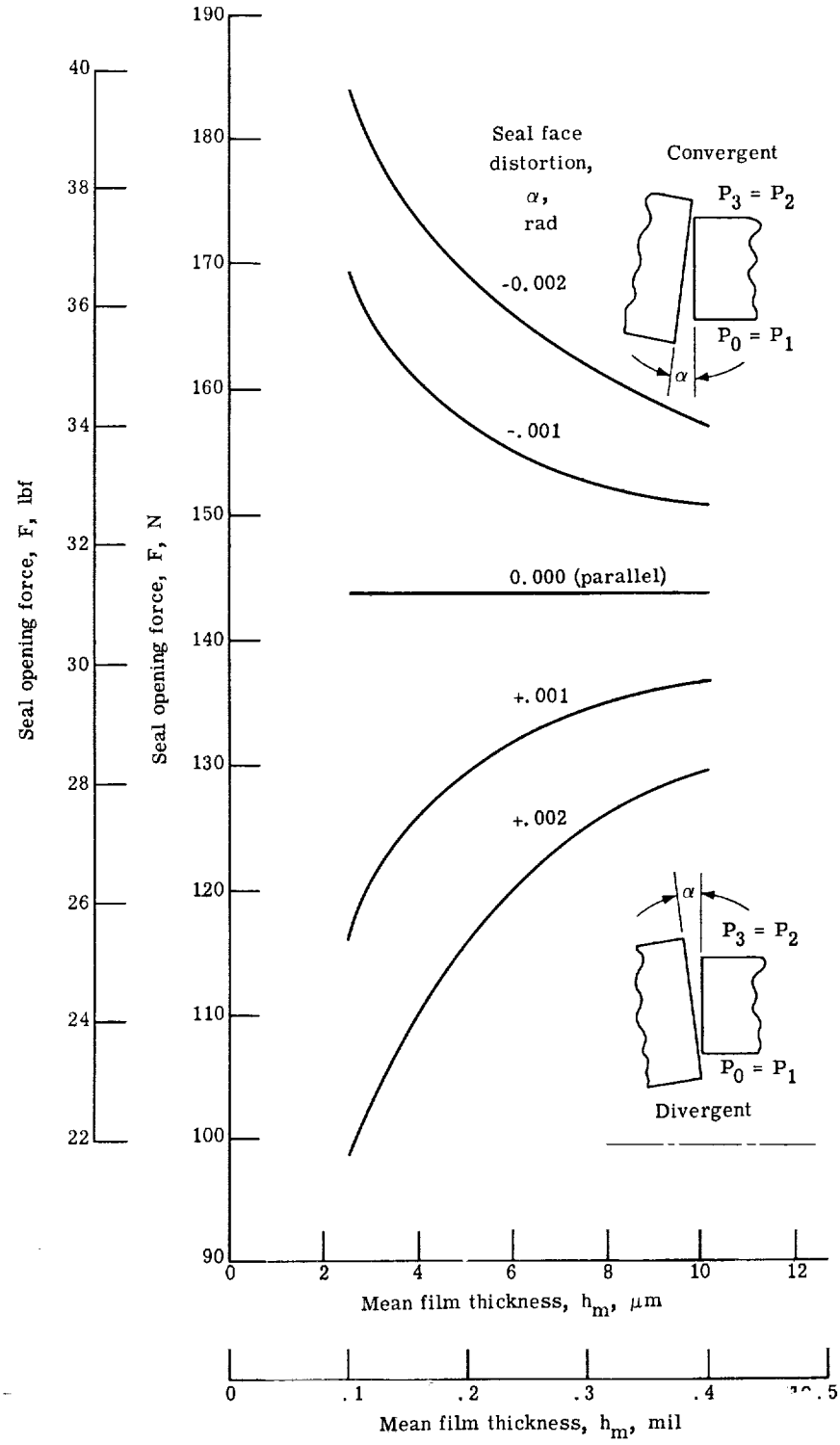

Figure 41. - Seal opening force as function of seal-face distortion. Sealed-gas pressure, P_0, 45 N/cm^2 abs (65 psia); sealed-gas temperature, T_0, 311 K (100° F); sump pressure, P_3, 10.3 N/cm^2 abs (15 psia); seal-face radial length, ΔR, 0.127 cm (50 mils).

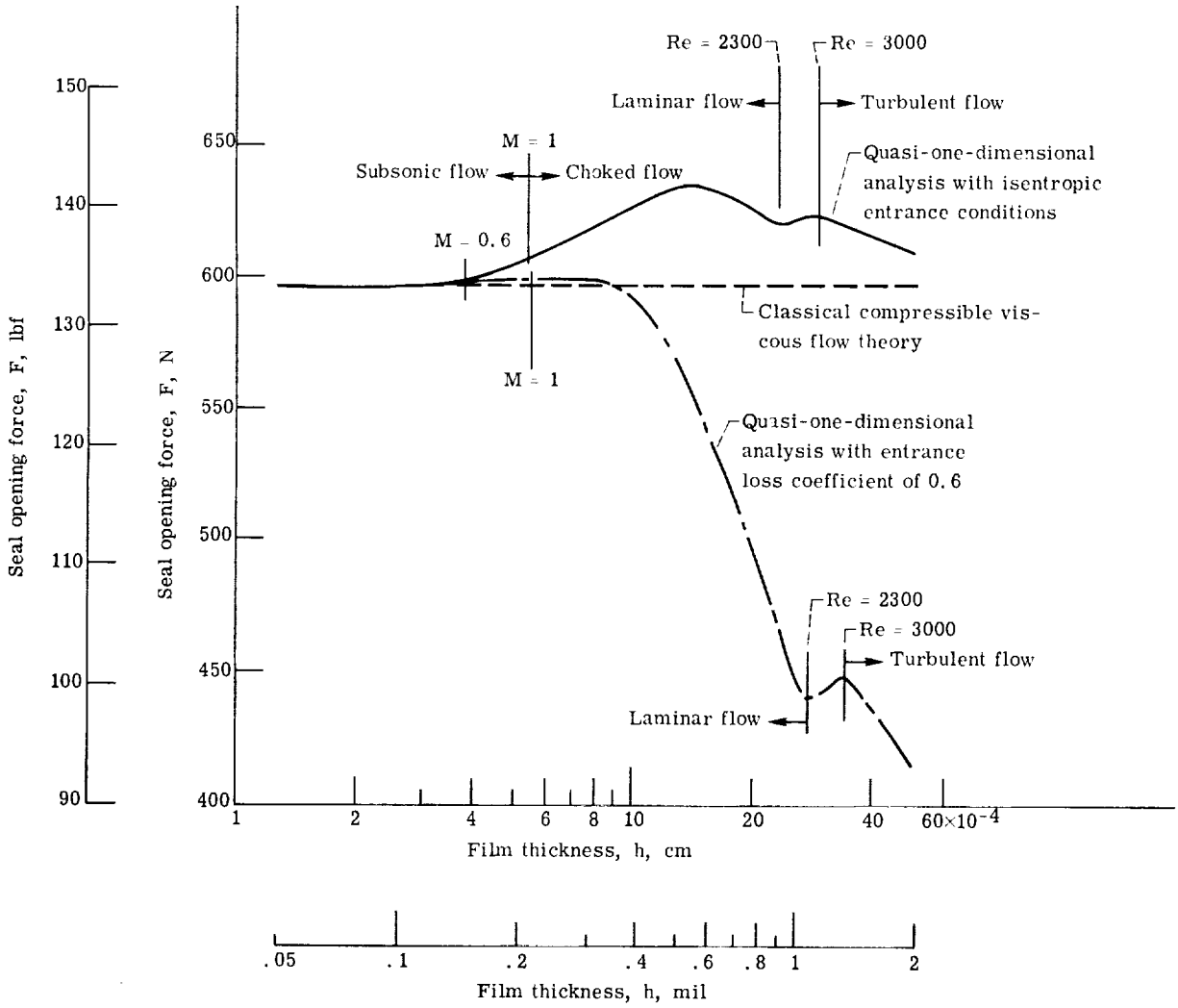

Figure 42. - Seal opening force as function of film thickness for parallel faces; comparison of classical viscous flow theory and quasi-one-dimensional analysis. Sealed-gas pressure, P_0, 148 N/cm^2 abs (215 psia); sealed-gas temperature, T_0, 700 K (800^o F); sump pressure, P_3, 10.3 N/cm^2 abs (15 psia); seal-face radial length, ΔR, 0.127 cm (50 mils).

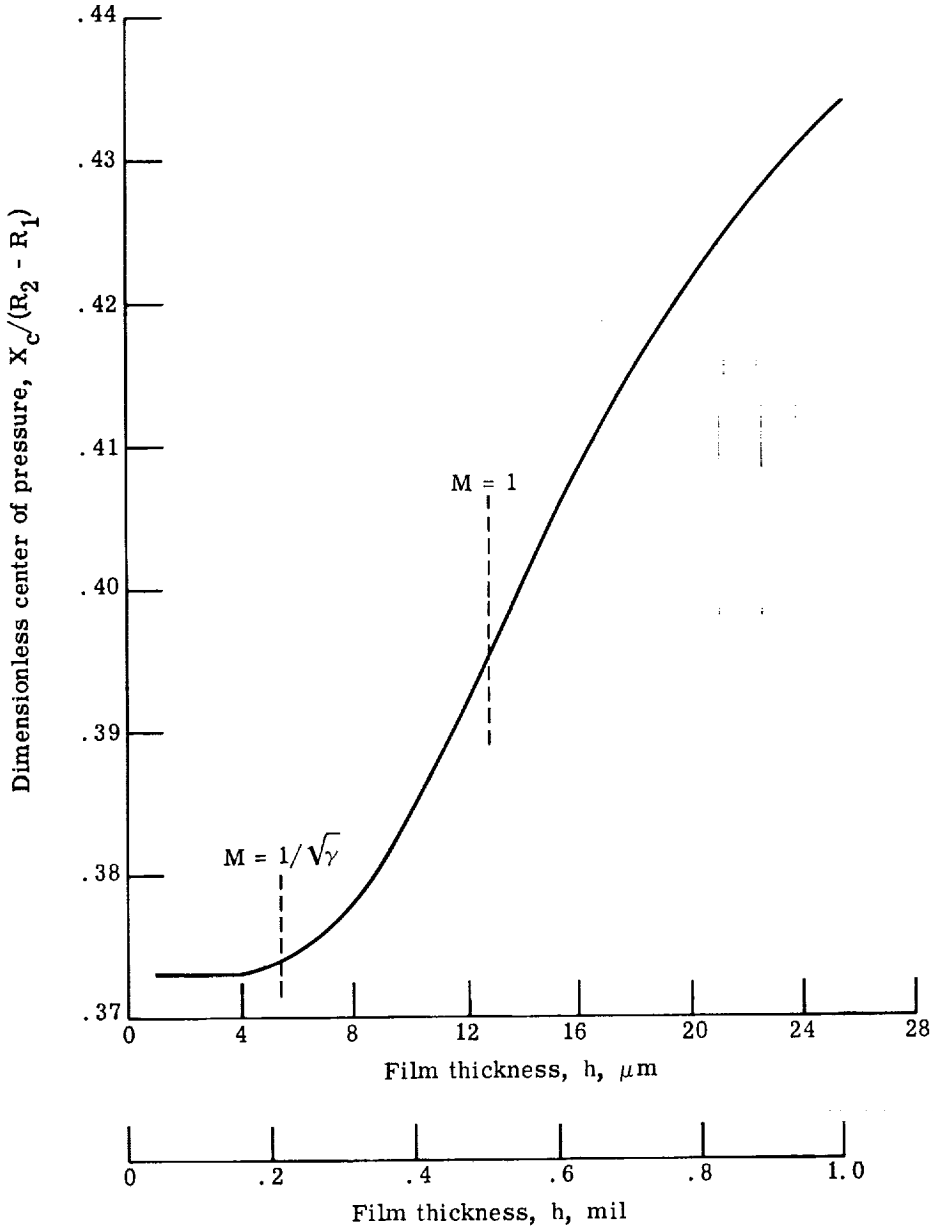

Figure 43. - Center of pressure as function of parallel-face film thicknesses representing subsonic and choked flow conditions. Sealed-gas pressure, P_0, 45 N/cm^2 abs (65 psia); sealed-gas temperature, T_0, 311 K (100^o F); sump pressure, P_3, 10.3 N/cm^2 abs (15 psia).

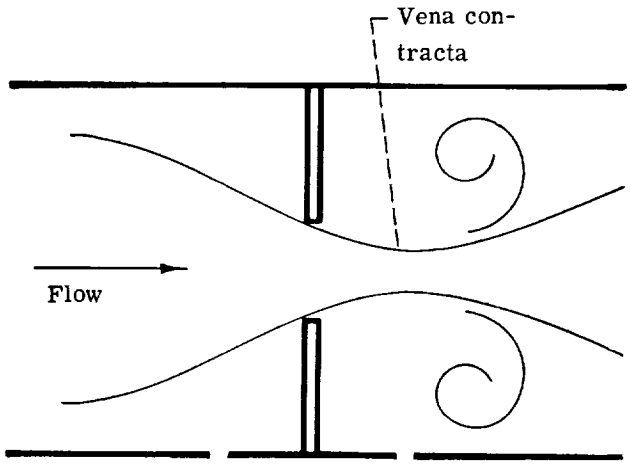

(a) Thin-plate orifice flow.

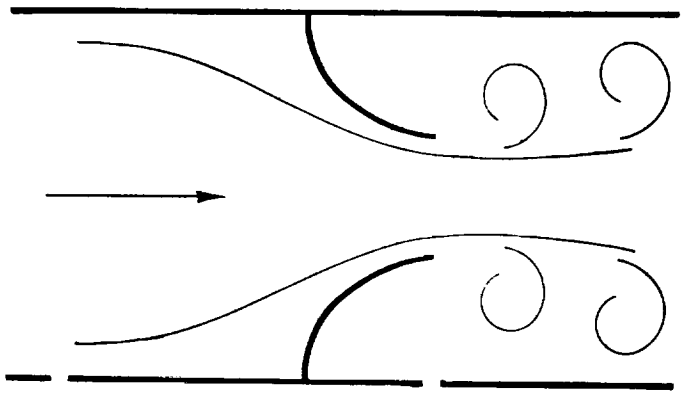

(b) Rounded nozzle flow.

Figure 44. - Vena contracta effects in thin-plate orifice and rounded nozzle flow.

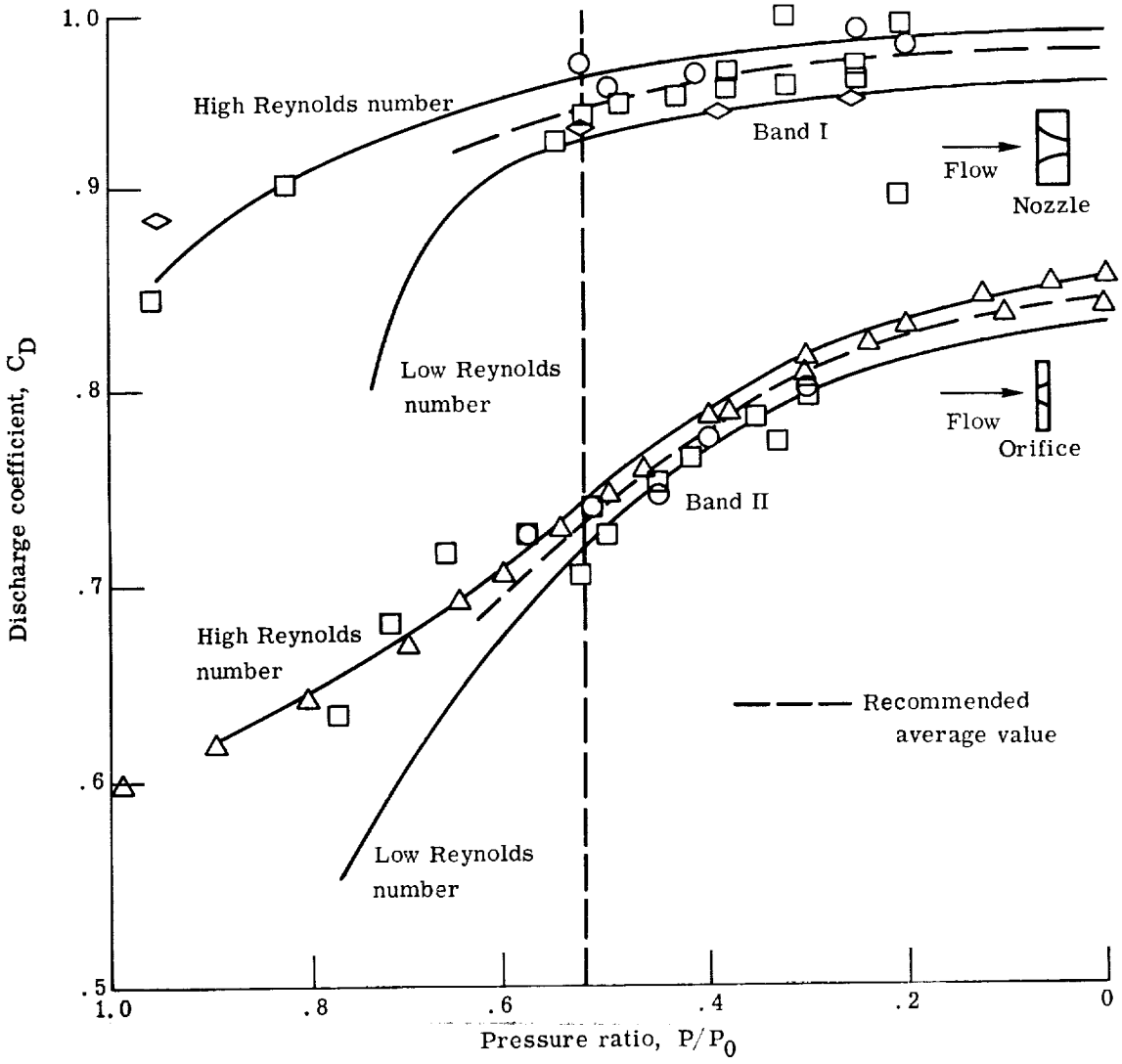

Figure 45. - Discharge coefficient as function of pressure ratio for nozzles and orifices. (From ref. 20; revised.)

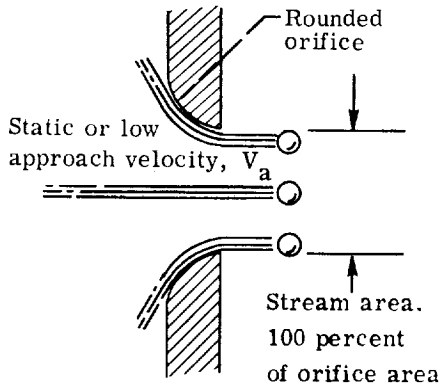

(a) Low-velocity flow through round-edge orifice.

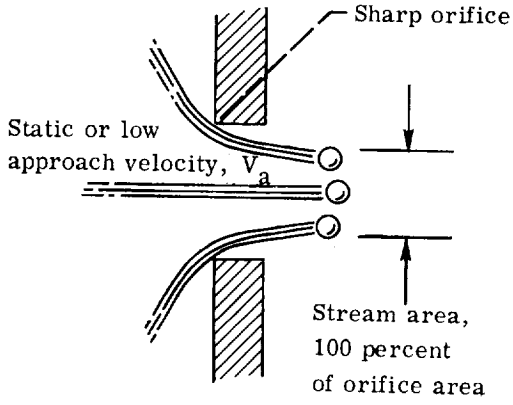

(b) Low-velocity flow through sharp-edge orifice.

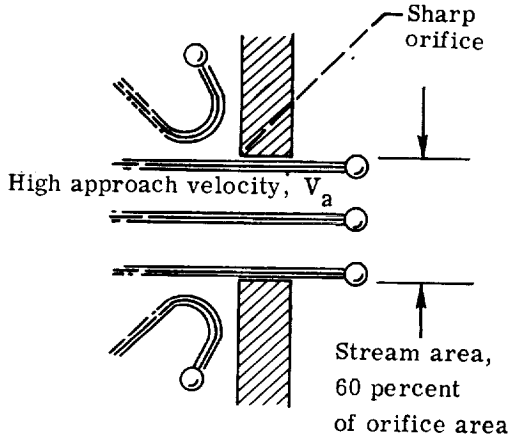

(c) High-velocity flow through sharp-edge orifice.

Figure 46. - Aerodynamic flow characteristics of air. (From ref. 21.)

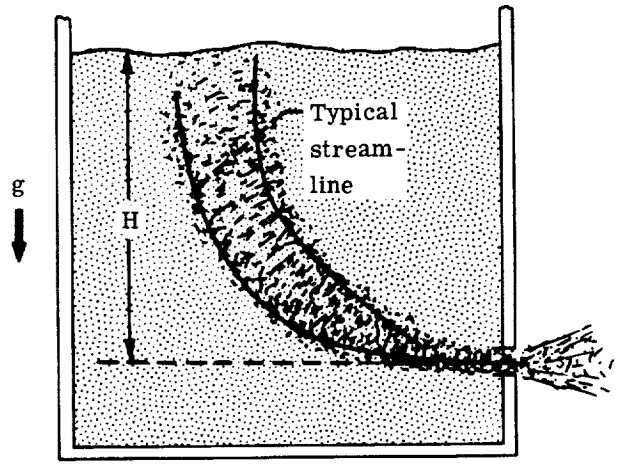

Figure 47. - Schematic representation of orifice flow driven by gravitational head.

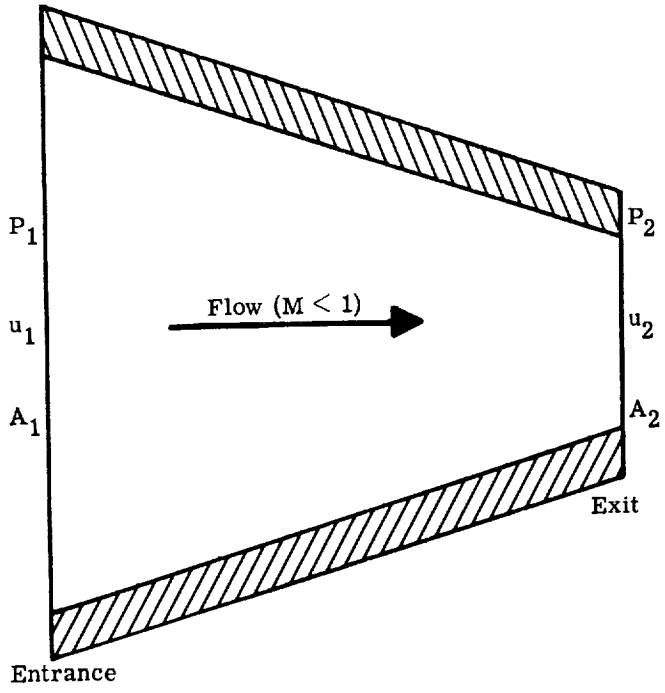

Figure 48. - Schematic of typical subsonic nozzle.

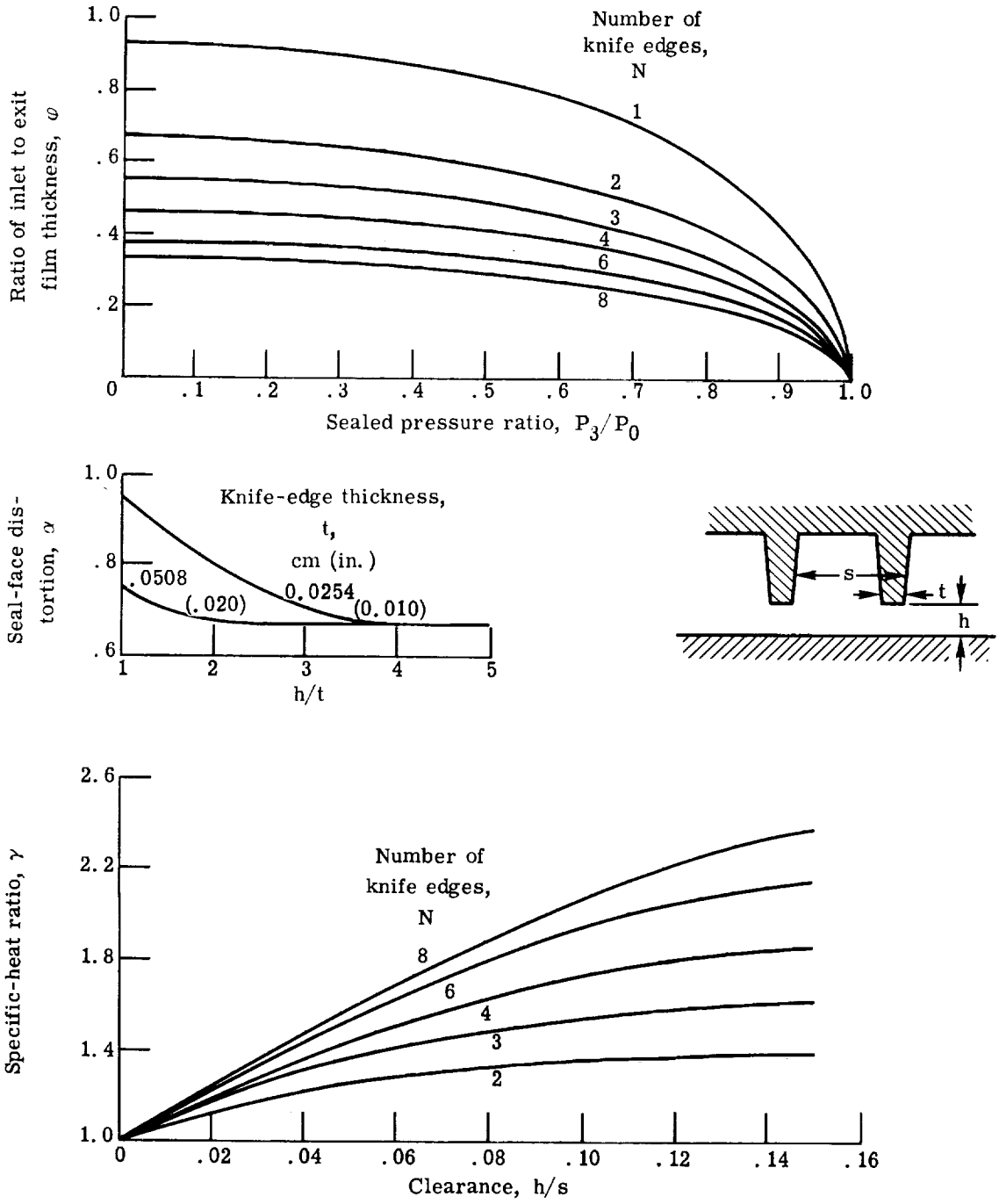

Figure 49. - Graphic representation of terms in Egli labyrinth seal leakage equation: $\dot{M} = A\alpha\varphi\gamma\sqrt{g\rho_0 P_0}$.

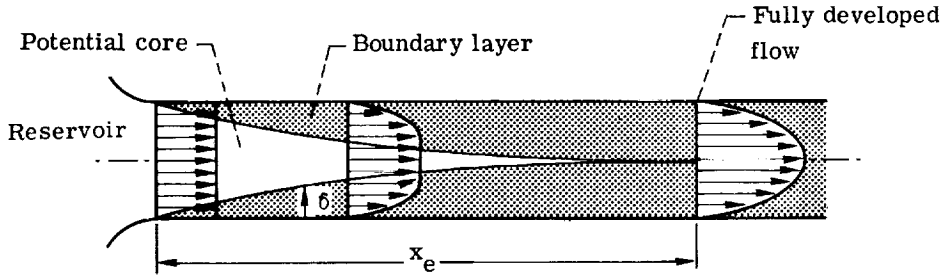

(a) Laminar flow in entry region of pipe.

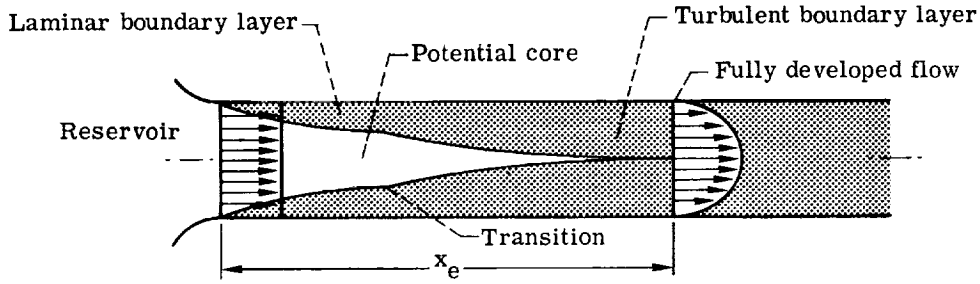

(b) Turbulent flow in entry region of pipe.

Figure 50. - Qualitative comparison of entrance lengths of laminar and turbulent flows with smooth (rounded) entrance lengths.

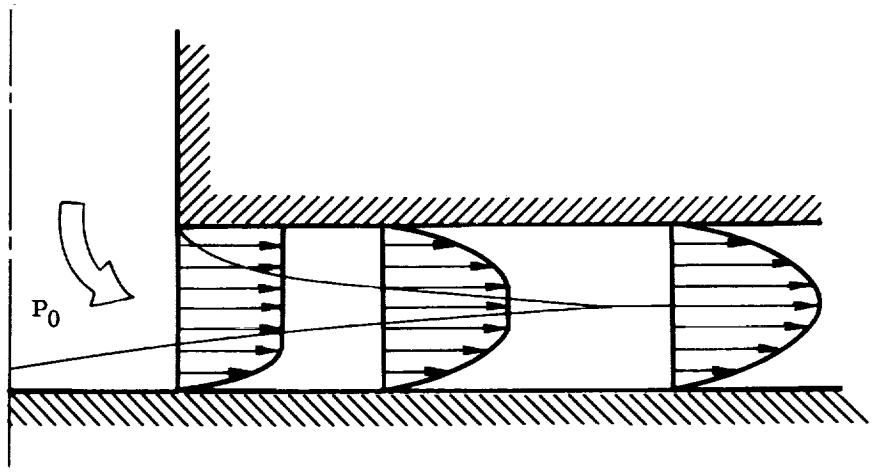

Figure 51. - Entrance loss mechanisms: turning (separated flow); wall shear (boundary layer growth); and momentum increase (less uniform velocity distribution).

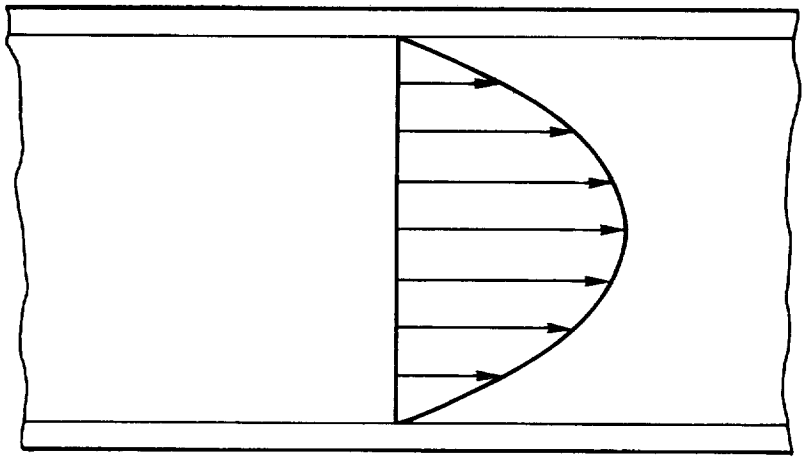

Figure 52. - Parabolic velocity distribution in viscous flow.

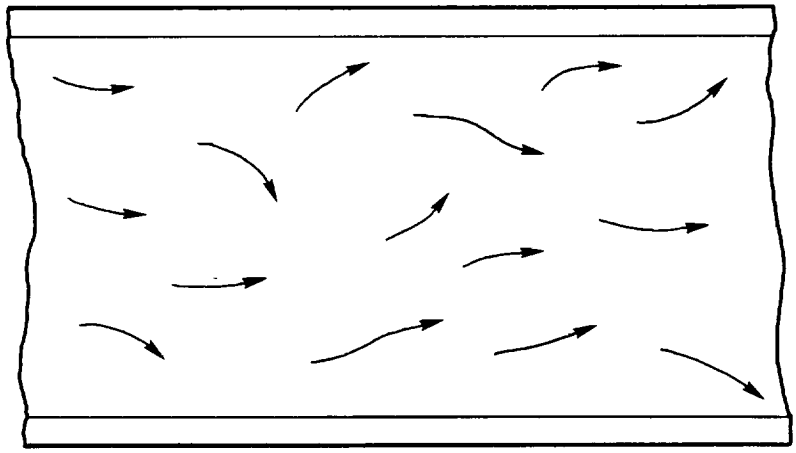

Figure 53. - Turbulent flow paths of fluid particles.

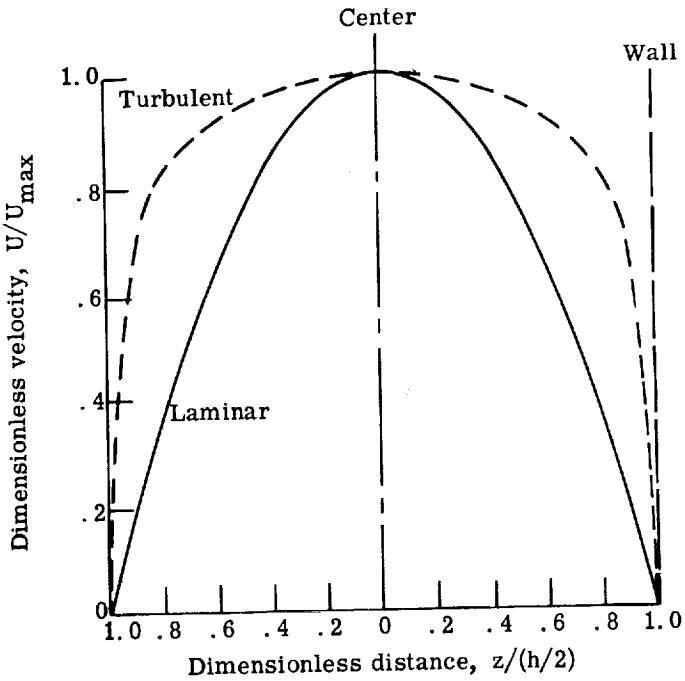

Figure 54. - Qualitative comparison of laminar and turbulent velocity distribution.

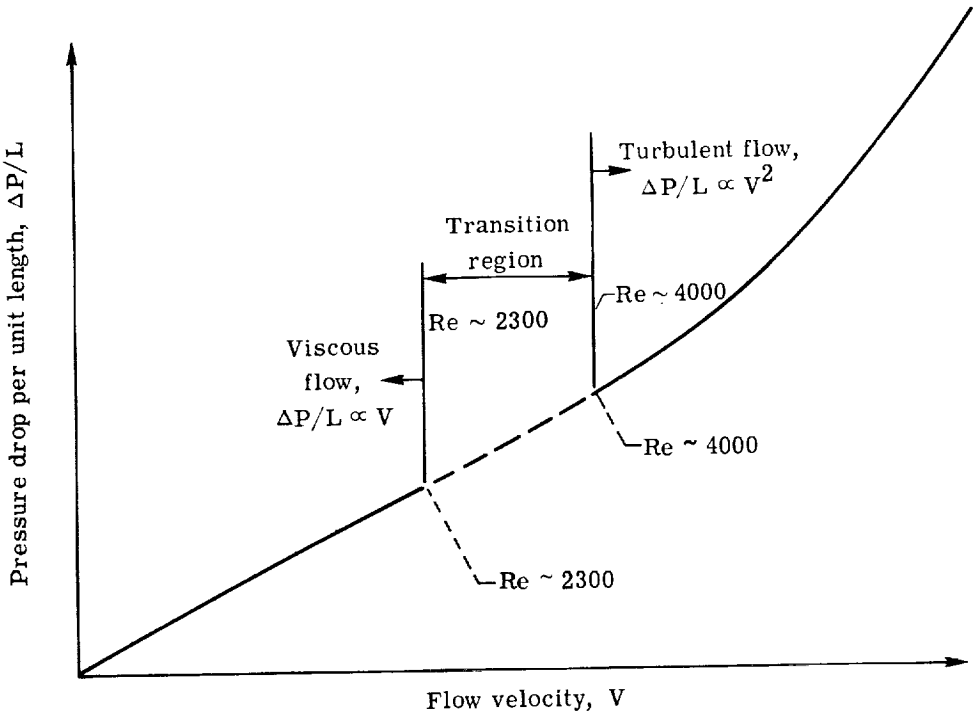

Figure 55. - Representation of pipe pressure drop for laminar, transition, and turbulent flow.

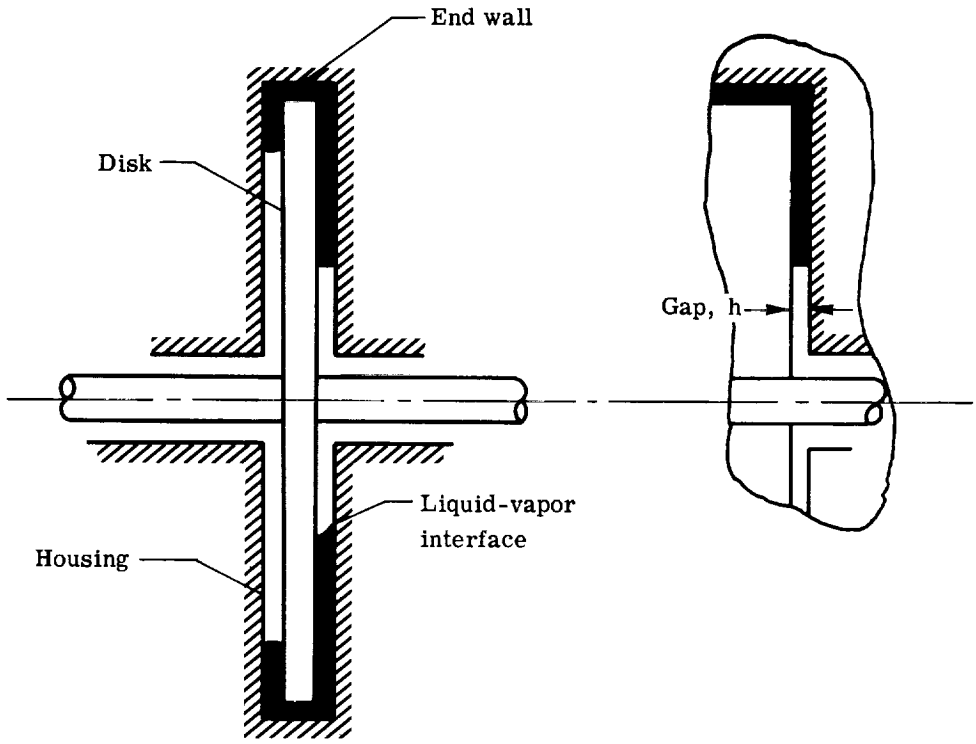

Figure 56. - Model of flow between partially wetted disks. (From ref. 31.)

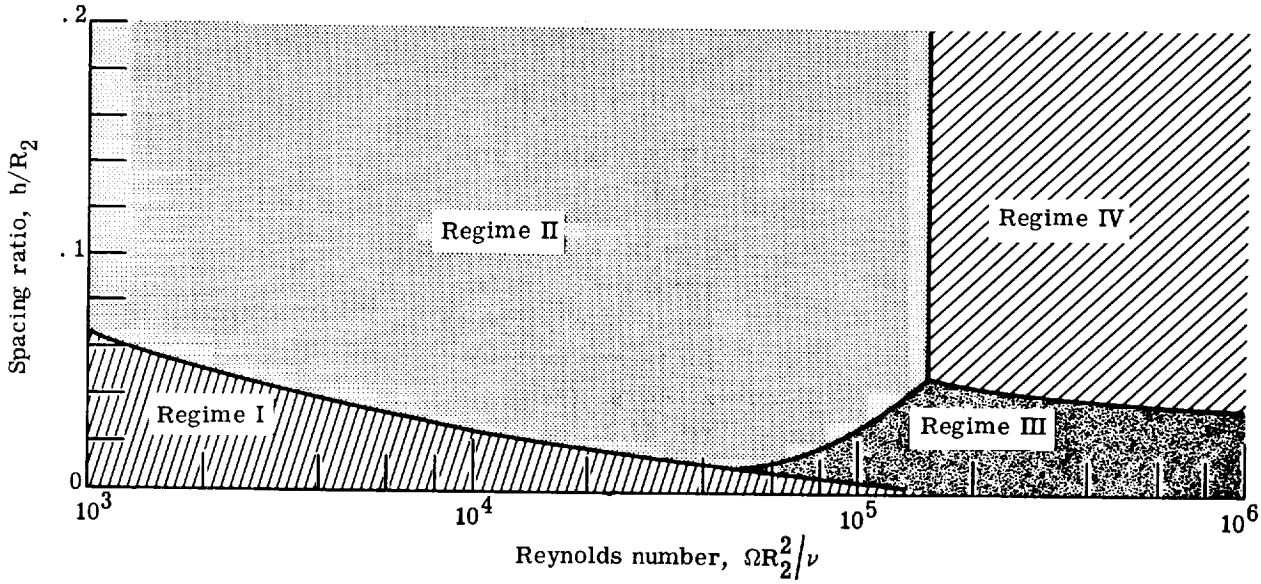

Figure 57. - Approximate operating flow regimes for rotating disks. (From ref. 31.)

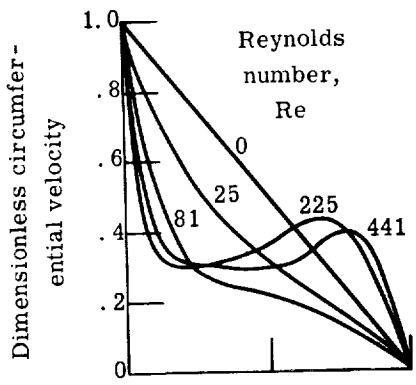

(a) Circumferential velocity profiles.

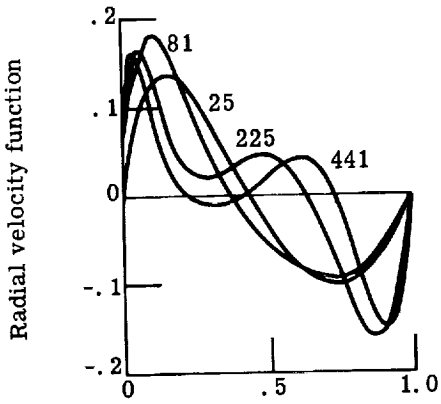

(b) Radial velocity profiles.

Figure 58. - Theoretical radial and circumferential velocity profiles for various Reynolds numbers. (From ref. 33.)

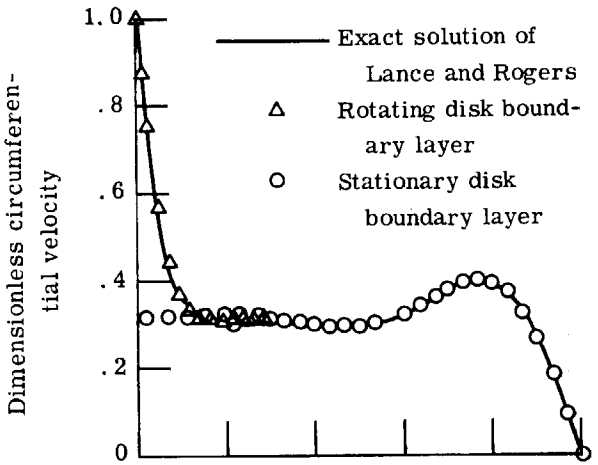

(a) Circumferential velocity profiles.

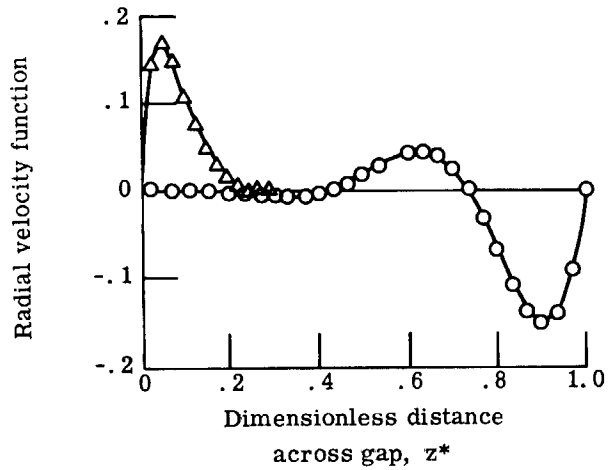

(b) Radial velocity profiles.

Figure 59. - Comparison of theoretical and experimental velocity profiles for boundary layer case (Re = 441). (From ref. 33.)

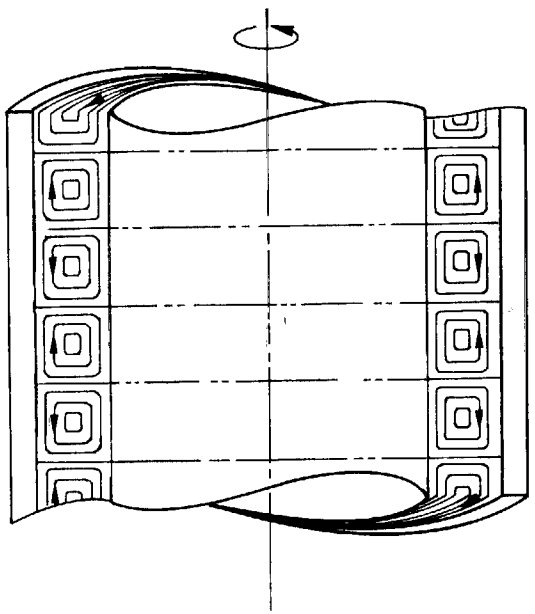

Figure 60. - Taylor vortex flow between concentric cylinders.

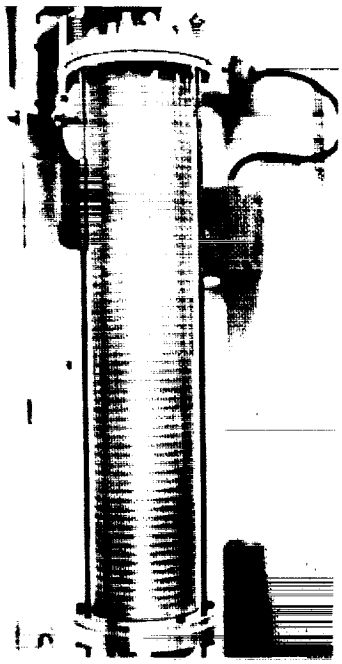

(a) Overall view

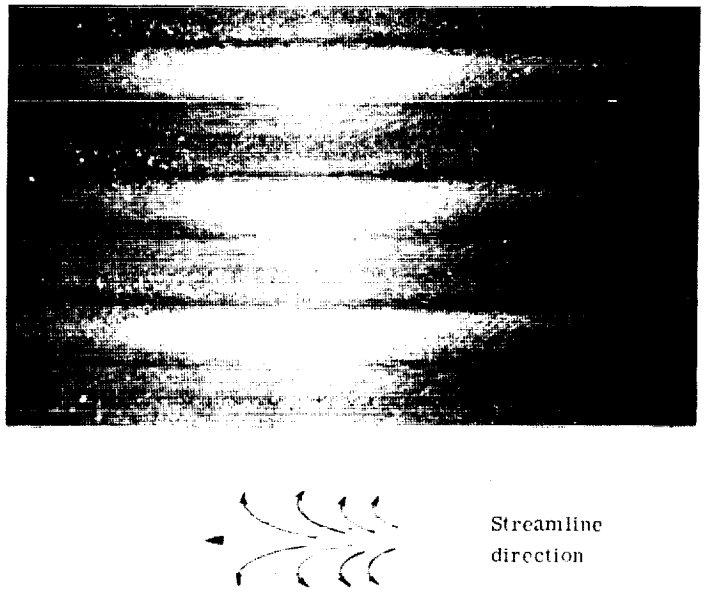

(b) Closeup of vortex flow, with diagram indicating streamline directions.

Figure 61. - Flow visualization of fully developed Taylor vortices for concentric cylinders with no axial flow. (From ref. 34.)

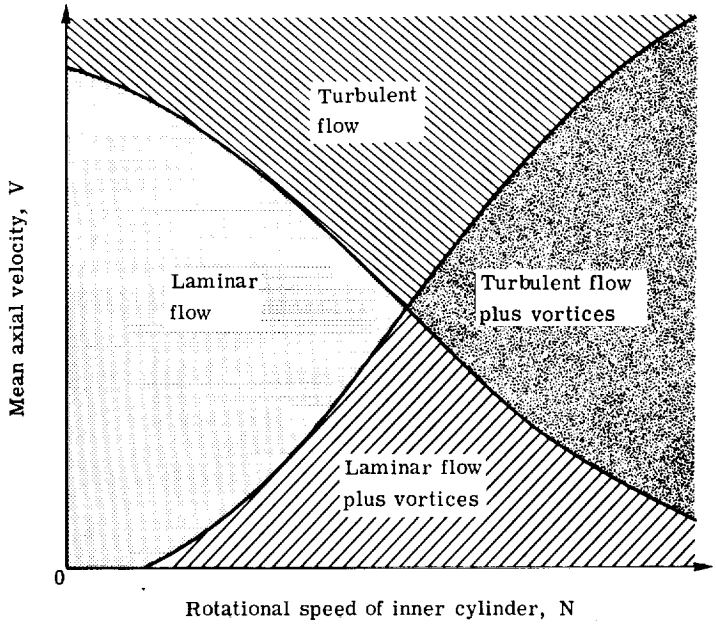

Figure 62. - Schematic representation of different flow regimes in an annulus with axial flow and inner cylinder rotating. (From ref. 36.)

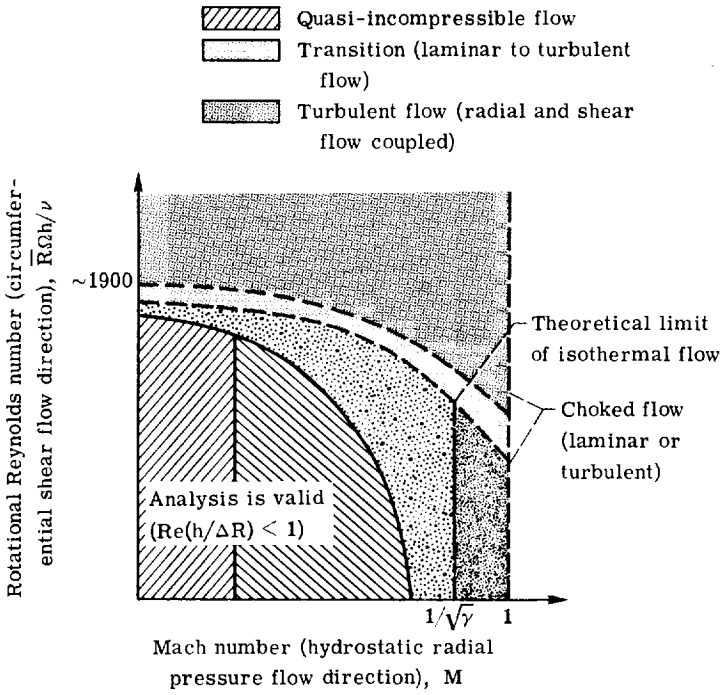

Figure 63. - Envelope of possible seal-face flow regimes for gases. (From ref. 38.)

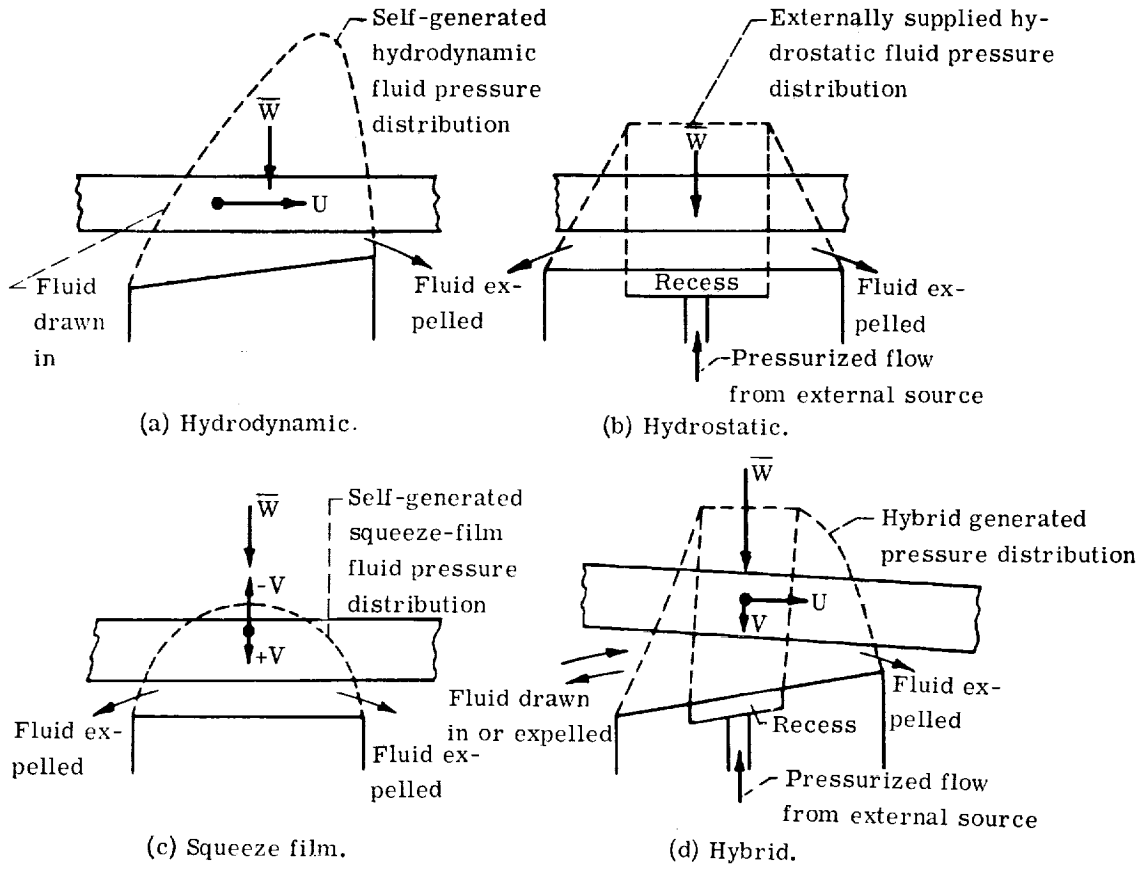

Figure 64. - Modes of fluid-film lubrication. (From ref. 39).

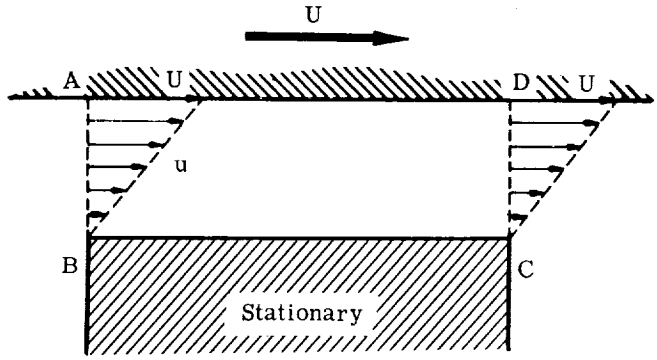

Figure 65. - Velocity distribution between two parallel plane surfaces in relative motion. (From ref. 40.)

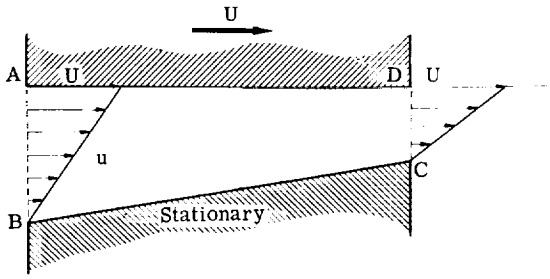

(a) Velocity distribution as a result of relative motion.

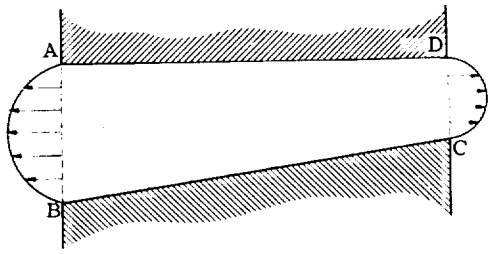

(b) Velocity distribution as a result of pressure buildup in lubricant film.

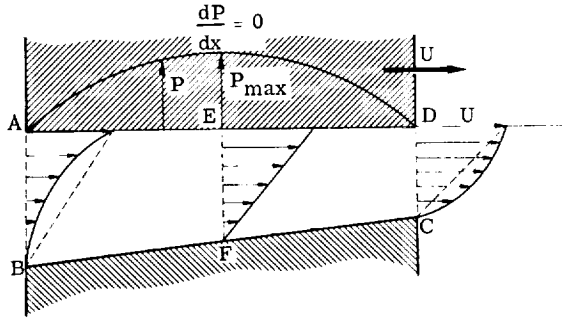

(c) Velocity distribution as a result of superimposed velocity and pressure flows.

Figure 66. - Flow between two inclined plane surfaces. (From ref. 40.).

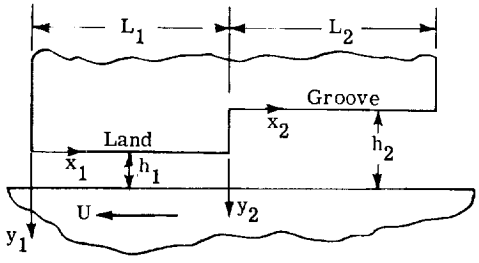

(a) Step bearing geometry.

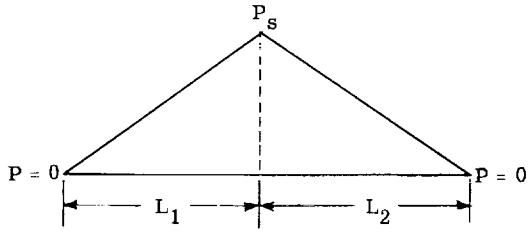

(b) Step bearing pressure distribution.

Figure 67. - Step bearing geometry and pressure distribution.

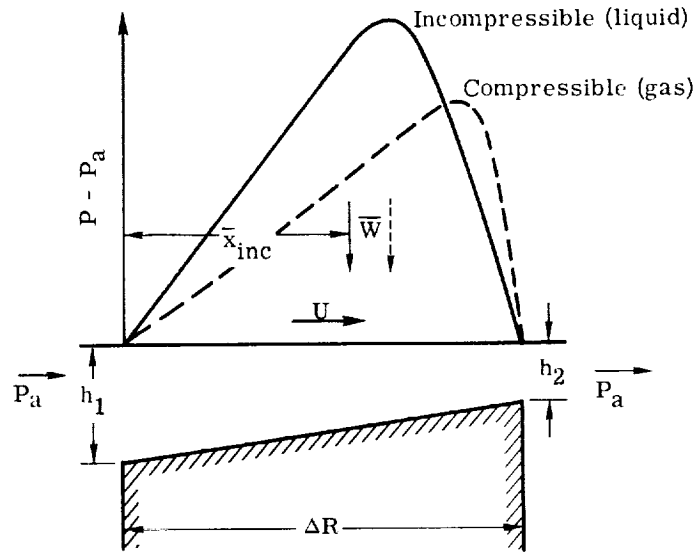

(a) Effect on pressure distribution.

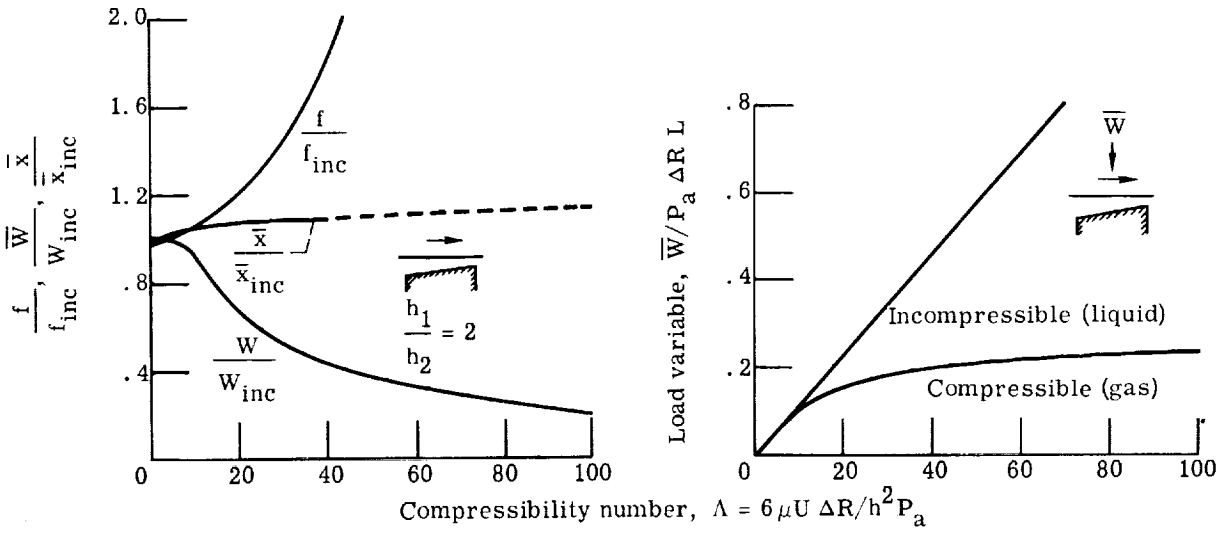

(b) Effect on friction, center of pressure, and load capacity. $\bar{x}_{inc} = 0.582\ \Delta R$; $f_{inc} = 11.0\ \Delta/\Delta R$; $W_{inc} = 0.069\ \mu U(\Delta R)^2 L/h_2^2$.

(c) Effect on load capacity.

Figure 68. - Typical compressibility effects in hydrodynamic bearings. Slider bearing; ratio of flow length to seal-face radial length, L/ΔR, 1; ratio of entrance to exit film thickness, h_1/h_2, 2. (From ref. 41.)

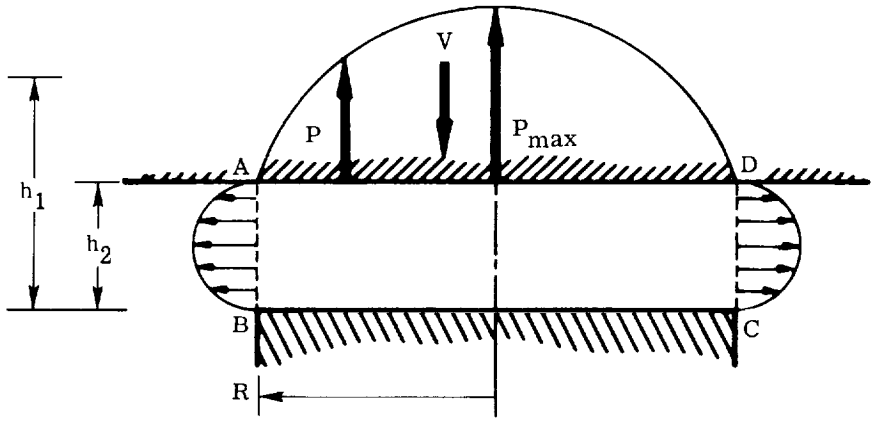

Figure 69. - Flow between parallel plane surfaces that approach each other. (From ref. 40.)

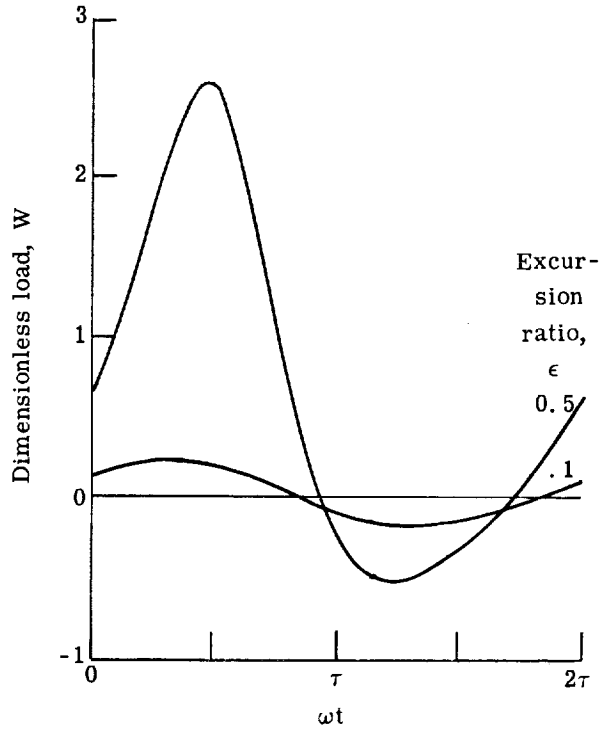

Figure 70. - Dimensionless squeeze-film force (load as function of time) for one cycle, for small and large excursion ratios. Squeeze number, σ, 10. (From ref. 43.)

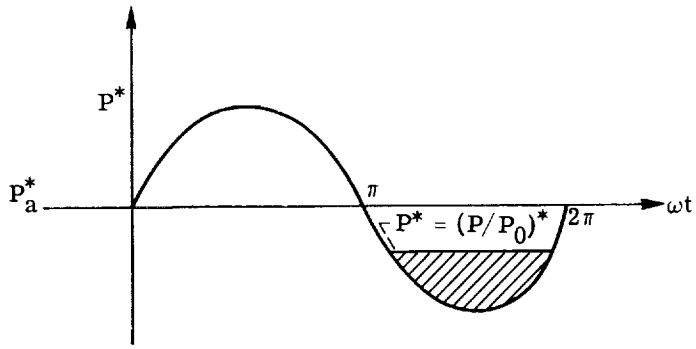

Figure 71. - Typical pressure profile found from incompressible flow solution, illustrating that "degassing" or cavitation will yield a net squeeze film force over a cycle.

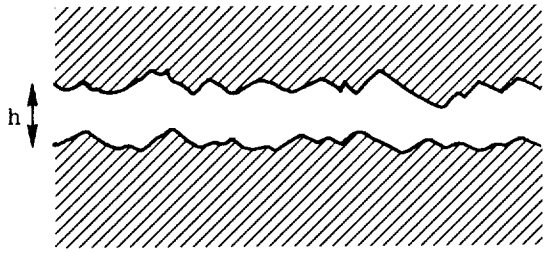

Figure 72. - Typical appearance of clearance between two seal surfaces. (From ref. 45.)

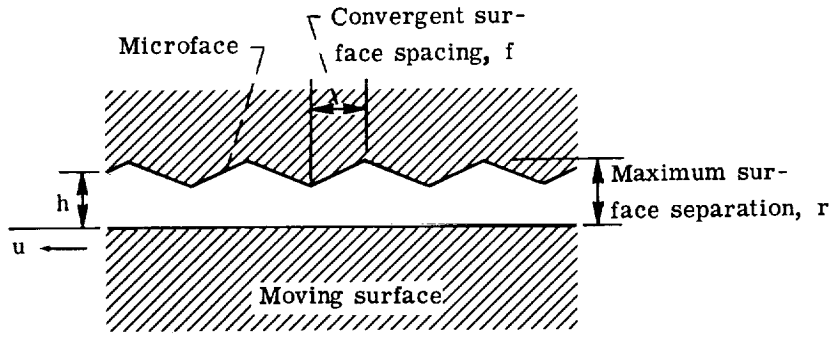

Figure 73. - Idealized appearance of clearance between two seal surfaces. (From ref. 45.)

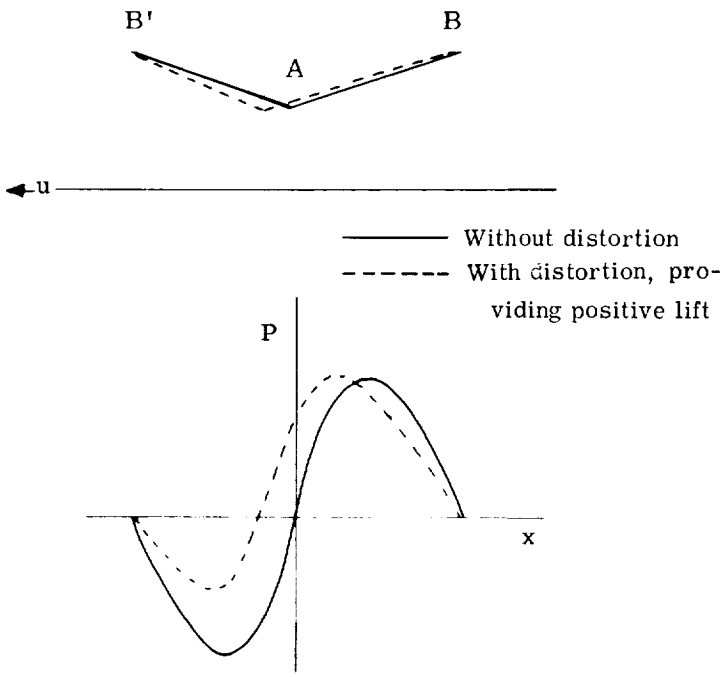

Figure 74. - Pressure distribution on a symmetrical microface pair. (From ref. 45.)

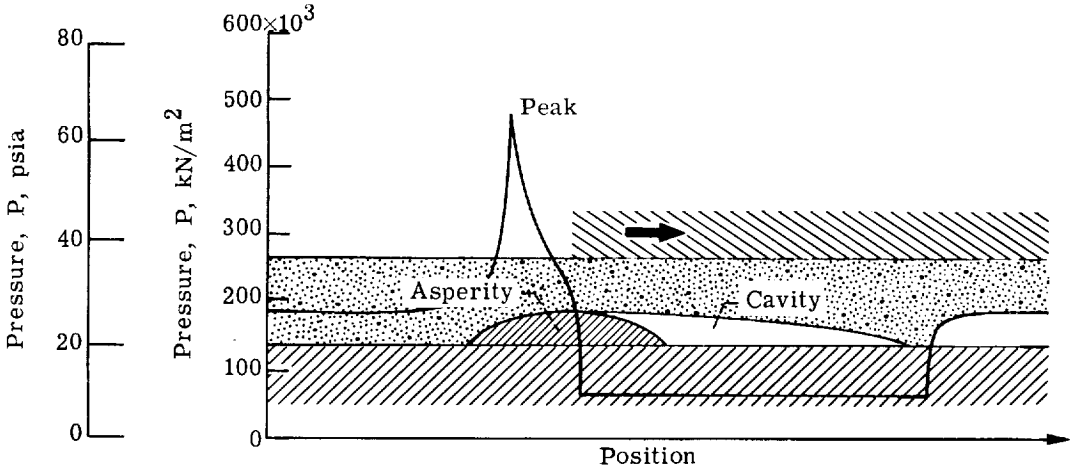

Figure 75. - Pressure measurement for large-scale asperity model. Ambient pressure, 177 kN/m^2 (25.7 psia); cavity pressure, 103 kN/m^2 (14.9 psia); peak pressure, 463 kN/m^2 (67.2 psia). (From ref. 46.)

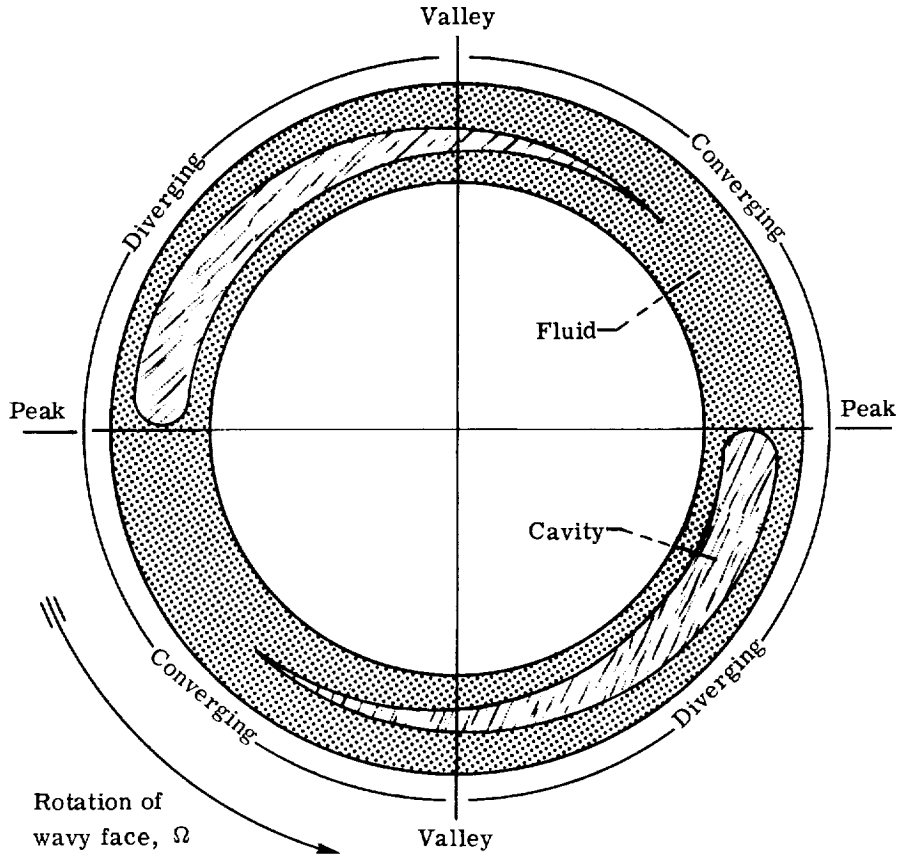

Figure 76. - Wavy face-seal surfaces, illustrating hydrodynamic pressure generation. (From ref. 47.)

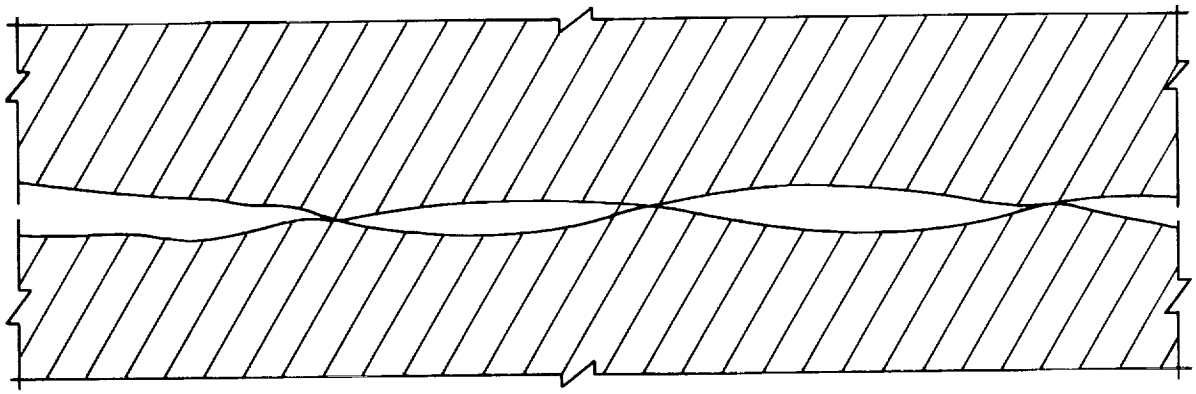

Figure 77. - Solid surfaces in contact. (From ref. 48.)

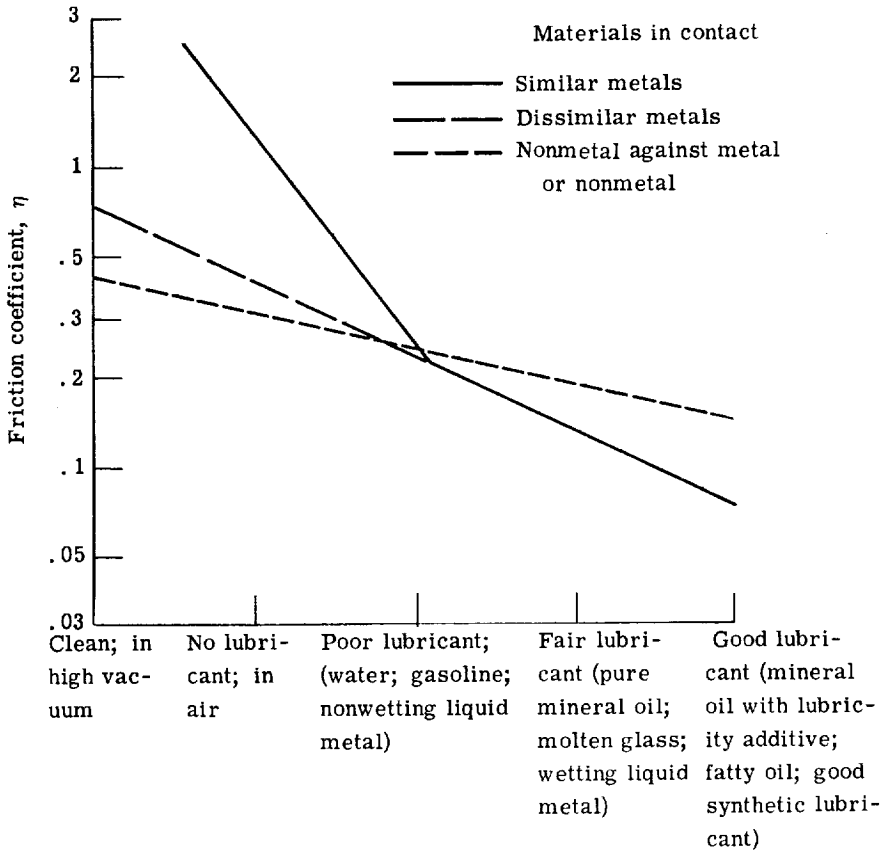

Figure 78. - Influence of contamination on friction coefficient for various material combinations. (From ref. 49.)

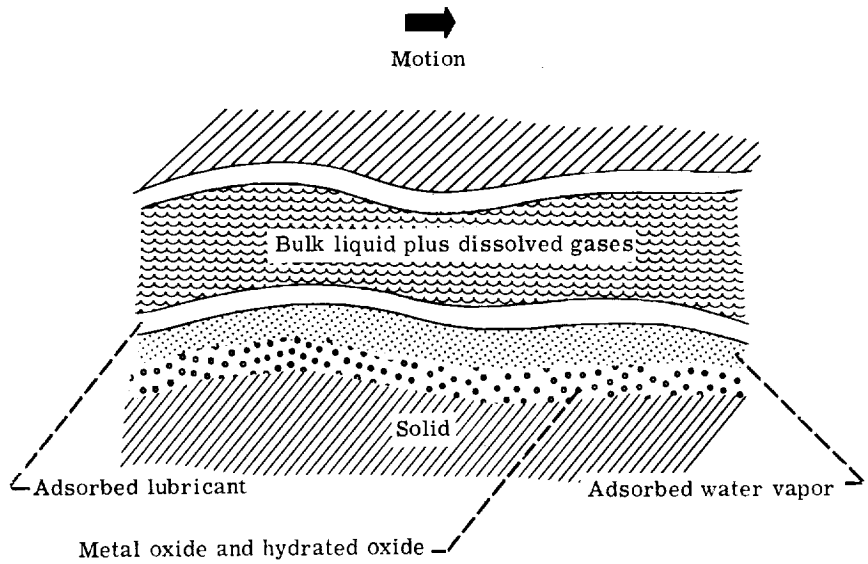

Figure 79. - Typical solid surface in contact with lubricant - undisturbed surfaces.

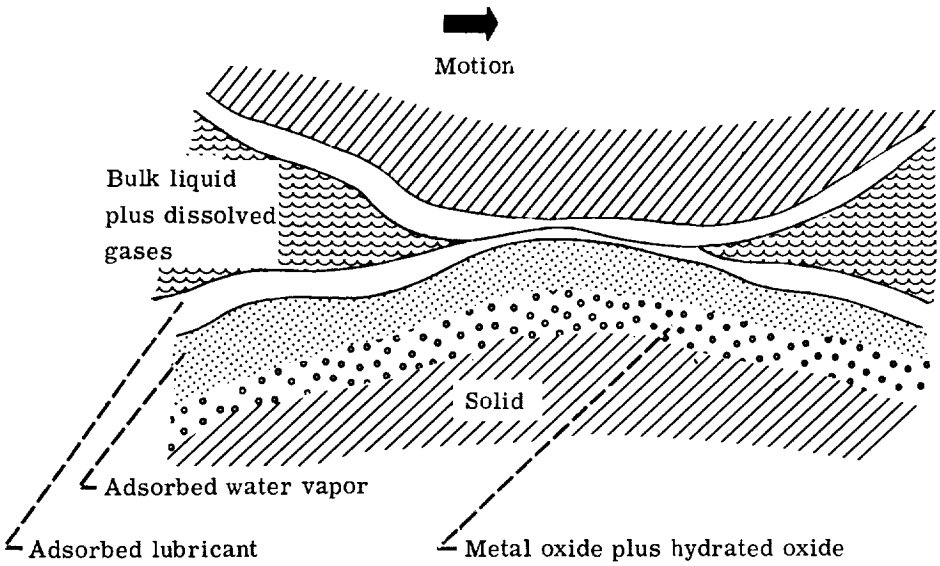

Figure 80. - Lubrication by adsorbed lubricant - lower effective shear strength (lower friction than solids in contact).

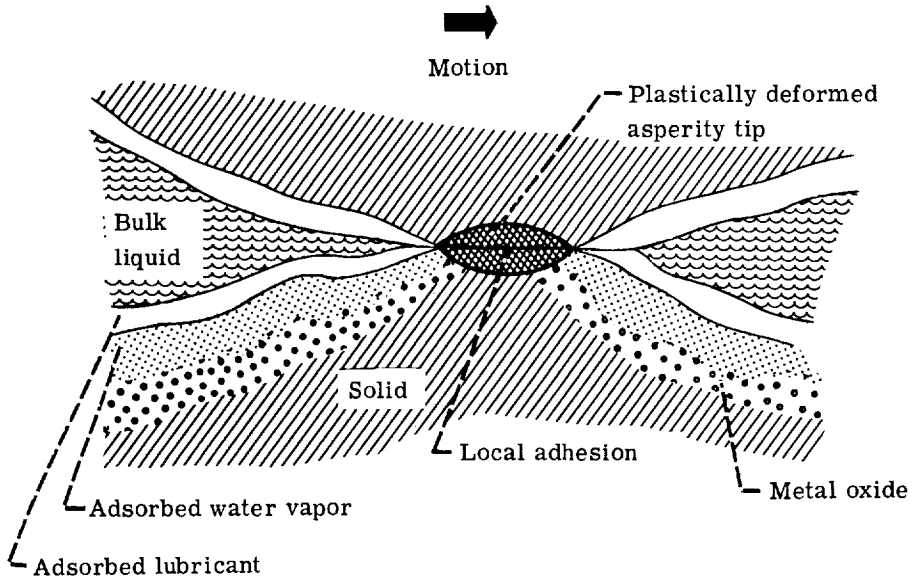

Figure 81. - Failure of surface films - friction increases and wear occurs.

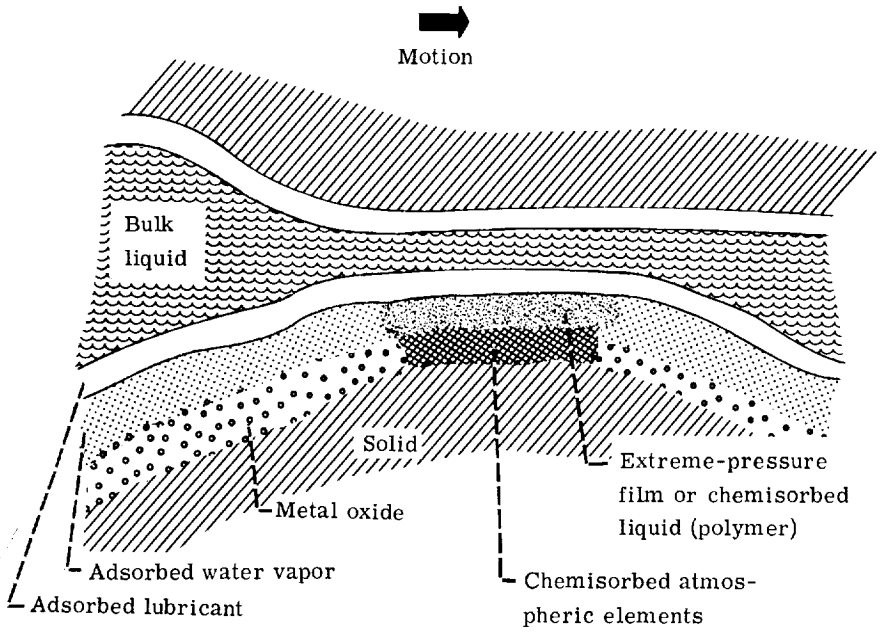

Figure 82. - Abraded surface after contact - oxide formation rate greater than removal rate.

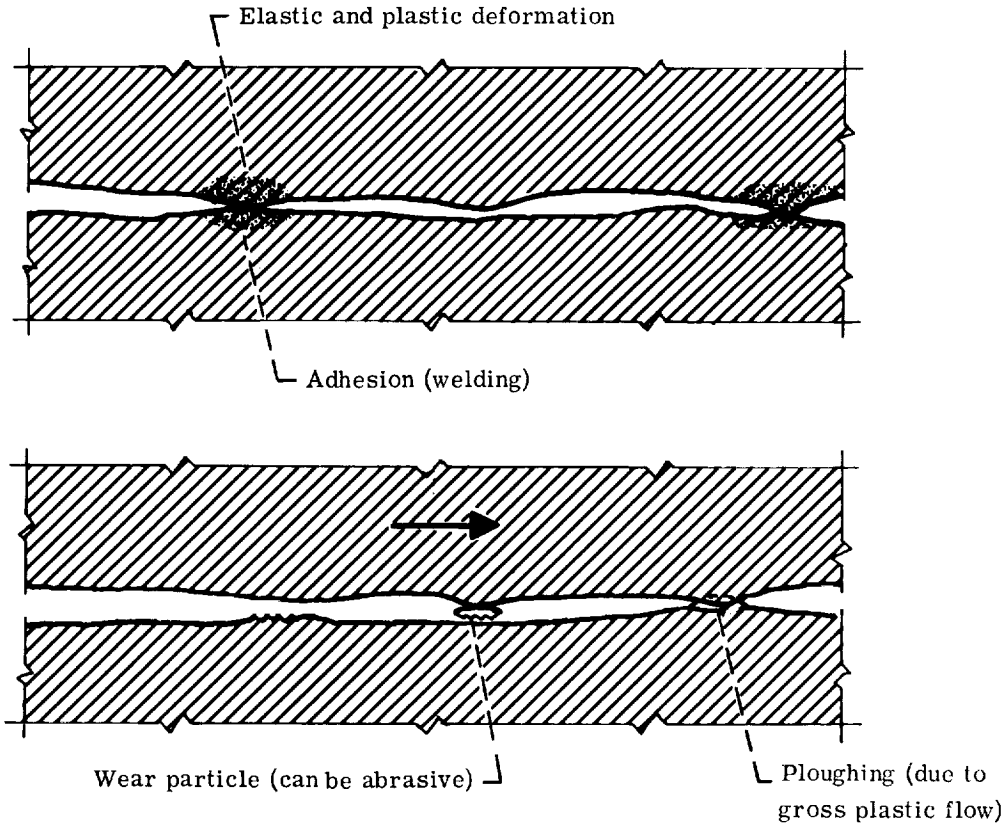

Figure 83. - Adhesive and abrasive wear mechanisms. (From ref. 48.)

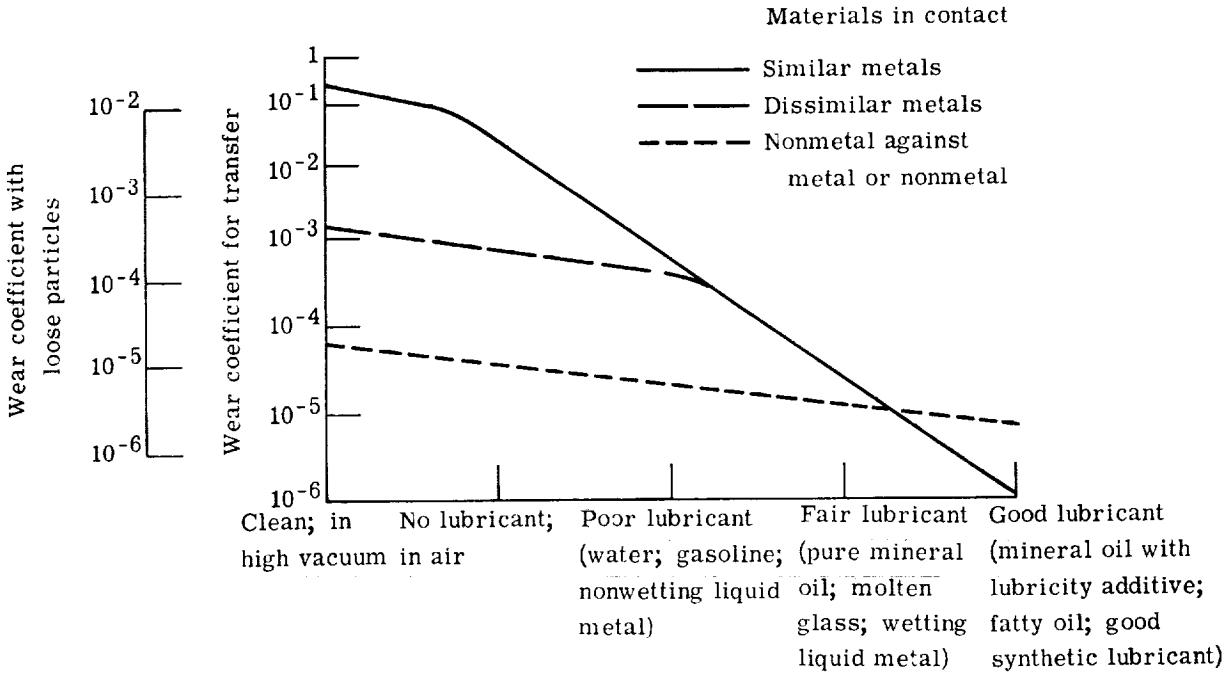

Figure 84. - Influence of contamination on wear coefficients for various material combinations. (From ref. 49.)

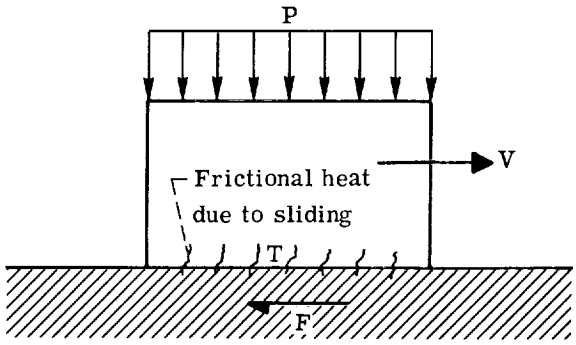

Figure 85. - Simplified model for deriving the pressure-velocity-limiting criterion based on heat generation.

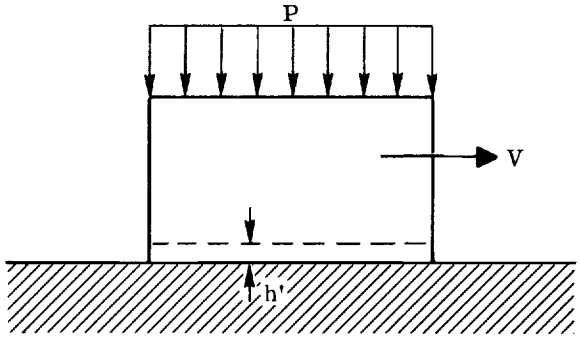

Figure 86. - Simplified model for deriving the pressure-velocity-limiting criterion based on wear.

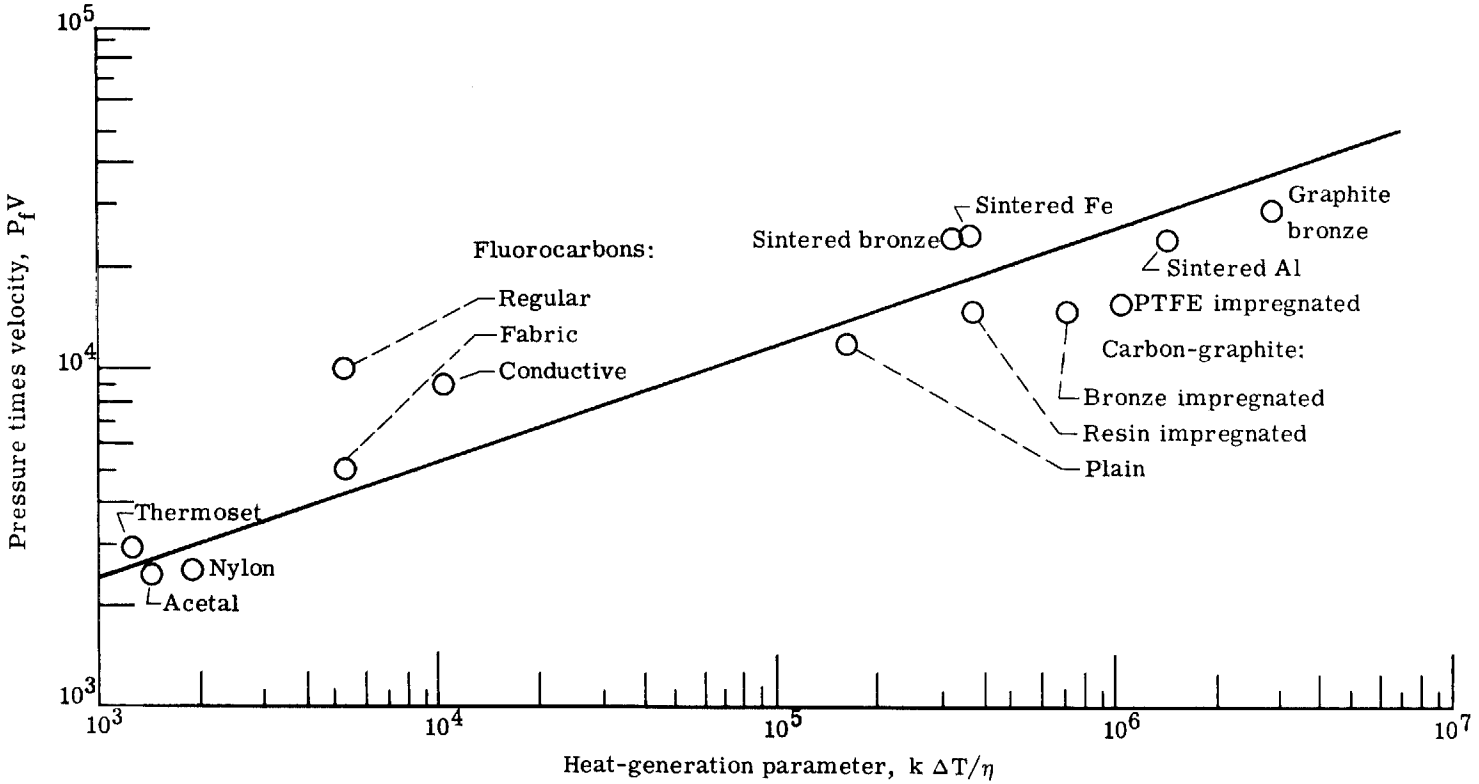

Figure 87. - Pressure times velocity as function of heat-generation parameter for some bearing materials. (From ref. 41.)

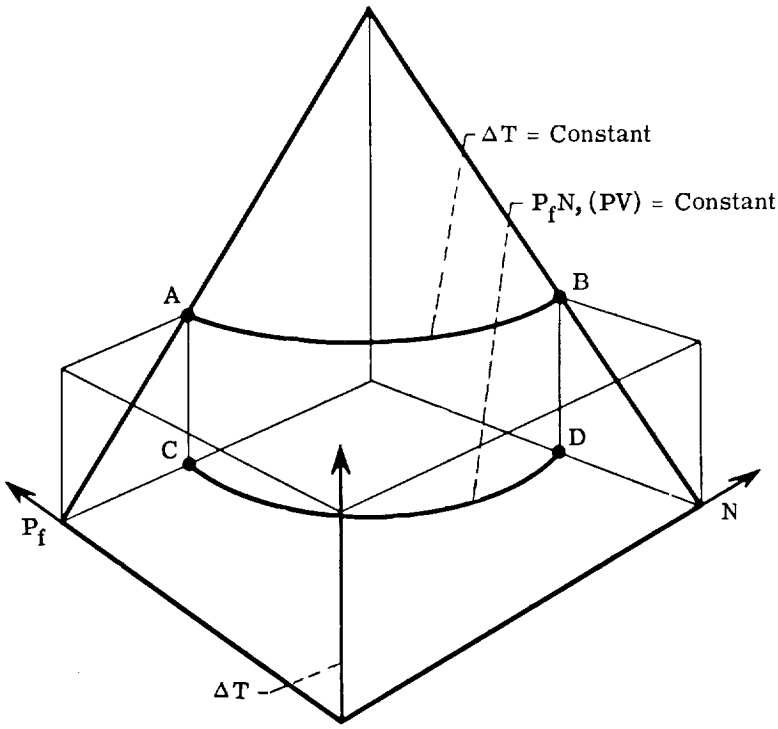

Figure 88. - Graphical representation of relation P_fN, (P_fV) = Constant. (From ref. 41.)

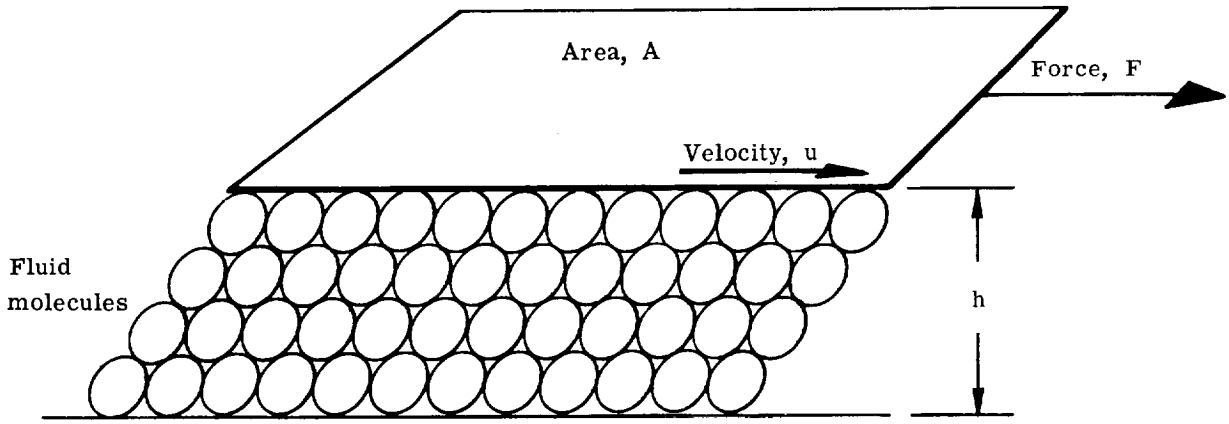

Figure 89. - Newton's law of viscosity: $F = \mu(AU/h)$ or $\mu = (F/A)/(u/h)$ = Shear stress/Shear rate, where μ is viscosity, U is leakage flow reference velocity, h is film thickness, and A, u, and F are defined in sketch.

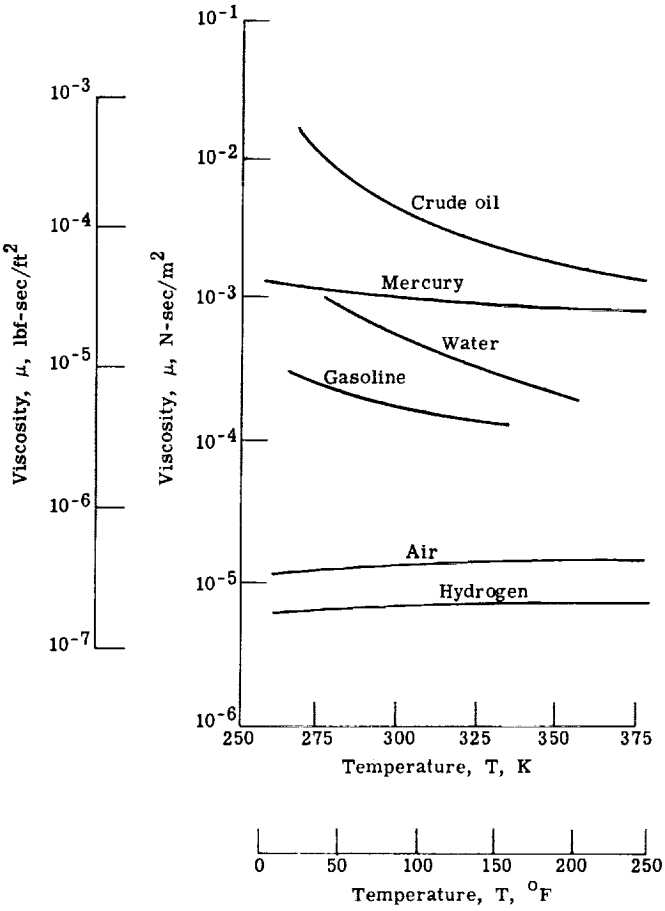

Figure 90. - Absolute viscosity of some fluids.

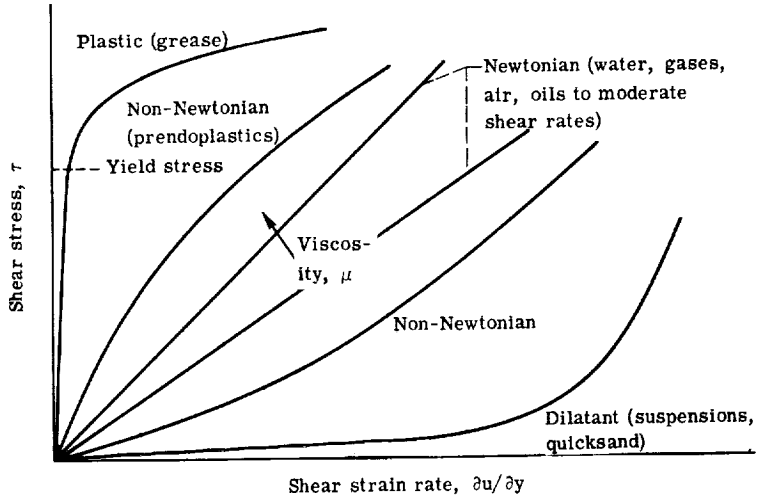

Figure 91. - Shear stress as function of shear strain rate for various types of viscous and plastic fluids.

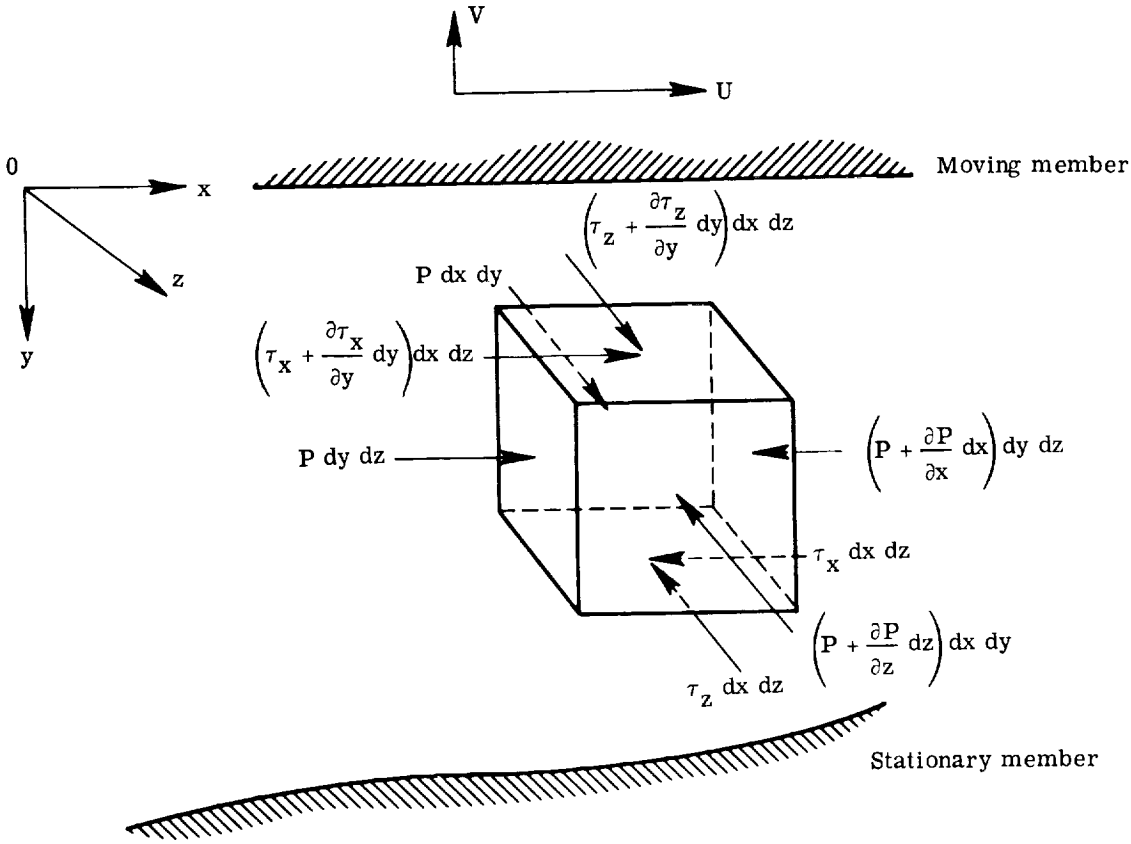

Figure 92. - Stressed element in fluid film. (From ref. 40.)

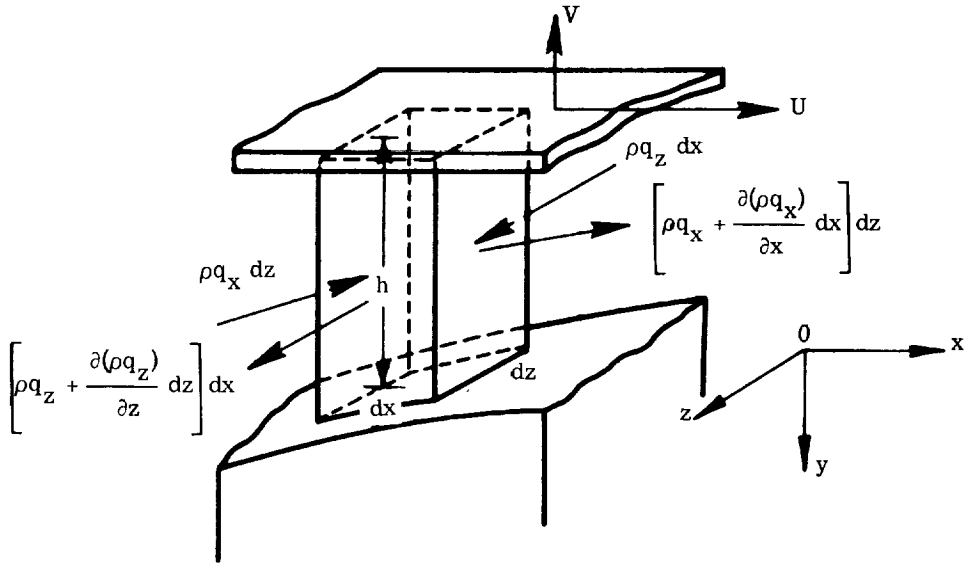

Figure 93. - Flow components into and out of fluid volume. (From ref. 40.)